THE UNIVERSITY OF CHICAGO

NOVEL IMMUNE RESPONSES IN LUNG INJURY AND FIBROSIS

A DISSERTATION SUBMITTED TO
THE FACULTY OF THE DIVISION OF THE BIOLOGICAL SCIENCES
AND THE PRITZKER SCHOOL OF MEDICINE
IN CANDIDACY FOR THE DEGREE OF
DOCTOR OF PHILOSOPHY

COMMITTEE ON IMMUNOLOGY

BY
YOUNG ME YOON

CHICAGO, ILLINOIS
JUNE 2023

TABLE OF CONTENTS

LIST OF FIGURES

LIST OF TABLES

LIST OF ABBREVIATIONS

ABSL	animal biosafety level
ALI	acute lung injury
ARDS	acute respiratory distress syndrome
a-SMA	alpha-smooth muscle actin
ASVs	amplicon sequence variants
AT1	alveolar type 1 cells
BLM	bleomycin
CTD-ILD	connective tissue disease-associated ILD
FMT	fecal microbiota transfer
FVC	forced vital capacity
GC	germinal center
GF	germ-free
gLN	gut-draining lymph node
HLA	human leukocyte antigen
HP	hypersensitivity pneumonitis
ILC	innate lymphoid cells
ILD	interstitial lung disease
Immune-ILD	immune-associated ILDs (For this sutdy: CTD-ILD, HP, IPAF)

IPAF	interstitial pneumonia with autoimmune features
IPF	idiopathic pulmonary fibrosis
KRT-17	cytokeratin-17
LLN	lung-draining lymph nodes
MHC	major histocompatibility complex
MPC	mesenchymal progenitor cells
NK	natural killer
PCA	principal component analysis
PCoA	Principal coordinate analysis
PF-ILD	progressive-fibrosing ILD
PhIP-seq	phage immunoprecipitation sequencing
RA	rheumatoid arthritis
RLBA	radioligand binding assay
SLE	systemic lupus erythematosus
SPF	specific pathogen-free
STAMP	statistical analysis of metagenomic profiles
Tcon	T conventional cell
TCR	T cell receptor
Tfh	follicular helper T cell

Tfr	follicular regulatory T cell
Th	helper T cell
Th17	T helper 17 cell
Treg	regulatory T cell
Trm	resident memory T cell
UCTD	undifferentiated connective tissue disease
UIP	usual interstitial pneumonia
UMAP	uniform manifold approximation and projection
WT	wild-type

ACKNOWLEDGMENTS

I have a village of colleagues and mentors that supported me throughout my academic journey. Foremost, I would like to express my biggest gratitude to my advisor Prof. Anne Sperling for the continuous support of my scientific endeavor as well as my personal goals. I appreciate how she always made herself available and introduced me to her colleagues to let me benefit from such a rich network of collaborators and mentors. I'm grateful to have learned how to manage a large collaborative project and how to effectively present science in both oral and written formats from Anne. Through her trust and encouragement, I became a more confident and well-rounded scientist and a professional.

I would like to thank all the past and present members of the Sperling Lab. I am fortunate to have a collegial and supportive group of people as my colleagues. Especially, I want to thank Dr. Tania Velez for being a great partner in human ILD study. I appreciate Maile Hollinger, Kelly Blaine, Donna Decker, Rebecca Voogt, Gabe Barron, Dr. Cara Hrusch, Dr. Paulette Krishack, and Lexi Cassano for all the guidance and great fellowship.

I would also like to express my sincere gratitude to Prof. Marcus Clark. I appreciate him for taking me under his roof and supporting me to able to complete my dissertation projects. With his encouragement, I was able to take a leap of faith in the middle of my graduate training to expand my areas of expertise. I would like to thank all the members of the Clark Lab. I appreciate Nathaniel Wright, Dr. Malay Mandal, Dr. Lily Ai, Margaret Veselits, Dr. Deepjyoti Ghosh, Thao Cao, Gabriel Casella, Greer Gurewitz, and Dr. Madeleine Durkee for all the support and inspiration.

It was a privilege to have great scientists on my thesis committee. I would like to thank Dr. Bana Jabri, Dr. Samantha Riesenfeld, and Dr. Robert Guzy for contributing their time and insight to guide me to be a deep thinker and a better scientist. I must also acknowledge a team of clinician mentors Dr. Katie Lee, Dr. Mary Strek, and Dr. Deji Adegunsoye. I appreciate them for inviting me to the clinic and MDD meetings to help me learn about ILD

disease and for paving the ground for the ILD study at University of Chicago.

I am tremendously grateful to ILD patients, organ donors, and their families for allowing me to study their lungs and blood samples. Also, I thank my collaborators at UCSF, Dr. Vaibhav Upadhyay, Dr. Sara Vazquez, Dr. Anthony Shum, Dr. Joseph DeRisi, Dr. Mark Anderson, and Christopher Law, for their mentorship and being instrumental to the antigen discovery study. Also, I acknowledge my collaborators in the microbiome study, Dr. Na Fei, Dr. Vanessa Leone, and Dr. Abigail E. Overacre-Delgoffe, for their guidance.

I am fortunate to have been a part of the Committee on Immunology, a community of truly brilliant and fun people. I want to thank every members but especially Dr. Pete Savage, Dr. Daria Esterhazy, Dr. Anita Chong, Dr. Marisa Alegre, and Dr. Melody Swartz for being great mentors to me. I appreciate Amber Chatellier and Beth Morrissey for making all the committee activities happen. Also, I acknowledge the University of Chicago core facilities: Cytometry and Antibody Technology Core, Integrated Light Microscopy Core, Human Tissue Resource Center, Animal Resource Center, and DFI Microbiome Metagenomics Facility. I couldn't have completed my dissertation without all the help that I received from experts in these facilities.

To my friends, Augusta, Geoff, Jen, and Histones, thank you for your unwavering support and love. I am happy that so many fun memories in graduate school were built together with you guys. To my Thursday Women's Group, thank you for being there for me at my most vulnerable times. I got courage to break down and build myself back up with your support.

To my deerest husband DongHo Kim, thank you for being the brainstem of our house and providing so much whether it is emotional support or scientific advice. You have always been by my side not only in life, but also in lab while I work late nights and weekends. Thank you for always caring and cheering for me. I owe this PhD to you. Finally, I thank my parents and sisters, SoYoung, JiYoung, and AhRam, for always believing in me and supporting me to reach for the best.

ABSTRACT

Fibrotic interstitial lung disease (ILD) is a group of heterogeneous conditions characterized by progressive respiratory decline and early death. Current understanding of the disease mechanisms depends on etiological and morphological classification of ILD subtypes. A prevailing paradigm is that immune cells play a pathogenic role in immune-associated ILDs, whereas their role in idiopathic pulmonary fibrosis (IPF) is controversial. However, patients with fibrotic ILDs commonly have enlarged lung-draining lymph nodes (LLN), which correlate with mortality. Our study revealed converging adaptive immune landscapes in LLNs of end-stage fibrotic ILD patients, characterized by the enrichment of germinal centers (GC), antigen-stimulated T cells, and regulatory T cells with an aberrant phenotype. The presence of GC B cells in LLNs was associated with worse respiratory decline in patients. A proteome-wide screening identified 17 novel auto-antigens to which circulating antibodies in ILD patients are reactive. Autoantibody responses to ABLIM1, a protein highly expressed in fibrotic lungs, correlated with frequencies of follicular helper T cells and regulatory T cells in patients' LLNs. These findings suggest that antigen-driven immune responses could be a key immunopathology that is common to end-stage fibrotic ILDs, even in IPF. Furthermore, we demonstrated that subtle differences in the gut microbiome compositions have a large impact in lung injury response of mice in specific pathogen-free barrier facilities. Presence of *Proteobacteria*, including *Helilcobacter hepaticus* and *Desulfovibrio sp.*, in the gut was associated with increased weight loss and mortality during lung injury responses in mice. These data support the gut-lung axis and highlight the potential benefit of specific alterations to the gut microbiome compositions to control lung injury outcomes. Together, my dissertation developed a comprehensive understanding of the human immune responses and the effect of the host-microbiota interaction during lung injury and fibrosis. This work will inform the development of models for mechanistic studies and patient endotypes for effective therapeutic intervention.

CHAPTER 1

INTRODUCTION

1.1 Pulmonary physiology and immunology

1.1.1 The lungs

The lungs are vital organs in mammals required for gas exchange to supply oxygen and remove carbon dioxide from the bloodstream. Lungs are organized into multiples lobes, three on the right and two on the left in humans, and air travels through a series of passages including the trachea, bronchial tubes, and bronchioles. At the end of bronchioles are clusters of air sacs called alveoli, which are surrounded by blood capillaries and are where gas exchange occurs. Connective tissue in the space between alveolar membranes and capillary endothelium are collectively termed the lung interstitium. Most medical conditions of the lungs affect either the airway (i.e. asthma and chronic obstructive pulmonary disease) or the interstitium (i.e. pulmonary fibrosis and sarcoidosis).

In addition to facilitating breathing, the lungs are a mucosal organ that functions as a primary barrier between the external environment and the body. With a total surface area as large as a tennis court, lungs are one of the largest organs in direct contact with the external environment(Ananda Rao and Johncy, 2022). Specialized epithelial cells lining the airway provide frontline defense against inhaled insults through mucociliary clearance and alarmin secretion. Furthermore, intricate functions played by multiple immune cells through interconnections among the tissue, vascular, lymphatic systems are key to ensuring the health of an individual.

1.1.2 Innate immunity in lungs

The immune system is largely divided into two arms, innate and adaptive immunities, with innate-like lymphocytes residing on a spectrum between the two systems. In general, the innate immune system depends on germ-line encoded receptors to recognize pathogens and provide immediate defense. Some innate immune cells such as alveolar and interstitial macrophages, tissue-resident natural killer cells and innate lymphoid cells reside within the lungs to function as phagocytes and secretors of soluble factors that instruct neighboring cells. Other innate immune cells such as eosinophils and neutrophils are rapidly recruited to the lungs in response to chemokines secreted upon insults.

Eosinophils play a major role in allergic airway inflammation. Activated by type 2 cytokines, especially by IL-5, eosinophils degranulate to release multiple pro-inflammatory substances, including IL-13, TGF-β, eosinophil peroxidase and major basic protein, which promote mucus hypersecretion, goblet cell hyperplasia, extracellular matrix secretion, epithelial cell remodeling, and mast cell activation(McBrien and Menzies-Gow, 2017; Travers and Rothenberg, 2015). Neutrophils clear extracellular pathogens and apoptotic cells through phagocytosis and the release of granules and neutrophil extracellular traps (Mantovani et al., 2011). Neutrophils are also a substantial source of matrix metalloproteinases, which play a crucial role in extracellular matrix modeling (Cundall et al., 2003; Ardi et al., 2007). Pro-inflammatory proteins released by eosinophils and neutrophils are beneficial for clearing pathogens, but uncontrolled such response can also induce tissue damage such as acute lung injury (ALI) and pulmonary fibrosis (Corbel et al., 2001; Henry et al., 2002).

1.1.3 Adaptive immunity in lungs

Adaptive immune cells, consisting of T cells and B cells, are equipped with 10^7 – 10^8 unique, somatically rearranged receptors that are antigen-specific and capable of imparting context-

dependent mechanisms of protection (Qi et al., 2014; Soto et al., 2020). Initiation of an adaptive immune response is spearheaded by antigen presenting cells, which pick up antigens from the lungs and migrate to lymph nodes where they present the antigens as peptides in the context of major histocompatibility complex (MHC) to T cells. Naïve T cells in blood constantly circulate through lymph nodes via a specialized post-capillary venule, high endothelial venules, until they encounter cognate antigens on an APC. Naïve T cells that have received three signals: (1) T cell receptor (TCR) engagement, (2) co-stimulation, and (3) cytokines from APC are programmed to perform specific effector functions, some of them as memory cells. Effector T cells exit lymph nodes through efferent lymphatics and traffic to the lungs via the thoracic duct to mount a response.

Effector T cells in the lungs come in many flavors. $CD8^+$ T cells are cytotoxic and promote viral clearance through secretions of IFN-γ, TNF, and granzymes. Following a viral challenge, some $CD8^+$ T cells become resident memory T cells (Trm) in lungs to provide effective protection against secondary infections (Hogan et al., 2001; Jozwik et al., 2015). For this reason, generation of $CD8^+$ Trm cells has been a focus of vaccine development against respiratory viruses in recent years (Lee et al., 2021b; Si et al., 2018). Though necessary for protection from pathogens, the antiviral response of $CD8^+$ T cells can also cause immunopathology such as acute respiratory distress syndrome (ARDS). TNF mediates weight loss and lung damage (Hussell et al., 2001; Rutigliano and Graham, 2004), and prolonged production of IFN-γ and TNF can trigger a cytokine storm, which causes life-threatening systemic inflammation (Fajgenbaum and June, 2020; Walsh et al., 2014).

$CD4^+$ T cells play various effector functions after differentiating into one of the helper T (Th) cell subtypes such as Th1, Th2, Th17, and follicular helper T cells (Tfh). Like $CD8^+$ T cells, Th1 cells are cytotoxic but are also specialized in clearing intracellular microbes that infect phagosomes such as Mycobacterium tuberculosis (Mogues et al., 2001; Tubo and

Jenkins, 2014). Differentiation of Th1 cells is orchestrated by the transcription factor T-bet, which is induced by IL-12 and type 1 interferon signaling. Th2 cells differentiate in response to epithelial damage often caused by allergens or injury in the lungs. Damaged epithelium secretes alarmins, such as IL-33, and initiates a cascade of cellular events including the secretion of IL-4 by ILC2 followed by GATA3 activation for Th2 cell differentiation (Kokubo et al., 2022). In the lungs, Th2 cells are the main culprit of allergic airway disease since IL-4, IL-5 and IL-13 produced by these cells activate eosinophils, goblet cells and promote IgE class switching. Type 2 cytokines also promote tissue repair by enhancing extracellular matrix production (Crosby and Waters, 2010). Th17 cells are defined by RORγt and are specialized in protection from extracellular bacteria through secretion of IL-17. Specialized lung dendritic cells promote Th17 differentiation via a IL-1β dependent mechanism when there is a bacterial invasion through the intranasal route (Caucheteux et al., 2017; Linehan et al., 2015; Pepper et al., 2010). Th17-mediated inflammation promotes neutrophilia for the pathogen clearance, and it is also involved in neutrophilic asthma in the lungs. Finally, the STAT3 pathway is activated via IL-6 and IL-21 signaling during antigen stimulation and induces differentiation of Tfh cells, which are players in germinal center (GC) responses required for generation of affinity matured and class switched antibodies (Ray et al., 2014).

Defined by the transcription factor FOXP3, regulatory T cells (Treg) play key roles in maintaining tolerance to self-antigens and regulating effector T cell activities. General mechanisms of immune suppression by Treg cells include the inhibition of CD80 and CD86 signaling by CTLA-4, absorption of IL-2 using a high affinity receptor to interfere with conventional T cell proliferation/survival, and secretion of immune suppressive cytokines IL-10 and TGF-β (Sakaguchi et al., 2020). Treg subpopulations can express other transcription factors traditionally associated with effector T cells such as T-BET (Koch et al., 2009), GATA3 (Wohlfert et al., 2011), and RORγt (Yang et al., 2016). These Treg subsets elicit enhanced suppressive function against the Th cell type with matched transcription factor

expression. For example, a loss of GATA3 from Treg cells resulted in increased Th2 cytokine secretion in the skin, which led to spontaneous activation of fibroblasts and dermal fibrosis (Kalekar et al., 2019). Similarly, other studies support anti-fibrotic roles for total Treg cells in mouse models of kidney and cardiac injury and fibrosis (do Valle Duraes et al., 2020; Kanellakis et al., 2011). In the lungs, it has been shown that Treg cells regulate inflammation and injury response through modulating the infiltration of inflammatory myeloids such as $Ly6C^{hi}$ cells via IL-13 secretion following the direct sensing of the alarmin IL-33 (Liu et al., 2019). However, cytokines secreted by Treg cells including IL-13 and TGF-β have pro-fibrotic properties (Lee et al., 2001), and Treg cells have been associated with pathogenic roles in lung fibrosis (Birjandi et al., 2016; Kaviratne et al., 2004; Lo Re et al., 2011). Therefore, further investigation is needed to understand the exact role of Treg cells during lung injury and fibrosis.

One of the important roles of B cells is to generate antibodies. Antibody generation requires the GC, which is a specialized microstructure maintained by chemokine gradients established by stromal cells in secondary lymphoid organs. GCs are typically divided into light zone and dark zone. The light zone is enriched with follicular dendritic cells, which are antigen reservoirs, and Tfh cells that secrete cytokines that enable survival and differentiation. GC B cells with high-affinity antigen receptors that can effectively acquire antigens from follicular dendritic cells are selected by Tfh cells in the light zone through secretion of IL-4 and IL-21 and engagement of co-stimulatory receptors including CD40, ICOS, and PD-1 (Good-Jacobson et al., 2010; Ise et al., 2018; Liu et al., 2015; Weinstein et al., 2016). Selected GC B cells enter the dark zone to undergo proliferation and somatic hypermutation (Bannard et al., 2013). A dichotomy between cellular division and mutation is important to prevent genomic instability in GC B cells. Dark zone is further compartmentalized into specialized niches, a proliferation region rich with tingible body macrophages and a differentiation region (Kennedy et al., 2020). After iterative selection

and proliferation, B cells exit the GC and become either memory B cells or plasma cells to respond rapidly in future GC responses or to secrete antibodies, respectively (Stebegg et al., 2018).

Together with Tfh cells, follicular regulatory T cells (Tfr) are a key cell type found in the GC. Tfr cells express markers shared with both Tfh and Treg cells including CXCR5, PD1, BCL6 and FOXP3. Our current understanding of the origin and role of Tfr cells is incomplete. Canonical Tfr cells primarily stem from Treg cells, and the TCR repertoire of Tfr cells is shared with Treg but not with Tfh cells (Chung et al., 2011; Linterman et al., 2011; Maceiras et al., 2017; Wollenberg et al., 2011). Tfr cells are generally thought to repress the Tfh cells in GC, but the effect of Tfr cells seems to be multifaceted and includes the overall suppression of antibody responses (Sage et al., 2014), the selection of antigen-specific, high-affinity B cells (Linterman et al., 2011), and prevention of autoantibody production (Fu et al., 2018). However, a recent study demonstrated that some Tfr phenotype cells arise from Tfh cells during the resolution phase of a GC response, and these cells contribute to GC contraction (Jacobsen et al., 2021). Though challenged by the lack of lineage specific markers that can distinguish Tfr from Treg or Tfh cells, the role of Tfr cells needs further investigation especially in the context of autoimmune disease.

1.2 Interstitial lung disease (ILD)

1.2.1 ILD subtype classification and treatment strategies

Interstitial lung disease (ILD) is an umbrella term that describes over 200 different clinical conditions characterized by inflammation or fibrosis of the connective tissue between the air sacs and lung capillaries, thereby compromising respiratory function (Kalchiem-Dekel et al., 2018). The prevalence of ILD is estimated at 74 cases per 100,000 in the United States (Noth et al., 2020). Risk factors for ILD are genetics, occupational exposures,

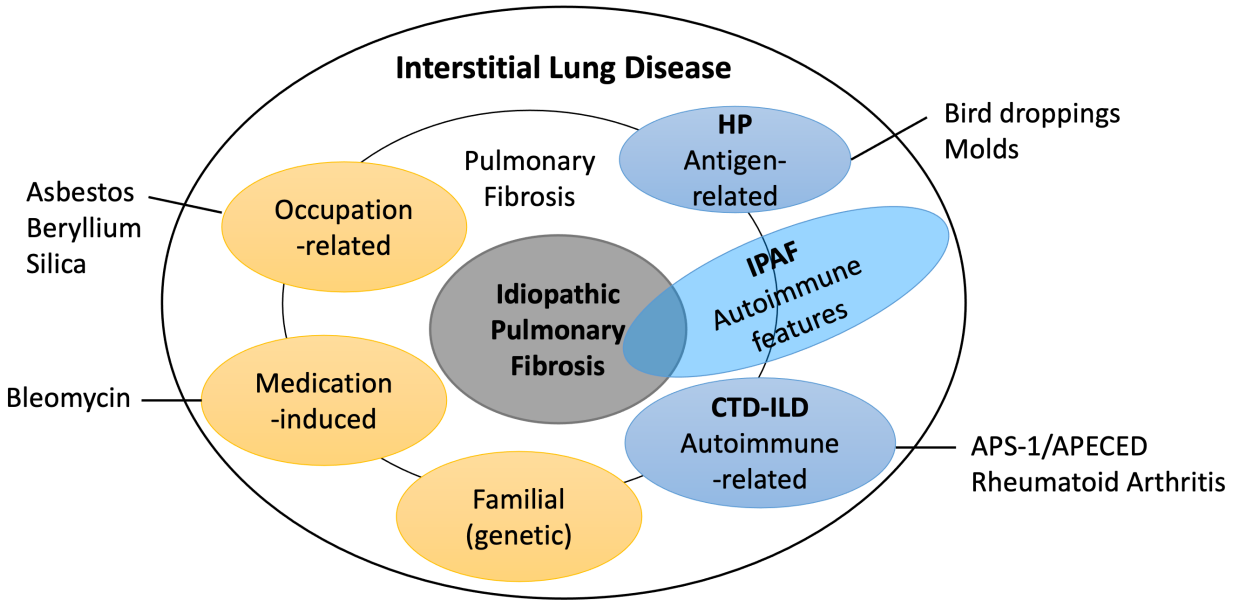

Figure 1.1: **ILD classification: from an immunologist's perspective.** Blue color indicates an immune-associated ILD. HP: hypersensitivity pneumonitis, IPAF: interstitial pneumonia with autoimmune features, CTD-ILD: connective tissue disease-associated ILD. SOURCE, Kalchiem-Dekel et al. (2018) with some modifications.

radiation, chemotherapy, smoking, age, and autoimmunity. Despite heterogeneity in diagnosis, patients with ILDs often present with a progressive fibrosing phenotype with similar presentations on high-resolution CT scan, lung function decline, and early mortality (Noth et al., 2020; Wijsenbeek and Cottin, 2020). A hallmark of fibrotic ILD is idiopathic pulmonary fibrosis (IPF), which is one of the most common types of ILDs with a prevalence of 8.3 cases per 100,000 in the United States. Up to 40% of other ILD conditions can also develop overlapping clinical, genetic, and pathophysiological features consistent with fibrotic ILD phenotypes (Cottin et al., 2018). Interestingly, ILDs that often present with lung fibrosis include hypersensitivity pneumonitis (HP) and connective tissue disease-associated ILD (CTD-ILD), which are immunologically mediated conditions associated with reactivities to environmental antigens and self-antigens, respectively (Figure 1.1).

IPF has no known cause and poor prognosis since 5-year survival is 56% despite the

recent development of anti-fibrotic medications (Zurkova et al., 2019). Nintedanib and Pirfenidone, a tyrosine kinase inhibitor and an inhibitor of the collagen synthesis and fibroblast proliferation, respectively, can improve patients' life expectancy on average by 2.5 years but are unable to reverse disease progression (Fisher et al., 2017). Further, these drugs have side-effects that are difficult for many patients to tolerate. IPF is associated with a characteristic radiologic feature, called usual interstitial pneumonia (UIP), but this pattern alone is not sufficient for a definitive diagnosis since other ILD conditions may also present with UIP. Therefore, IPF diagnosis requires exclusion of all known causes of pulmonary fibrosis through multidisciplinary discussions among clinicians, radiologists, pathologists, and other health care providers (Wuyts et al., 2014).

HP is mediated by inflammation of the lungs due to repeated exposure to inciting agents which are usually protein antigens derived from microorganisms such as molds, birds, and bacteria (Raghu et al., 2020). Patients with fibrotic HP have variable radiological presentations, but often have signs of airway abnormalities and fibrosis in the mid-zone of the lungs. Assessment of the exposure history is key to both diagnosis and treatment of HP since avoiding antigens is an important intervention (Fernandez Perez et al., 2013). It has been hypothesized that inflammation may be caused by some common epitopes among environmental antigens and that sensitization to one antigen may result in hypersensitivity to multiple agents. However, it is unknown why some patients with HP develop irreversible fibrosis while others have non-fibrotic subtype.

CTD-ILD is defined by radiologic demonstration of pathology consistent with ILD in the presence of an established connective tissue disease (CTD) (Solomon et al., 2020). Most common CTDs associated with ILD are rheumatoid arthritis (RA) and systemic sclerosis, which are autoimmune diseases with multi-organ involvement. CTD-ILD patients typically have non-specific interstitial pneumonia, which is characterized by homogeneous infiltration of the interstitium with inflammatory cells. CTD-ILD patients have a heterogenous degree

of fibrosis, but they can also have UIP (Vij and Strek, 2013). The degree of fibrosis and the symptoms of lung function impairment vary among CTD-ILD patients.

While anti-fibrotic therapies might commonly benefit fibrotic ILD patients (Maher et al., 2020), potentially distinct underlying disease mechanisms for different ILDs could have a large impact on patient outcomes. For example, immunosuppressive therapies such as corticosteroids, azathioprine, and mycophenolate are often used for HP and CTD-ILD, but they are detrimental for IPF patients (Idiopathic Pulmonary Fibrosis Clinical Research et al., 2012; Vasakova et al., 2017). Therefore, understanding key cellular mechanisms that underly initiation and progression of IPF in comparison to other fibrotic ILDs is critical for developing more efficient diagnostic and therapeutic strategies.

1.2.2 Role of the immune system in development and progression of IPF

Fibrosis is defined by the thickening of tissues due to excessive accumulation of extracellular matrix components, which is a result of a dysregulated wound healing process. It is believed that chronic inflammation is typically linked to fibrosis, while there could be a wide range of known and unknown triggers for the inflammation (Wynn, 2008). Therefore, a historical perspective on IPF is that the disease initiation is likely mediated by some inflammation of the lungs despite an unknown etiology. Multiple immunohistological studies of IPF patient lungs have shown that T cells and B cells accumulate within the lung tissues (Daniil et al., 2005; Marchal-Somme et al., 2006; Parra et al., 2007). The number of lung infiltrating CD3 T cells and CD8 T cells have negative associations with patient survival and lung function, indicating that T cells may be involved in IPF pathology. A study from our group, demonstrating a significant association between the enlargement of lung-draining lymph nodes and early deaths in fibrotic ILD patients, further supports that the adaptive immune response may be involved in IPF and other fibrotic ILDs (Adegunsoye et al., 2019).

Unlike HP and CTD-ILD, the argument for IPF being an immune disorder has been

weakened by the fact that various efforts to suppress the immune response, including prednisone, azathioprine, N-acetylcysteine, and anti-TNFα, have been unsuccessful at improving IPF patient survival (Douglas et al., 2000; Idiopathic Pulmonary Fibrosis Clinical Research et al., 2012; Raghu et al., 2008). In fact, treating patients with three immunosuppressants in combination resulted in a nearly ten-fold increase in mortality compared with placebo treatments, suggesting that some immune responses may be required for protecting IPF patients (Idiopathic Pulmonary Fibrosis Clinical Research et al., 2012). Because attempted immunotherapies such as prednisone and azathioprine suppress the immune system in non-specific manners, the outcome of these clinical studies does not entirely rule out the involvement of specific immune cells in IPF pathophysiology. For example, it was shown that specific depletion of B cells and plasma antibodies improves pulmonary function and patient survival in a small cohort of IPF patients who are undergoing acute exacerbation (Donahoe et al., 2015). To this end, it is critical to delineate specific roles for different adaptive immune cells in IPF and to understand whether they may be different from their roles in other fibrotic ILDs.

One current paradigm of IPF pathophysiology is that dysregulated alveolar epithelial cell regeneration, but not inflammation, is a fundamental driver of lung fibrosis. It is believed that alveolar type 1 cells (AT1), which are the building blocks of thin alveolar walls, are lost due to some microinjuries, and subsequently dysregulated AT1 cell differentiation leads to the replacement of AT1 cells with fibroblasts (Selman and Pardo, 2002). Epithelial cell-intrinsic dysregulation of regeneration has been demonstrated by Xia et al. (2014), where the authors showed that mesenchymal progenitor cells (MPC) isolated from IPF lungs present a distinct transcriptional profile compared to MPC from healthy lungs. IPF patient-derived MPC could give rise to fibroblasts in immunodeficient mouse lungs when injected intravenously (Xia et al., 2014). Furthermore, aberrant lung resident cells that co-express lineage-determining transcripts for both epithelial and mesenchymal

lineages have been identified through independent investigations of late stage IPF lungs via single cell RNA sequencing (Adams et al., 2020; Habermann et al., 2020). Nevertheless, it remains to be determined why AT1 cells are lost in the first place and what contributes to pathogenic reprogramming of progenitor cells in IPF. Since immune cells are abundant populations in the lungs in close contact with AT1 cells, it would be important to examine the role of immune cells even after the epithelial cell dysregulation has been established.

1.2.3 Autoimmunity in ILD

Some ILDs are associated with autoimmunity, which range from a definitive connective tissue disease to clinical autoimmune features. For example, RA is a type of connective tissue disease that can co-manifest with the lung pathology as CTD-ILD. In fact, the lungs are most frequently affected organs outside of joints in RA, and around 10% of RA patients develop an ILD (Kadura and Raghu, 2021). Though smoking, inhalational exposures, and genetic predisposition have been identified as risk factors for developing a CTD-ILD, underlying immunological mechanisms involving the lungs are not well understood. In addition, IPF patients, in the absence of a bona fide autoimmune disease, can show subtle features of autoimmunity including antinuclear antibodies, clinical signs of Raynaud's phenomenon, and distal digital fissuring (Fischer et al., 2015). These ILD patients are being increasingly recognized and classified as interstitial pneumonia with autoimmune features (IPAF) according to the official guideline of the American Thoracic Society (Fischer et al., 2015; Strek et al., 2016). Besides, around 29% of IPF patients tested positive for autoimmune serologies, suggesting that a significant subset of IPF patients may have underlying autoimmunity or a break in humoral tolerance as a result of ILD progression (Moua et al., 2014).

Associations with human leukocyte antigen (HLA) alleles have been well established in many autoimmune diseases, including rheumatoid arthritis, type 1 diabetes, celiac disease,

and multiple sclerosis (Hollenbach and Oksenberg, 2015; Miyadera and Tokunaga, 2015). Identifying disease-associated HLA haplotypes provides key insight for elucidating cellular mechanisms of pathogenesis because molecular structures of MHC encoded by HLA genes govern antigen peptide repertoires, which are presented to T cells for both establishing tolerance and eliciting adaptive immunity. When combined with a known antigen specificity, peptide-MHC pair can be identified and used as a tool for mechanistic research and potentially for patient diagnosis. A genome-wide association study of over a thousand non-Hispanic white patient population revealed that three HLA alleles, DQA1*01:02, DQB1*06:02 and DRB1*15:01, are significantly associated with fibrotic idiopathic interstitial pneumonia (Fingerlin et al., 2016). In particular, DRB1*15:01 association is consistent with a previous study of a smaller IPF cohort recruited from multiple institutions across the US, but not with a study of a patient population in Mexico (Falfan-Valencia et al., 2005; Xue et al., 2011). Though more than one mechanisms may lead to the pathology consistent with the current clinical definition of IPF, it is clear that autoimmunity could be associated with at least a subset of IPF.

IPF patients do not share a common history of exposure to environmental antigens or pathogens. Instead, studies suggest that reactivities to self-antigens could be contributing to IPF pathogenesis. Antibodies in IPF patient plasma were shown to be reactive to human cell lysates (Feghali-Bostwick et al., 2007). Few autoantigens, including HSP 70, vimentin and BPIFB1, have since been identified and shown to be associated with IPF patient survival, using targeted approaches (Kahloon et al., 2013; Li et al., 2017; Shum et al., 2013). All autoantigens discovered to date in the context of IPF are summarized in Table 1.1. Furthermore, IPF patients have increased complement deposition in lungs, which could support a hypothesis that some autoantibodies bind to lung tissues and form antibody-complement complexes to mediate tissue damage (Okamoto et al., 2018). Alternatively, autoantibodies may arise during late-stage disease only as a result of tissue

Table 1.1: Previously described ILD auto-antigens

Antigen	Disease	Method	Reference
Vimentin	IPF, NSIP	Immunoblot patient sera against lung fibroblast cell line extract (MRC5)	1, 2
Cytokeratin8	IPF, cryptogenic fibrosing alveolitis	Screened sera using a cDNA phage library of AT II carcinoma cell line (A549)	3, 4
Cytokeratin18	IPF	Immunoblot patient sera against bovine CK18	5
Cytokeratin19	IPF	Immunoblot patient sera against recombinant huCK19	6
IL1a	IPF	Radioimmunoassay of patient sera against IL1a	7
Collagen V	IPF	Flow analysis using col V coated beads	8
Hsp72	IPF	ELISA against Hsp72 using serum and BALF	9
Hsp70	IPF, Acute exacerbation	Screened sera against lung and lymphoblast cell line extract (K562)	10
Grp78	IPF	Screened sera against lung and lymphoblast cell line extract (K562)	10
Annexin1	IPF, Acute exacerbation	Screened sera using a phage library of AT II carcinoma cell line cDNA (A549)	11
BPIFB1	Idiopathic ILD, CTD-ILD	First discovered in Aire-/- mouse and then RLBA using patient sera	12
KCNRG	APS1 with lung disease	Screened patient sera against a bovine cDNA library in phage	13
Periplakin	IPF	Immunoblot patient sera against A549 cell lysates	14

1. Yang, et al. *Clin Exp Immunol.* 2002, 2. Li, et al. *JI* 2017, 3. Kurosu, et al. *JI* 2008, 4. Dobashi, et al. *Thorax* 1998, 5. Dobashi, et al. *Lung* 2000, 6. Dobashi, et al. *Lung* 1999, 7. Ogushi, et al. *J Med Invest* 2001, 8. Vittal, et al. *Plos One* 2013, 9. Mills, et al. *J Immunol Res.* 2019, 10. Kahloon, et al. *AJRCCM* 2013, 11. Kurosu, et al. *JI* 2008, 12. Shum, et al. *Science Trans Med* 2013, 13. Alimohammadi, et al. *PNAS* 2009, 14. Taille, et al. *AJRCCM* 2011

damage. Even if the autoantibodies are not involved in disease initiation or progression, they could serve as biomarkers to indicate important biological processes in patients. Therefore, further studies are needed to determine the extent of lung autoantigens and whether these autoantibodies are pathogenic in ILD.

1.3 Animal models of lung injury and fibrosis

Intratracheal instillation of bleomycin (BLM) in mice is a model of lung injury and fibrosis. Bleomycin is an anti-cancer antibiotic that induces cell death by generating reactive oxygen species and double-stranded DNA breaks (Burger et al., 1981). First reported as a side effect during clinical trials for cancer therapy, lungs are susceptible to inflammation and fibrosis in response to BLM (Sleijfer, 2001). BLM administration in an experimental model induces neutrophilic alveolitis and increases lung permeability during the first few days before the onset of fibrosis (Aeffner et al., 2015; Hrusch et al., 2018; Matute-Bello et al., 2008). Though not a perfect recapitulation of human diseases, the acute phase of BLM

response in mice models a lung injury response and the later phase models pulmonary fibrosis. Furthermore, BLM-induced lung fibrosis in mice can be spontaneously resolved, whereas patients experience irreversible lung fibrosis. Despite these limitations, the BLM model is among the most commonly used models in studies of lung injury and fibrosis. Though refined over the years, the BLM dosage used to perpetuate pathology in animals varies widely among investigators (Scotton and Chambers, 2010). The need for a varying amount of BLM even for the same strain of mice suggests that some environmental factors, such as diet and microbiome, may contribute to the susceptibility to BLM-induced lung injury.

Intratracheal BLM challenge primarily induces epithelial injury, while endothelial damage is predominant in patients with lung injury such as acute respiratory distress syndrome (ARDS) (Matute-Bello et al., 2008; Millar et al., 2016). Similarly, the incidence and prognosis of ARDS among critically ill patients are heterogenous. The development of ARDS is most often associated with respiratory infection induced-pneumonia, non-pulmonary sepsis, aspiration of gastric and/or esophageal contents, and major trauma (Matthay et al., 2019). However, the development and outcome of ARDS in patients are highly unpredictable since only a third of hospitalized COVID-19 patients develop ARDS (Tzotzos et al., 2020) and outcomes of ARDS can be 1) full recovery 2) irreversible lung damage or 3) death (Herridge et al., 2016). Understanding the factors that determine lung injury susceptibility using the BLM model could lead to improved prediction and treatment strategies for ARDS.

1.3.1 Impact of the gut microbiota on lung injury and fibrosis

Increasing evidence based on both clinical and experimental studies suggests that the gut microbiome is closely linked to many inflammatory pulmonary conditions. The term gut-lung axis refers to the microbiota-mediated crosstalk between the two organs, which is

exemplified by associations between occurrences and outcomes of inflammatory gastrointestinal diseases and pulmonary conditions (Rutten et al., 2014; Sencio et al., 2021; Yazar et al., 2001). Translocation of gut-trophic microbes to the lungs, even in the absence of systemic bacterial infection, is a risk factor for developing ARDS (Dickson et al., 2016; Panzer et al., 2018). The enrichment of lungs with enteric microbe Enterobacteriaceae has been shown to correlate with ARDS development among mechanically ventilated patients with severe trauma (Panzer et al., 2018). Furthermore, anaerobic gut commensals including Bacteroides and Enterococcus faecalis were abundantly found in lungs and correlated with survival in an experimental sepsis model (Dickson et al., 2016). Based on the above data and others (Grier et al., 2018; Madan et al., 2012), the gut and lung microbiota seem to be interconnected and to have a direct impact on health despite the two organs having different anatomical and oxygen environments.

Alternative to the gut commensal microbes having a direct impact in the lungs, the gut-lung axis may be facilitated by modulating the systemic immune response (Chiu et al., 2017). Studies have shown that some immune cells, such as Th17 cells and inflammatory neutrophils that are differentiated due to gut microbiota interactions can migrate and affect the lung health during inflammation (Felix et al., 2018; Ivanov et al., 2009). Also, specific gut microbiomes induce increased serum levels of short-chain fatty acids, which are metabolites with beneficial effects on barrier integrity (Trompette et al., 2014). However, it has been suggested that the local microbiome in the lungs, but not the gut microbiome, has more eminent impact in lung inflammation and fibrosis (Yang et al., 2019). Therefore, specific roles of the site-specific microbiota, as well as the impact of long-distance immunity, need to be further delineated.

1.4 Aims and significance

My dissertation project aims to understand immunopathology of lung injury and fibrosis in both human and animal models. The first chapter of my thesis focuses on defining the characteristics and specificity of adaptive immune responses in fibrotic ILD patients. We established that activated T cells and germinal center B cells are highly enriched in the enlarged lung-draining lymph nodes of fibrotic ILD patients, even in IPF patients. We tested a hypothesis that adaptive immune activation is driven, in part, by self-antigens expressed in the lung parenchyma. To our knowledge, our work is the first comprehensive investigation of fibrotic ILD patients' lymph node cells, as well as the first proteome-wide screening for ILD autoantigens. The use of a robust methodology and an extensive biobank enable us to identify novel antigens, as well as to define key cellular responses. As identifying antigen-specific responses can have a substantial impact on understanding the disease mechanism, this gain in knowledge can be used to improve prognosis prediction and targeted therapy development. In the second chapter, we test a hypothesis that the gut microbiota can alter immunologic responses to BLM-induced lung injury. We demonstrate that specific microbial communities have dominant negative effects on the morbidity of lung injury and identified candidate commensal species that may be responsible for such effects. This work provides a better understanding of how the microbiota composition could be a determining factor for the susceptibility and mortality outcomes of ALI, which are often unpredictable among critically-ill patients.

CHAPTER 2

MATERIALS AND METHODS

2.1 Experiments using mice

2.1.1 Animal husbandry

C57BL/6 mice were bred and maintained in two designated animal housing facilities at the University of Chicago. Both facilities were maintained at SPF barrier I level with the use of positively pressurized and individually ventilated caging with automated reverse osmosis watering system. Caging and bedding were autoclaved and changed in biological safety cabinets. Facility A mice were provided with NIH-31 Modified Open Formula (7913, Harlan-Envigo, Indianapolis, IN), and Facility B mice were provided with Teklad Global 18% Protein Rodent Diet (2918, Harlan-Envigo, Indianapolis, IN). Male age-matched germ-free C57BL/6 recipient mice were bred in the University of Chicago Gnotobiotic Research Animal Facility. All animal studies were performed in agreement with the approved IACUC Animal Care and Use Protocol.

2.1.2 Bleomycin model

Bleomycin for Injection USP (Teva Pharmaceuticals USA, Sellersville, PA) was reconstituted at 3U/mL in endotoxin-free PBS and stored at $-80°$C until use. Mice were anesthetized with intraperitoneal injection of ketamine and xylazine cocktail at 200–300mL (adjusted based on body weight), and intratracheally administered 1U/kg bleomycin in 50μL volume. Control mice received 50μL endotoxin-free PBS. Mice were monitored and weighed daily and euthanized if weight loss surpassed 25% of the original weight or if their wellness scores dropped.

2.1.3 Fecal microbiota transfer

Conventionalization of germ-free mice in SPF facilities was done by adding dirty bedding and feces from neighboring mouse cages in the respective SPF facilities, twice a week. For FMT between SPF mice, fresh fecal pellets from donor mice were suspended in 1mL of PBS per pellet (each fecal pellet weighed 60–70mg), and 0.2mL of fecal slurry from each donor was combined and passed through an 18G needle 10 times. Mice received 0.2mL of pooled fecal slurry via oral gavage, three times a week.

2.1.4 Flow cytometry analysis of mouse cells

Perfused mouse lungs were dissociated by mincing with scissors for 1 min, followed by digestion with 150U/mL Collagenase D (Gibco, Waltham, MA) and 0.02mg/mL DNase I (Worthington, Lakewood, NJ) in 10mL of DMEM (Gibco, Waltham, MA) plus 5% FCS (X&Y Cell Culture, Kansas City, MO) for 1.5h. Following digestion, cell suspensions were pipetted up-and-down for 50 times, filtered through nylon cell strainers, and washed. Samples were treated with 1mL of ACK lysis buffer for 5 min and then washed with 9mL of DMEM with 5% FBS to remove residual red blood cells.

For flow cytometry, 0.5–1$\times 10^6$ cells were suspended in 100μL of PBS and live/dead stained using Zombie Fixable Viability dye at 1:2500–5000 (BioLegend, San Diego, CA) for 20 min at RT. Cells were washed with FACS buffer (PBS with 1% BSA, 0.1% sodium azide), blocked using 10μL of 2.4G2 hybridoma supernatants (anti-CD16/32) and without washing, stained with 50μL of the surface antibody cocktail containing 10μL of brilliant stain buffer plus (BD, Franklin Lakes, NJ) for 30 min at 4°C. For all intracellular staining, cells were washed with FACS buffer twice and fixed with 50–100μL of fix/perm solution from the Foxp3/Transcription Factor Staining Buffer Set (eBioscience, Waltham, MA) for 1 hour at dark in RT. Fixed cells were washed in perm buffer from the Foxp3/Transcription Factor Staining Buffer Set twice at 350xG. The cells were blocked with 10μL of

Table 2.1: Anti-mouse antibodies used for flow cytometry

Antigen	Fluorophore	Clone	Company	Dilution Factor
CD3	BUV395	17A2	BD	200
CD4	BUV805	GK1.5	BD	200
CD44	Pacific Blue	IM7	BioLegend	400
CD8	BV510	53-6.7	BioLegend	200
CD45	BV605, BV785, BUV805	30-F11	BioLegend	200
CD62L	BV711	MWL-14	BioLegend	200
CD25	BV786	3C7	BD	100
TCRgd	APC-Fire750	GL3	BioLegend	200
Helios	FITC	22F6	BioLegend	400
RORgt	PerCP-Cy5.5	Q31-378	BD	100
EOMES	PE	Dan11mag	Invitrogen	400
T-bet	PE-Cy7	4B10	BioLegend	200
Foxp3	APC	FJK-16s	Invitrogen	400
GATA3	PE-CF594	L50-823	BD	50
NK1.1	FITC	PK136	BioLegend	400
MHC II	PerCP-Cy5.5	M5/114.15.2	BioLegend	400
Ter119	APC	TER-119	BioLegend	200
F4/80	APC-eFluor780	BM8	eBioscience	200
NKp46	BV421	29A1.4	BioLegend	50
CD11B	BV510, PE-dazzle	M1/70	BioLegend	400
Ly6C	BV605, APC-cy7	HK1.4	BioLegend	200
Ly6G	BV711	1A8	BioLegend	200
CD19	BUV737	1D3	BD	200
Siglec F	PE, BV421	E50-2440	BD	200
CD11C	PE-cy7, APC	N418	BioLegend	200
CD80	FITC	16-10A1	BioLegend	600
CD86	BV605	GL-1	BioLegend	200
PDCA1	BV650	927	BioLegend	100
PD-L1	BV785	10F.9G2	BioLegend	200
CD24	BUV396	M1/69	BD	400
CD103	PE	2E7	BioLegend	800

heat-inactivated FBS, and then stained with intracellular antibodies in perm buffer overnight at 4°C. Antibody-stained cells were analyzed on an LSRFortessa (BD, Franklin Lakes, NJ) or Aurora (Cytek, Fremont, CA), and data analysis was performed using FlowJo (BD, Franklin Lakes, NJ). Antibodies and dilution factors used for staining are listed in Table 2.1.

2.1.5 Metagenomics

Metagenomics sequencing analysis of fecal samples from unperturbed SPF mice were performed by Transnetyx (Cordova, TN). Fresh mouse fecal samples were placed in barcoded sample collection tubes containing DNA stabilization buffer and shipped to Transnetyx where DNA extraction, library preparation, sequencing, and the initial analysis were performed. Briefly, genomic DNA was extracted using DNeasy 96 PowerSoil Pro QIAcube HT extraction kit (Qiagen, Germantown, MD) and was converted into sequencing libraries using the KAPA HyperPlus library kit (Roche, Basel, Switzerland). Unique dual indexed adapters were used to ensure that reads and/or organisms were correctly assigned. After quality control, the libraries were sequenced on Illumina NovaSeq platform (Illumina, San Diego, CA) using the shotgun sequencing method (a depth of 2 million 2x150 bp read pairs), which enables species and strain level taxonomic resolution. Raw data files were uploaded onto One Codex analysis software and analyzed against the One Codex database consisting of >115K whole microbial reference genomes, assembled from both of public and private sources. Sequence alignment and taxonomy classification were achieved using the One Codex analysis software through the following three steps. First, every individual sequence (NGS read or contig) was compared against the One Codex database by exact alignment using k-mers where k=31 (Ames et al., 2013, 2014; Wood and Salzberg, 2014). Second, based on the relative frequency of unique k-mers in the sample, sequencing artifacts were filtered out of the sample. Third, the relative abundance of each microbial

species was estimated based on the depth and coverage of sequencing across every available reference genome.

2.1.6 16S rRNA gene sequencing

Sequencing of fecal samples from fecal microbiota transfer experiments was performed by the DFI Microbiome Metagenomics Platform at the University of Chicago. DNA was extracted from freshly frozen fecal pellets using the QIAamp PowerFecal Pro DNA Kit (Qiagen, Germantown, MD), and the V4–V5 region of the 16S rRNA genes were PCR amplified using barcoded dual-index primers. Illumina compatible libraries were generated using the QIASeq 1-step amplicon kit (Qiagen, Germantown, MD), and sequencing was performed on the Illumina MiSeq platform (Illumina, San Diego, CA) in the Functional Genomics Facility at University of Chicago using 2×250 paired end reads, generating 5000–10,000 reads per sample. Raw V4–V5 16S rRNA gene sequence data was demultiplexed and processed through the dada2 pipeline (Callahan et al., 2016) into Amplicon Sequence Variants (ASVs). ASVs were identified with the Bayesian RDP classifier up to the genus level and were BLASTed against RefSeq for species-level identification.

Alpha and beta-diversity analyses were performed in R using the 'phyloseq' package (McMurdie and Holmes, 2013). Alpha diversity was calculated by Shannon's diversity index (Peet, 1974). Principal coordinate analysis (PCoA) was performed based on weighted UniFrac distances (Yang et al., 2013), and permutational multivariate analysis of variance [PERMANOVA, R function adonis (vegan, 999 permutations)] was used to analyze paired statistical differences in beta diversity (Anderson, 2001). Significantly different taxa were determined using STAMP platform (Parks et al., 2014). Benjamini–Hochberg false discovery rate correction was used to correct for multiple hypothesis testing (Storey, 2002).

2.2 Experiments using human tissues

2.2.1 Collection of human lung, lymph node, and blood samples

Lung-associated lymph node cells and lung tissue sections were collected from ILD patients who underwent lung transplantation at the University of Chicago between August 2013 to December 2019. Control samples were obtained from the Illinois Gift of Hope Organ & Tissue Donor Network. Organs were processed within 48-hours of harvest. The lymph nodes were isolated from lung tissues using scissors and dissociated by filtering through a piece of Nytex mesh. Viable lymphocytes were purified through centrifuging the cells after being layered onto Histopaque-1077 medium (Sigma Aldrich, St Louis, MO) at 1750rpm for 20 min without break. The purified lymphocytes were aliquoted into cryovials and preserved using the Mr. Frosty Freezing Container (Thermo Fisher Scientific, Waltham, MA) in -80°C and stored in liquid nitrogen until use.

For histology, both freshly-frozen and formalin-fixed, paraffin-embedded (FFPE) blocks were prepared with ILD and control lung and lymph node tissues. Freshly-frozen tissue blocks were prepared by embedding a small piece of lung or lymph node tissues in optimal cutting temperature compound (OCT 4583, Fisher HealthCare, Waltham, MA) in a mold. Tissue blocks were snap froze on dry ice and stored in -80°C. For FFPE blocks, tissues were placed in individual cassettes and fixed in 10% formalin (Azer Scientific, Morgantown, PA). Fixed samples were washed in 70% ethanol and water and were embedded in paraffin wax by the Human Tissue Resource Center at University of Chicago.

Blood samples for PhIP-seq study were collected in Vacutainer Blood Collection tubes (BD, Franklin Lakes, NJ) from ILD patients during their clinic visits and at the time of transplantation. Bloods were diluted 1:1 in PBS and layered onto Histopaque-1077 medium (Sigma-Aldrich, St Louis, MO) and then spun at 1750rpm for 20 min without break. Plasma and mononuclear cells were isolated from the layers and cryopreserved in -80°C. Serum

samples from GOH organ donors were cryopreserved in −80°C. Control plasma samples were obtained from blood banks in San Fancisco and New York by the Laboratory of Dr. Joseph DeRisi.

The study is approved by the University of Chicago Institutional Review Board (IRB 14163A, IRB 14514A), and all patients included in the study signed informed consent.

2.2.2 Collection of clinical data

Diagnosis of ILD type was established at University of Chicago based on the multidisciplinary discussion of pulmonologists, dedicated chest radiologist, rheumatologists, and thoracic pathologist in concordance with the American Thoracic Society/European Respiratory Society criteria(Fischer et al., 2015; Raghu et al., 2018, 2020). From consented patients, race, ethnicity, date of birth, pulmonary function test, hospitalization records, and lymphadenopathy information were collected. Lymphadenopathy larger than 10 mm in diameter was noted in the radiology reports of high-resolution chest computerized tomography scan. Information on lymphadenopathy status and frequency and cause of hospitalization of patients that are included in this study were collected by pulmonologists through patient chart review. Patient information was de-identified and maintained with a randomly generated unique identifier specific to each subject.

2.2.3 Flow cytometry analysis of cryorecovered human cells

Cryopreserved human cells were thawed in a 37°C water bath with constant swirling just until some ice crystals float on top. Cells were resuspended in 4mL of HBSS (Gibco, Waltham, MA) containing 2% FBS (X&Y Cell Culture, Kansas City, MO) and 10μg/mL DNAse (Worthington, Lakewood, NJ) in a 15mL tube and layered on top of 3mL of histopaque-1077 (Sigma-Aldrich, St Louis, MO). After spinning at 1750rpm for 20min without break, live lymphocytes were collected from the interphase and washed once with

RPMI (Gibco, Waltham, MA) containing 2% FBS.

For antibody staining, 0.5–1.0x10^6 cells from each sample were aliquoted into 5mL round bottom tubes or 96-well U-bottom plates. Cells were washed with PBS and stained for viability using Zombie NIR Fixable Viability stain (1:2500, BioLegend, San Diego, CA) in PBS for 20 min at room temperature in dark. Cells were washed with FACS buffer, blocked with Human TrueStain FcX (1:200, BioLegend), and immediately stained with the surface antibody cocktail in FACS buffer for 30 min at 4°C in dark. All antibodies and dilutions used for staining are listed in Table 2.2 and Table 2.3. For intracellular staining, cells were fixed and permeabilized using the Foxp3/Transcription Factor Staining Buffer Set (eBioscience, Waltham, MA) as described in section 2.1.4. After staining, the cells were washed twice with perm buffer, once with FACS buffer, and resuspended in FACS buffer for analysis. Antibody-stained cells were analyzed on Cytek Aurora (Cytek Biosciences, Fremont, CA). For spectral unmixing, two sets of single stained controls were prepared using cells and UltraComp eBeads (Invitrogen, Waltham, MA) each. During analysis, single stained cells were used to perform initial spectral unmixing, and some controls were swapped with single stained beads as needed based on quality check on SpectroFlo (Cytek Biosciences, Fremont, CA).

2.2.4 Computational analysis of flow cytometry data

FlowJo (BD, Franklin Lakes, NJ) was used for compensation, conventional gating analysis, dimensionality reduction analysis (UMAP), and exporting specific cellular subsets. After importing the data files into FlowJo, fluorescence spillover in each channel was compensated by manually editing the compensation matrix based on single stained controls. Immune cell populations were quantified by using conventional gating strategies as summarized in Table 2.5. Frequencies of immune cell populations were exported for statistical analysis. For UMAP analysis, an equal number of cells was selected from every sample using the DownSample

Table 2.2: Flow cytometry panel for human T cell analysis

Antigen	Fluorophore	Clone	Company	Dilution Factor
PD1	BV421	MIH4	BD	25
CD19	BUV395	HIB19	BD	100
CD38	eFluor450	HIT2	Invitrogen	100
CD3	BV480	UCHT1	BD	100
CD45RA	BV510	HI100	Biolegend	400
CD8	BV570	RPA-T8	Biolegend	100
Va7.2	BV605	3C10	Biolegend	50
CD127	BV750	HIL-7R-M2	BD	100
HLA-DR	BV785	L243	Biolegend	200
CD25	BB515	2A3	BD	200
CCR7	AF488	G043H7	Biolegend	50
ICOS	PerCP-Cy5.5	C398.4A	Biolegend	200
CD1d PBS-57	PE	-	NIH tetramer facility	200
CD137	PE-Cy5	4B4-1	Biolegend	100
Vd1	PE-Cy7	TS8.2	Invitrogen	50
Vd2	PE-Cy7	B6	Biolegend	100
CD4	AF700	OKT4	Biolegend	200
BCL6	APC-Cy7	K112-91	BD	2500
RORgt	BV650	Q21-559	BD	50
GATA3	BV711	L50-823	BD	200
CD154	APC	24-31	Biolegend	50
FOXP3	AF647	206D	Biolegend	50
Zombie	NIR	-	BIolegend	2500

Table 2.3: Flow cytometry panel for human B cell analysis

Antigen	Fluorophore	Clone	Company	Dilution Factor
CD3	PE-Cy5	HIT3a	BD	200
HLA-DR	APC-Fire 750	L243	Biolegend	333
CD10	BV711	HI10a	Biolegend	100
CD14	BUV395	MΦP9	BD	100
CD16	BV650	3G8	Biolegend	333
CD19	PE-Cy7	HIB19	Biolegend	200
CD20	eFluor450	2H7	Invitrogen	100
CD24	BV510	ML5	Biolegend	200
CD27	APC-R700	M-T271	BD	100
CD38	APC	HIT2	Biolegend	100
CD44	AF488	BJ18	Biolegend	1000
CD116	BV421	hGMCSFR-M1	BD	333
CD138	PE-Dazzle	MI15	Biolegend	50
IgD	PerCP-Cy5.5	IA6-2	BD	100
IgM	BV785	MHM-88	Biolegend	333
ILT3	AF647	ZM4.1	BIolegend	333
ILT5	PE	MKT5.1	Biolegend	333
CD71	BUV805	L01.1	BD	100
CXCR4	BUV737	12G5	BD	3333
CD172	BV750	SE5A5	BD	333
CD11C	BUV661	B-ly6	BD	333
CD1C	BV605	F10/21A3	BD	333
CD26	BV480	L272	BD	100
Zombie	NIR	-	BIolegend	2500

plugin (FlowJo Exchange) and concatenated into a single data file. UMAP was generated using the UMAP plugin (FlowJo Exchange) and cluster analysis was performed using the FlowSOM plugin (FlowJo Exchange). The resulting FlowSOM clusters were projected onto UMAP for visualization and cellular frequencies exported using FlowJo functions.

For more multidimensional analysis and regression analysis, compensated channel values of specific cell populations from every sample were exported in csv format and analyzed using R. Principal component analysis (PCA) of flow cytometry data was performed using the prcomp function in R 4.1.2. PCA was performed separately for each experimental batch, and the statistical analysis of the median fluorescence intensity (MFI) of each parameter was performed with samples from all batches together. The batch effect was corrected by including batch terms when performing statistical tests using generalized linear models. R packges 'dplyr' and 'tidyverse' were used for data-wrangling, and 'ggplot2', 'ggpubr', 'ggrepel' and 'introdataviz' were used for generating graphs. For heatmap visualization, population frequencies were z-scored, separately in each experimental batch, using the scale function in R. The z-scored cellular frequencies from every batch was combined, and a heatmap was generated using the 'ComplexHeatmap' package in R.

2.2.5 Immunofluorescence staining of lung sections

Freshly frozen tissue blocks were cut into 8μm-thin slices to prepare serial tissue slides. Tissue sections were fixed with 4% PFA for 10 min, permeabilized with 0.1% NP-40 for 10 min, quenched with freshly made 0.1mg/ml NaBH4 for 5 min, and blocked with 10% normal donkey serum and Human TrueStain FcX (1:200, Biolegend 422302) for 30 min. Tissues were stained with primary antibodies for overnight at 4°C using rabbit anti-human ABLIM1 (1:200, Proteintech 15129-1-AP) and mouse anti-human cytokeratin 17 (1:100, Invitrogen MA 1-06325) diluted in PBS with 5% normal donkey serum. Tissues were washed and stained with the secondary antibodies: Alexa Fluor 647-donkey anti-rabbit (1:1000,

Invitrogen A31573) and Alexa Fluor 568-donkey anti-mouse (1:1000, Invitrogen A10037), in PBS with 5% normal donkey serum for 1 hour at room temperature. After washing, the sections were blocked with 10% mouse serum for 30 min, and then stained using a directly conjugated Alexa Fluor 488-anti-alpha-smooth muscle actin monoclonal antibody (1:250, Invitrogen 53-9760-82) for 2 hours at room temperature. The slides were washed and nuclear stained with Hoechst 33342 (1:1000, Invitrogen H3570) for 30 min. Finally, the slides were mounted with ProLong Gold Antifade Mountant (Invitrogen P36934) and cured for 24 hours at room temperature. For every sample, an adjacent section was stained with only secondary antibodies as a control. Slides were imaged by the University of Chicago Integrated Light Microscopy Core. Olympus VS200 Slideview Research Slide Scanner with a 40X objective was used to capture images. The images were analyzed using QuPath (https://qupath.github.io/) (Bankhead et al., 2017) and ImageJ (https://imagej.nih.gov/ij/) (Schneider et al., 2012).

2.2.6 Phage Immunoprecipitation-sequencing

Phage Immunoprecipitation-sequencing (PhIP-seq) was performed as previously described to screen circulating patient antibodies against approximately 700,000 different linear peptide segments, each at 49 amino acid length, spanning the entire human proteome (Vazquez et al., 2020b; O'Donovan et al., 2020; Larman et al., 2011b). Plasma or serum samples of ILD patients, rheumatoid arthritis patients, and individuals with no lung disease were aliquoted into 96-well plates and shipped on dry ice to the laboratory of Dr. Joseph DeRisi at UCSF, where PhIP-seq was performed. Another cohort of ILD sera (from the laboratory of Dr. Anthony Shum, UCSF) were sequenced and analyzed simultaneously. Briefly, the plasma/sera were incubated with phage library, and the phages recognized by plasma antibodies were immunoprecipitated using protein A/G beads, PCR amplified, and next-generation sequenced. For negative control for immunoprecipitation, phages were

mock immunoprocipitated using only protein A/G beads and included for sequencing. Non-diseased control sera included in the screening were sourced from New York blood bank and were provided by the laboratory of Dr. Joseph DeRisi. From the next-generation sequencing of immunoprecipitated phage genes, only sequencing reads with >100,000 counts were included in the downstream analysis. Patient antibody-bound peptide sequence counts were quantified as fold change (FC) over mock immunoprecipitated (A/G beads only, no serum) sequence counts. At this level to control for noise, we only considered sequences with greater than 10 FC over beads only controls. Next, to distinguish disease-relevant antigens, we normalized the FC values against the mean FC value of non-diseased controls for each given peptide sequence as z-scores. We used a z-score threshold at >50 to identify antigens that are strongly enriched in ILD patients over non-diseased controls. Finally, peptide sequences were aligned to genes, and antigenic genes that are positive in at least 2 ILD individuals but none in non-diseased controls were defined as shared ILD antigens.

2.2.7 Radioligand binding assay

The following cDNA sequences were selected for cloning: ABLIM1 isoform j (NM_001322888), CDHR5 isoform X2 (XM_011520188), and GIMAP1 (NM_130759), based on results of blasting all epitope sequences identified from PhIP-seq against all known splicing isoforms for each antigenic gene. Full length cDNA sequences led by the Kozak sequence (GCCACC) were cloned into pTNT vector (Promega L5610), and the constructs were validated using Sanger sequencing. Using the rabbit reticulocyte lysate system (Promega TNT Quick Coupled Transcription/Translation System), proteins were translated under the control of T7 promoter with 35S labels *in vitro*. Proteins were purified by passing through Nap-5 column (GE 17-0853-01) and quantified using the MicroBeta Trilux liquid scintillation counter (PerkinElmer). Translation of the full length proteins

were confirmed based on size after running on SDS-PAGE gels.

To quantify binding of patient antibodies to radiolabeled protein antigens, 5μL of plasma or serum samples were incubated with 5,000 – 20,000 counts of proteins for overnight. On the next day, the antibody complex was immunoprecipitated using protein A/G agarose beads at 4:1 A to G ratio (GE Healthcare) on 96-well plates with PVDF filter membrane. After washing the plate for 4 times using a vacuum apparatus and air drying for 30 min, the ionizing radiation from immunoprecipitated antibody-ligand complex was quantified using the scintillation counter. Every plate included A/G beads only negative controls and commercial antibody positive controls in triplicates. Commercial antibodies used as positive controls are anti-CDHR5 (Invitrogen PA5-89483), anti-GIMAP1 (Novus Biologicals, NBP159488), and anti-ABLIM1 (Novus Biologicals NBP198472).

The antibody index for each antigen for each plasma sample was calculated using the following formula.

$$\text{Antibody Index} = \frac{\text{sample value} - \text{mean}_{\text{ negative control}}}{\text{mean}_{\text{ positive control}} - \text{mean}_{\text{ negative control}}}$$

A samples was considered positive for having autoantibodies against an antigen if the antibody index was at 3 standard deviations above the mean antibody index of non-diseased controls for a given antigen.

2.2.8 Statistics

Statistical comparisons of specific cellular frequencies between disease groups and controls were achieved by non parametric Mann Whitney Wilcoxon Test and also by one-way ANOVA where there were three groups.

To test associations between having an ILD and immune protein expressions (MFI from flow cytometry data), a binomial logistic regression analysis was performed for each flow

parameter using the glm() function in R, where:

$$\text{disease state} = \beta_0 + \beta_1 * \text{MFI} + \beta_2 * \text{batch}$$

Likelihood ratio test (LRT) for β_1 was performed to test the significance of MFI of each flow parameter, and p-values were adjusted using Benjamini-Hochberg (BH) method using the p.adjust() function in R.

To test relationships between having an ILD and the enrichment of immune cell populations in LLN , a generalized linear model for each population was built with a Gaussian distribution, where:

$$ln(\frac{\text{cell frequency}}{1 - \text{cell frequency}}) = \beta_0 + \beta_1 * \text{disease state} + \beta_2 * \text{batch}$$

The p-value for β_1 was calculated by LRT and adjusted for multiple testing by BH method.

To test whether the enrichment of germinal center B cells in LLN is associated with changes in pulmonary function over time, a mixed effects model was built using STATA (StataCorp, College Station, TX). The status of germinal center B cell enrichment in each patient was converted into a binary response (GCB status: yes or no) using a cutoff of 1% of live cells in LLN. Longitudinally collected forced vital capacity (FVC) from ILD patients was used as a pulmonary function measurement. The amount of time between each pulmonary function test was calculated in years and included in the model, where:

$$E[\text{FVC}|\text{GCB status, year}] = \beta_0 + \beta_1 * \text{GCB status} + \beta_2 * \text{year} + \beta_3 * \text{GCB status * year}$$

The coefficient and p-value for the interaction term between GCB status and year were reported to determine how much FVC change per year differs between GCB-positive and GCB-negative patients.

Simple linear regressions were performed to test relationships between the antibody index against ABLIM1 and immune cell proportions in LLN. The Goodness of fit (R-squared value) and p-value were obtained using GraphPad Prism (GraphPad Softwares, San Diego, CA).

CHAPTER 3

RESULTS

3.1 Antigenic responses are hallmarks of fibrotic interstitial lung diseases independent of underlying etiologies

3.1.1 Abstract

Interstitial lung diseases (ILD) are heterogeneous conditions that lead to progressive fibrosis, which can result in death. Despite diversity in clinical manifestations, enlargement of lung-associated lymph nodes (LLN) in all fibrotic ILD patients predicts worse survival. Herein, we revealed a common adaptive immune landscape in LLNs of all ILD patients including idiopathic pulmonary fibrosis (IPF), characterized by highly activated germinal centers and antigen-activated T cells. T regulatory cells (Tregs) expanded in ILD LLN and had an aberrant phenotype similar to phenotypes seen in some autoimmune diseases. Proteome-wide screening, using phage immunoprecipitation sequencing, identified reactivity to 17 novel auto-antigens in ILD patients' sera. Autoantibody response to ABLIM1, an actin-binding protein highly expressed in aberrant basaloid cells of fibrotic lungs, correlated with LLN frequencies of T follicular helper cells and Tregs in ILD patients. Together, we demonstrate that end-stage ILD patients have converging adaptive immune mechanisms that may contribute to the disease.

3.1.2 Introduction

Fibrotic interstitial lung disease (ILD) is a heterogeneous group of conditions characterized by inflammation and scarring of the lung parenchyma. Current diagnosis and treatment strategies for ILD subtypes are largely based on the underlying etiology. The most common type of ILD is idiopathic pulmonary fibrosis (IPF). IPF is diagnosed based on the

presence of a specific radiologic pattern, usual interstitial pneumonia, in the absence of an identifiable underlying cause (Raghu et al., 2022). In addition to IPF, several other ILDs including hypersensitivity pneumonitis (HP) and connective tissue disease ILD (CTD-ILD) can also progress to pulmonary fibrosis (Kern et al., 2015; Yusen et al., 2014). HP is clearly driven by inflammatory responses against inhaled environmental antigens, such as molds and bird droppings (Raghu et al., 2020). However, other pulmonary fibrosis patients have either underlying CTD-ILD (Vij and Strek, 2013) or features of autoimmunity, including serum autoantibodies, without meeting the full diagnostic criteria for an autoimmune disease (Ghang et al., 2019; Oldham et al., 2016). Immunosuppressants are commonly used to improve symptoms and disease progression in HP and other immune-associated ILD patients. In contrast, broadly suppressing the immune system in IPF patients has been ineffective at improving patient outcomes, and instead increased the risk for hospitalization and death (Idiopathic Pulmonary Fibrosis Clinical Research et al., 2012). As a result, the prevailing mechanistic paradigm is that IPF is driven by epithelial dysfunction, while HP and CTD-ILD are proposed to be driven by immune mechanisms (Wolters et al., 2018).

While the immune system may not be the primary driver of IPF, there is growing evidence of abnormal immune activation in fibrotic ILDs. For example, many immune-associated receptors and ligands have been identified as biomarkers for IPF (DePianto et al., 2015; Herazo-Maya et al., 2013; Parra et al., 2007; Vuga et al., 2014), and activated T cells and B cells in IPF patient lungs correlate with patient survival (Marchal-Somme et al., 2006; Todd et al., 2013). Furthermore, the enlargement of lung-draining lymph nodes (LLN) is prevalent and predicts survival outcomes in all ILD patients, including IPF (Adegunsoye et al., 2019). As lymph nodes are structures where adaptive immune cells are recruited and proliferated in response to antigens from the tissues, the association between LLN size and patient survival suggest that the adaptive immune response could contribute to the pathophysiology of IPF. This idea is supported by findings that compared to healthy controls, IPF patients have

higher levels of circulating autoantibodies (Heukels et al., 2019) that are reactive to various proteins in cellular extracts (Feghali-Bostwick et al., 2007). While efforts at characterizing patients with autoantibodies and no defined CTD-ILD are ongoing (Fischer et al., 2015), the extent of autoantibody specificities and their functional implications in fibrotic ILD are incompletely understood. Thus, determining specific immune pathways that impact disease progression and the antigenic specificity of the response are critical for developing mechanistic understanding of pathology and effective therapeutic strategies for IPF and other fibrotic ILD.

To understand the complexity of immune responses in fibrotic ILD, we investigated phenotypes of adaptive immune cells in LLNs isolated from explanted lungs of end-stage ILD patients and age-matched controls. We hypothesized that the immune response in IPF LLNs is distinct from immune-mediated ILD patients and that there are autoantigen responses driving immune activation. To test this hypothesis, we first investigated cellular composition and phenotypes of LLN cells by flow cytometry. Strong immune activation profiles that are consistent with antigen-stimulation of T cells and germinal centers (GC) were identified across all ILD LLN, including IPF. Furthermore, Tregs were elevated and had unique phenotypes in ILD LLNs compared to controls, suggesting that failure to control antigen responses in ILD is potentially due to Treg dysregulation. To identify antigens that drive immune activation in ILD, we employed a human peptidome phage library to screen patients' serum antibodies against autoantigens. We discovered 17 novel autoantigens that are shared among ILD patients regardless of subtypes. Strikingly, many ILD patients have circulating antibodies against ABLIM1, an actin-binding protein that is specifically upregulated in structural cells of the fibrotic lungs, suggesting a common antigenic stimulation in fibrotic ILD patients. Thus, we demonstrate that all ILD patients' enlarged lymph nodes contained evidence of antigen-induced activation that was dysregulated, and we identified a novel autoantigen that could be a part of common

immunopathology in pulmonary fibrosis.

3.1.3 Results

Distinct T cell and B cell landscapes in fibrotic ILD lung lymph nodes compared to age-matched controls

To investigate the enlarged lung lymph nodes in ILD patients, we conducted comprehensive profiling of adaptive immune cells in biobanked LLN from end-stage fibrotic ILD patients and organ donors who were free of known lung disease. For this study, groups were matched for age (median ages of 63 and 60) and sex (72% and 67% male) for ILD and controls, respectively (Table 3.1). ILD subtype was determined via multidisciplinary diagnosis using ATS/ERS criteria (Fischer et al., 2015; Raghu et al., 2018, 2020). Idiopathic pulmonary fibrosis (IPF: n=30) was most prevalent in our study cohort, followed by interstitial pneumonia with autoimmune features (IPAF: n=7), connective tissue disease-associated ILD (CTD-ILD: n=5), hypersensitivity pneumonitis (HP: n=4), and other ILDs (n=4). In the CTD-ILD group, 3 patients had rheumatoid arthritis (RA), 1 patient had anti-synthetase syndrome, and 1 patient had anti-neutrophil cytoplasmic antibody-associated ILD. The other ILD group included patients with short telomeres, pleuroparenchymal fibroelastosis, and unclassifiable ILD.

We designed two antibody panels for spectral flow cytometry to investigate compositions and phenotypes of T cells and B cells. Due to the large number of samples, the flow cytometry was performed in 4 batches on different days. Batches 1-3 consisted of ILD samples with age matched controls, and batch 4 consisted of ILD samples only (IPF and HP). We found that ILD patients and control donors had similar levels of total T cell enrichment in their LLN (Figure 3.1a,b). However, principal component analysis (PCA) using 19 T cell markers revealed a clear separation between ILD and control groups,

Table 3.1: Demographics of the explanted LLN flow study cohort

		ILD (n=50)	**Control** (n=36)
Sex, n (%)	Male	36 (72%)	24 (67%)
	Female	14 (28%)	12 (33%)
Age, median (range)		63 (43 – 72)	60 (44 – 76)
Race, n (%)	African American	6 (12%)	8 (22%)
	Asian	2 (4%)	
	Caucasian	36 (72%)	26 (72%)
	Hispanic	1 (2%)	2 (6%)
	Other	1 (2%)	
	Unknown	4 (8%)	
Diagnosis, n (%)	IPF	30 (60%)	
	IPAF	7 (14%)	
	CTD-ILD	5 (10%)	
	HP	4 (8%)	
	Other ILD	4 (8%)	

consistently across batches (Figure 3.1c-e). To investigate which markers are associated with the distinct T cell phenotypes, we performed logistic regression analyses across all samples, with adjustments for batch effects, and found that expression of 11 markers were significantly different between ILD and control groups (Figure 3.1f, Figure 3.2a). Interestingly, a costimulatory molecule CD154 (CD40L), and a regulatory T cell (Treg) marker FOXP3, were among the most significantly associated and highly expressed markers in ILD patient T cells. Other markers that are associated with activation (HLA-DR and ICOS) and Th2-lineage determining transcription factor GATA3 were also upregulated in ILD T cells. In contrast, significantly lower CCR7 expression in ILD LLN T cells suggested that these T cells are poised to exit lymph nodes traffic to the lungs. Expressions of cytokine receptors, CD25 (IL-2R) and CD127 (IL-7R), were also

downregulated in ILD T cells. To visualize protein expression patterns at the cellular level, we performed a uniform manifold approximation and projection (UMAP) with T cells from batch 1 (Figure 3.2b,c). We found that CD154 and FOXP3 were not co-expressed, while FOXP3-high cells also expressed CD25, ICOS, HLA-DR, and CD137 (Figure 3.2c). Furthermore, some ICOS-positive cells co-expressed PD1 and BCL6, which are consistent with the follicular helper T cell (Tfh) phenotype. Overall, these data suggest that T cells in ILD LLNs have unique phenotypes compared to controls.

Similar to T cells, there was no significant difference in the frequency of total B cells in the LLN between ILD and controls (Figure 3.1g,h). PCA analysis of B cells based on 12 parameters demonstrated that distinct B cell phenotypes exist in ILD LLNs compared to controls (Figure 3.1i-k). Based on regression models, we found 5 B cell markers are significantly associated with ILD (Figure 3.1l, Figure 3.2d). Expression of CXCR4 was the most significant association and also was the only marker downregulated in ILD patients. Other markers upregulated in ILD patients included HLA-DR, CD10, IgD, and CD1c. UMAP analysis of the B cells revealed differential islands of cells between the two groups (Figure 3.2e,f). CD10 expression was confined to one region where there was high expression for CD38, which is known to be highly expressed on germinal center (GC) B cells and plasma cells in LN (Figure 3.2f). These data indicate that B cells also have distinct phenotypes in ILD patients compared to controls.

Effector T cells and Tregs display activated phenotypes in fibrotic ILD LLN

To interrogate which T cell subsets are driving the ILD phenotype, we analyzed CD4 and CD8 T cells separately. We found no difference in frequencies of total CD4 T cells (Figure 3.3a) and CD8 T cells (Figure 3.3b), but interestingly there was a significantly higher ratio of CD4 T cells to CD8 T cells (Figure 3.3c). The expression of several markers including HLA-

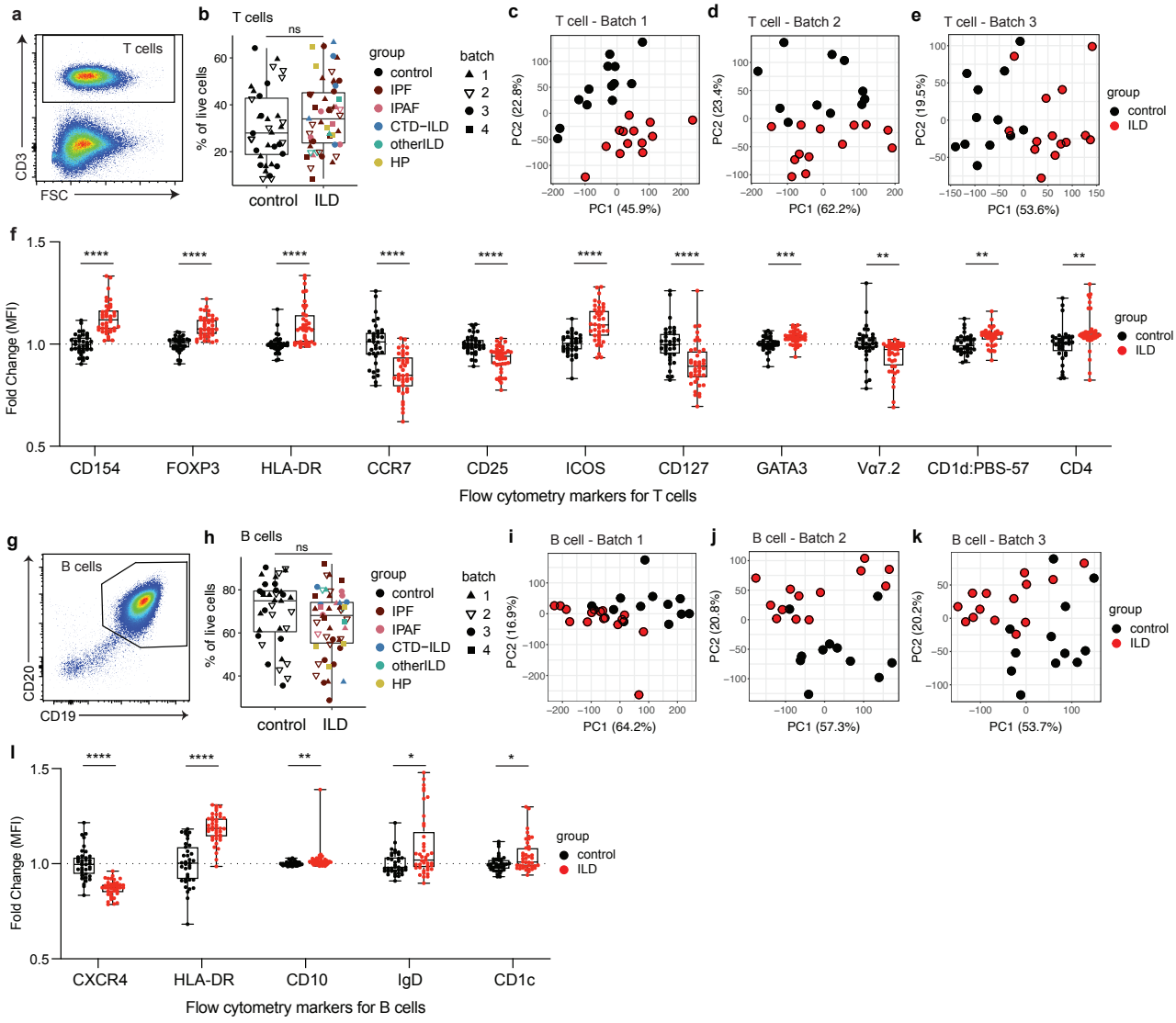

Figure 3.1: Distinct T cell and B cell landscapes in LLNs from ILD patients compared with matched controls. a. Representative flow cytometry gating for the total T cells in LLNs. Cells were pre-gated on live cells. **b.** Frequencies of T cells in live cells in control vs ILD LLNs. Statistical significance was tested by the Wilcoxon rank sum test. **c-e.** PCA of total T cells based on fluorescence intensities of 19 parameters: CD154, FOXP3, HLA-DR, CCR7, CD25, ICOS, CD127, GATA3, Vα7.2, PBS-57 loaded CD1d tetramer, CD4, CD8, Vδ, PD1, RORγt, BCL6, CD38, CD45RA and CD137. An analysis was run with 10,000 cells, 8,000 cells, and 10,000 cells for batch1, batch2, and batch 3, respectively.

Figure 3.1: continued. **f.** Box plots comparing the median fluorescence intensity of individual T cell markers between ILD and controls, based on all samples in batches 1-3. Fold change was calculated relative to the mean values of control samples, separately for each batch. Parameters that are significantly associated with ILD based on a likelihood-ratio test on each logistic regression coefficient are shown. Non-significant parameters are shown in Figure 3.2. P-values were adjusted by Benjamini-Hochberg correction. **g.** Representative flow cytometry gating for B cells in LLNs. Cells were pre-gated on live cells. **h.** Frequencies of B cells in live cells in control vs ILD LLNs. Statistical significance was tested by the Wilcoxon rank sum test. **i-k.** PCA of B cells based on fluorescence intensities of 12 parameters: CXCR4, HLA-DR, CD10, IgD, CD1c, CD44, CD138, CD11C, CD24, CD27, CD38, IgM. An analysis was run with 10,000 cells for each batch, separately. **l.** Box plots comparing the median fluorescence intensity of individual B cell markers between ILD and controls, based on all samples in batches 1-3. Calculations of fold changes and adjusted p-values were done as described above (f). $P<0.05$ (*), $P<0.01$ (**), $P<0.001$ (***), $P<0.0001$ (****).

DR on CD8 T cells were associated with ILD (Figure 3.3d-h). For CD4 T cells, we analyzed CD4 T conventional cells (Tcon) (Figure 3.4a-f) and Tregs (Figure 3.4g-l) separately since these two populations play opposite roles in immune response. Interestingly, PCA of CD4 Tcon cell phenotypes distinguished ILD patients from controls (Fig 2c-e), and ILD patients showed higher expression of activation markers CD154, HLA-DR, and ICOS on Tcon cells (Figure 3.4f, Figure 3.3i). Unlike Tcon and CD8 T cell populations in LLN, Treg proportions were elevated in ILD LLNs compared to controls (Figure 3.4g,h). As recent studies showed that Tregs can express a variety of effector transcription factors and activation markers that identify their function, we performed PCA and found that Tregs from the LLN of ILD patients have phenotypes that are distinct from control LLNs (Figure 3.4i-k). Intriguingly, expression of 7 markers were associated with ILD, five of which are activation markers such as PD1, HLA-DR, CD137, ICOS and CD154 (Figure 3.4l, Figure 3.3j). Surprisingly, CD25 was the most significantly associated with ILD and was downregulated in ILD patients' LLN compared to controls. These findings indicate that effector T cells and Tregs accumulate in ILD LLNs at end-stage disease, have distinct phenotypes, and therefore may have different functional roles compared to non-diseased organ donors.

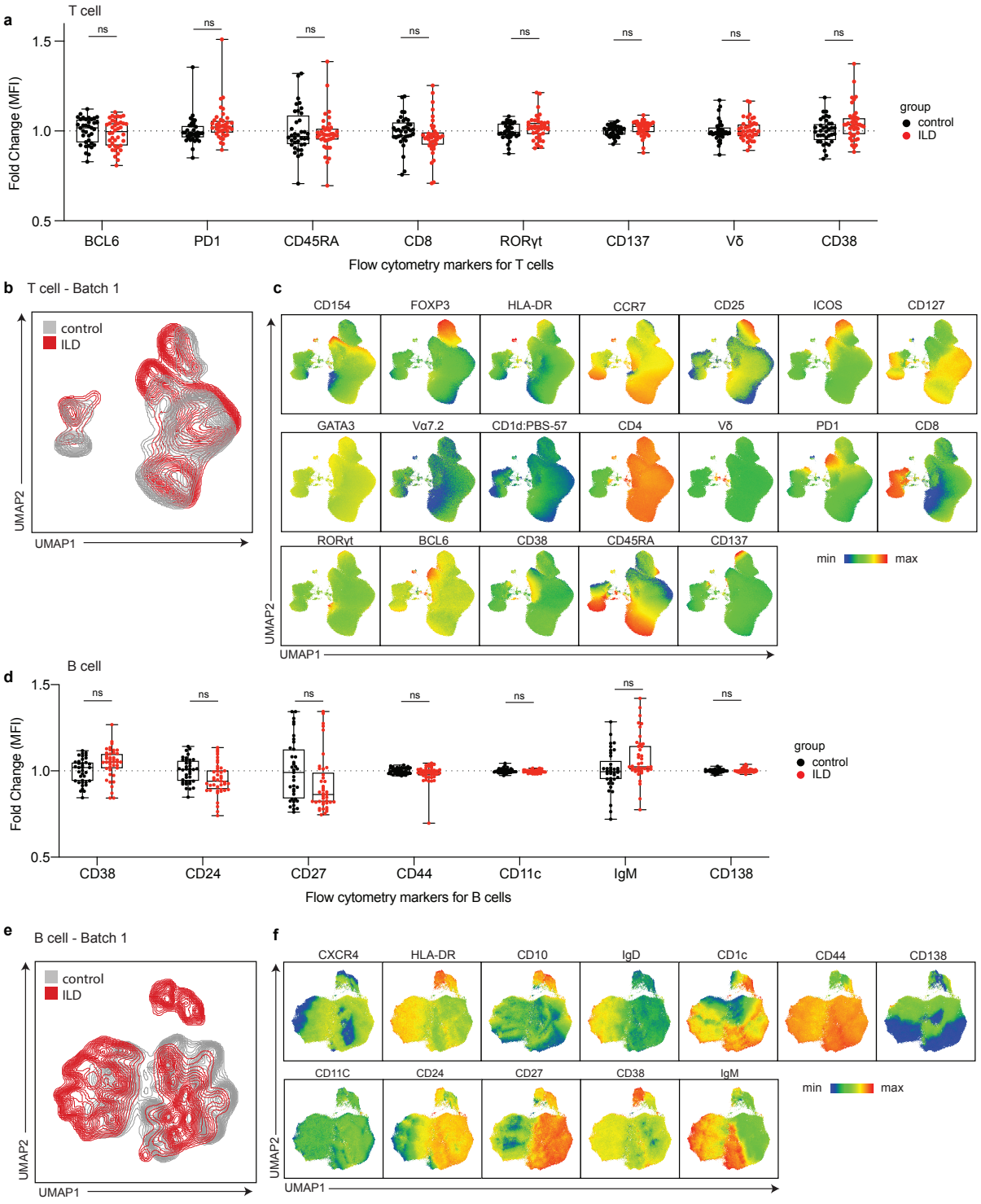

Figure 3.2: Expression of T cell and B cell markers in explanted LLNs from ILD patients and controls.

Figure 3.2: continued. **a.** Box plots comparing the median fluorescence intensity of individual T cell markers between ILD and controls, based on all samples in batches 1-3. Fold change was calculated relative to the mean values of control samples, separately for each batch. **b.** Representative UMAP of T cells. Each group (control vs ILD) contains 130,000 T cells concatenated from 13 individuals (10,000 cells per individual) in batch 1. **c.** Fluorescence intensity of each T cell parameter overlayed on the UMAP plot. **d.** Box plots comparing the median fluorescence intensity of individual B cell markers between ILD and controls, based on all samples in batches 1-3. Fold change was calculated relative to the mean values of control samples, separately for each batch. **e.** Representative UMAP of B cells. Each group (control vs ILD) contains 130,000 B cells concatenated from 13 individuals (10,000 cells per individual) in batch 1. **f.** Fluorescence intensity of each B cell parameter overlayed on the UMAP plot.

Adaptive immune activation signatures define the ILD lymph node landscape

Using conventional flow cytometry gating, we identified and quantified a total of 39 unique T cell and B cell populations in LLNs (Figure 3.5, Figure 3.6). Hierarchical clustering based on frequencies of individual immune cell populations demonstrated that almost all ILD samples are clustered away from controls, suggesting specific immune cells are correlated with ILD (Figure 3.7). Statistical comparisons of cellular abundance between ILD and control LLNs determined that 25 cell populations were differentially enriched between the two groups (Figure 3.8a). Immune populations upregulated in ILD LLNs with greatest significance were Tcon cells expressing co-stimulatory molecules CD154, ICOS, and PD1. Consistent with immune activation, T cells with effector and memory phenotypes were more abundant in ILD LLNs. Furthermore, robust enrichment of Tfh cells, follicular regulatory T cells (Tfr), and GC B cells indicate activated germinal center response in ILD LLN. Also, Tregs and $CD25^{low}$ subset of Tregs were highly enriched in ILD LLN. Only 4 populations were downregulated in ILD LLNs, and these include central memory CD4 T cells, naïve CD8 T cells, switched memory B cells and Th2 cells. These data suggest that expansion of effector memory T cell proportions was at the expense of central memory and naïve T cells, and

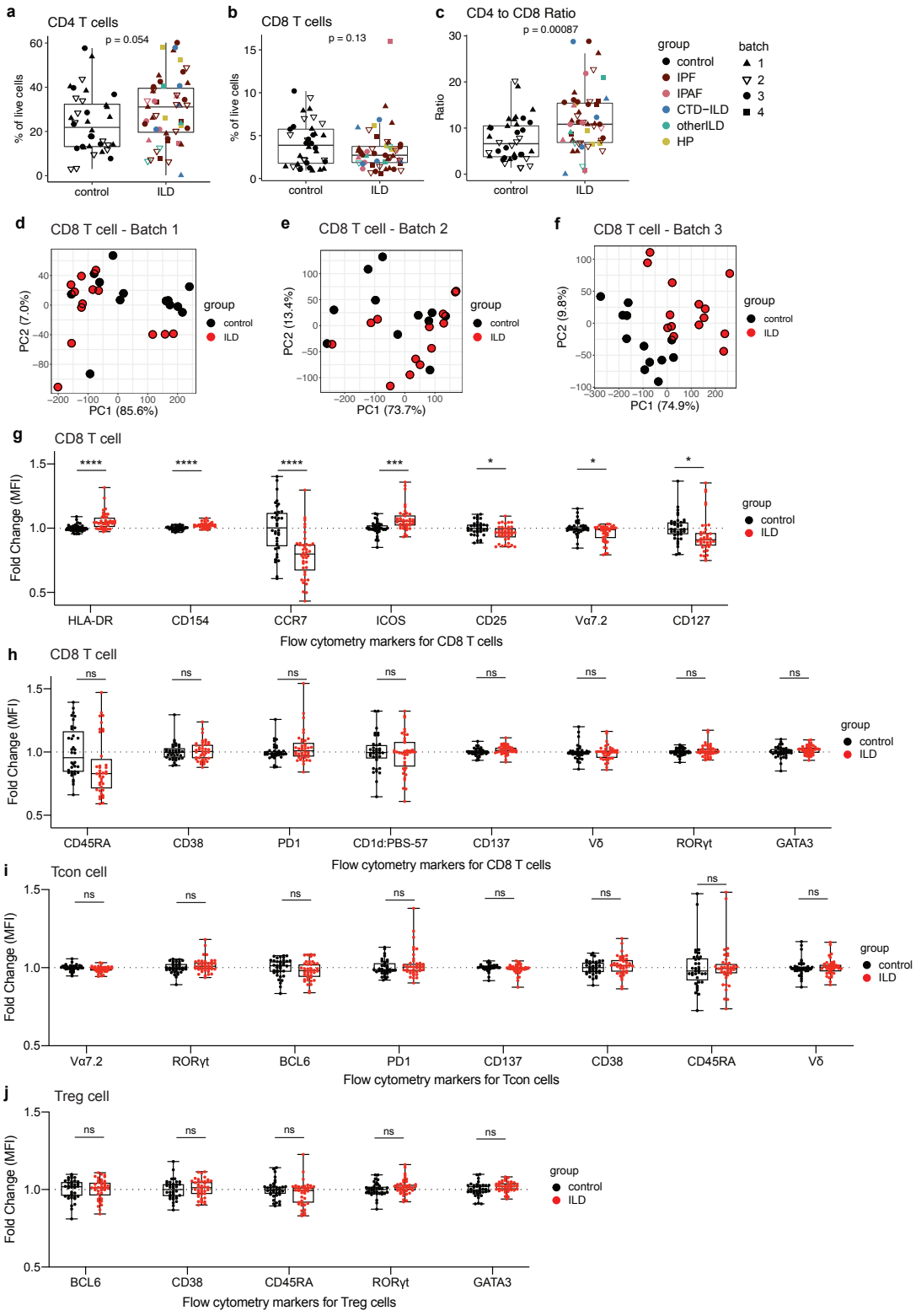

Figure 3.3: T cell subpopulations in LLNs from ILD patients compared with matched controls.

Figure 3.3: continued. **a.** Comparison of CD4 T cell frequencies between control and ILD LLNs. **b.** Comparison of CD8 T cell frequencies between control and ILD LLNs. **c.** Comparison of CD4 to CD8 T cell ratio between control and ILD LLNs. **d-f.** PCA of CD8 T cells based on fluorescence intensities of 15 parameters: CD154, HLA-DR, CCR7, CD25, ICOS, CD127, GATA3, Vα7.2, PBS-57 loaded CD1d tetramer, Vδ, PD1, RORγt, CD38, CD45RA and CD137. An analysis was run with 1,600 cells, 669 cells, and 1,100 cells for batch1, batch2, and batch 3, respectively. **g-h** Box plots comparing the median fluorescence intensity of individual CD8 T cell markers between ILD and controls, based on all samples in batches 1-3. **i.** Box plots comparing the median fluorescence intensity of individual Tcon markers between ILD and controls, based on all samples in batches 1-3. **j.** Box plots comparing the median fluorescence intensity of individual Treg markers between ILD and controls, based on all samples in batches 1-3. For all split violin plots, fold change was calculated relative to the mean values of control samples, separately for each batch. Parameters that are significantly associated with ILD based on a likelihood-ratio test on each logistic regression coefficient are shown. P-values were adjusted by Benjamini-Hochberg correction.

such phenomenon can support a hypothesis that there are ongoing immune responses in the lymph nodes of ILD patients.

T cell phenotypes are associated with clinical phenotypes

Given that the enlargement of LLNs at diagnosis is correlated with survival outcomes (Adegunsoye et al., 2019), we next investigated whether the presence of lymphadenopathy at the time of diagnosis was associated with accumulation of any specific adaptive immune cell types in LLNs at end-stage disease. Surprisingly, we found that naïve T cells, both CD4 and CD8 cells, are more abundant in LLNs of ILD patients who presented at diagnosis with lymphadenopathy compared to patients who did not have enlarged lymph nodes (Figure 3.8b,c). Increase in naïve T cells in enlarged LLN were accompanied by a decrease in PD1 expression on T cells, which is a marker of activation and exhaustion (McLane et al., 2019) (Figure 3.8d,e). Furthermore, another activation phenotype, which is the co-expression of HLA-DR and CD38, was lower in ILD patients who presented with lymphadenopathy compared to patients who did not have enlarged lymph nodes (Figure

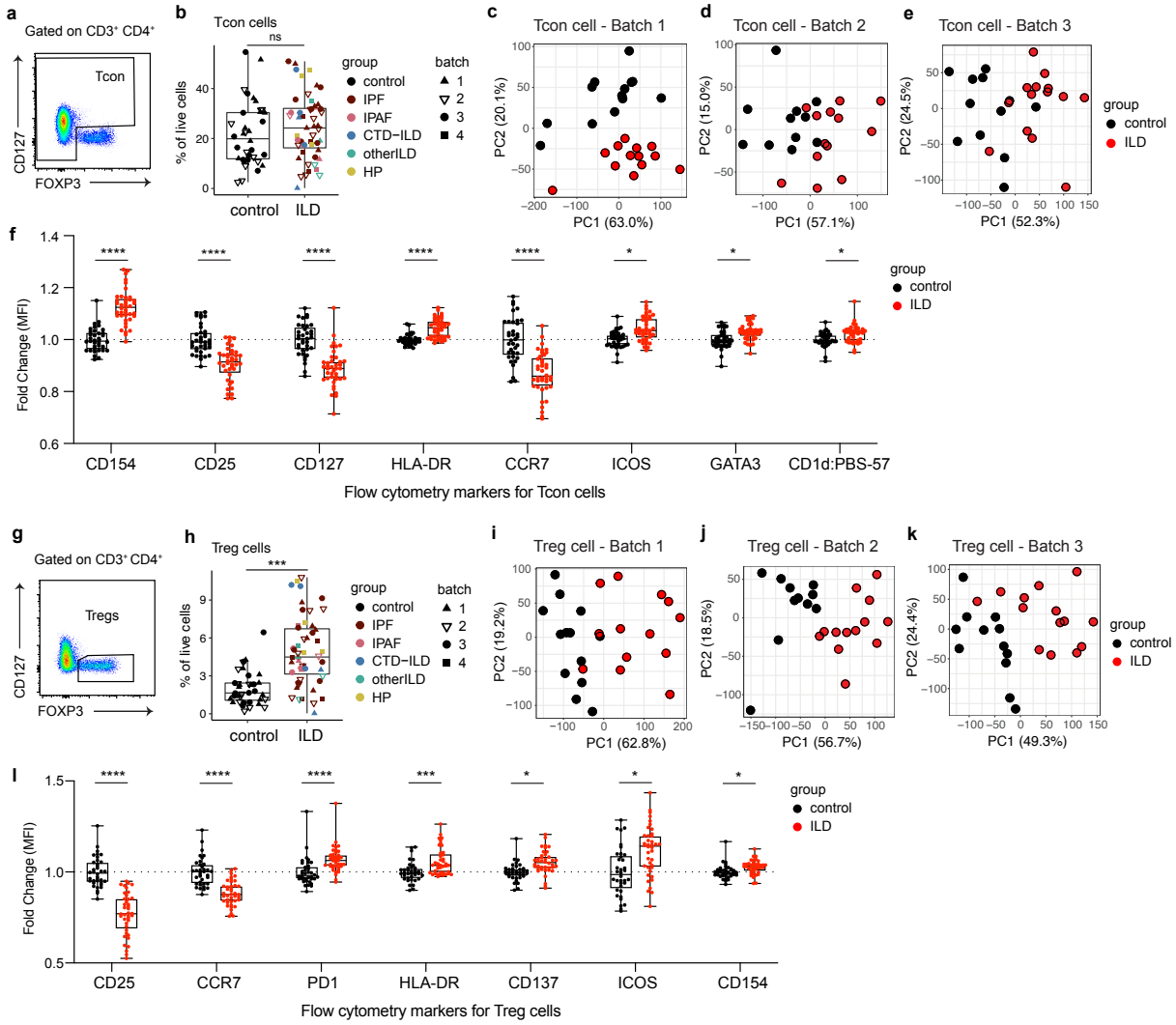

Figure 3.4: ILD patients have elevated Treg with unique phenotypes compared to controls. a. Representative flow cytometry gating for Tcon cells in LLNs. Cells were pre-gated on live, CD3+, CD4+ cells. **b.** Frequencies of Tcon cells in live cells in control vs ILD LLNs. Statistical significance was tested by the Wilcoxon rank sum test. **c-e.** PCA of Tcon cells based on fluorescence intensities of 16 parameters: CD154, CD25, CD127, HLA-DR, CCR7, ICOS, GATA3, PBS-57 loaded CD1d tetramer, Vα7.2, RORγt, BCL6, PD1, CD137, CD38, CD45RA, Vδ. An analysis was run with 10,000 cells, 2,300 cells, and 10,000 cells for batch1, batch2, and batch 3, respectively. **f.** Split violin plots comparing the median fluorescence intensity of individual Tcon markers between ILD and control, based on all samples in batches 1-3. Fold change was calculated relative to the mean values of control samples, separately for each batch. Parameters that are significantly associated with ILD based on a likelihood-ratio test on each logistic regression coefficient are shown. Non-significant parameters are shown in Figure 3.3. P-values were adjusted by Benjamini-Hochberg correction.

Figure 3.4: continued. **g.** Representative flow cytometry gating for Treg cells in LLNs. Cells were pre-gated on live, CD3+, CD4+ cells. **h.** Frequencies of Treg cells in live cells in control vs ILD LLNs. Statistical significance was tested by the Wilcoxon rank sum test. **i-k.** PCA of Treg cells based on fluorescence intensities of 12 parameters: CD25, CD154, HLA-DR, CCR7, ICOS, GATA3, RORγt, BCL6, PD1, CD137, CD38, CD45RA. An analysis was run with 1,000 cells, 269 cells, and 1,300 cells for batch1, batch2, and batch 3, respectively. **l.** Split violin plots comparing the median fluorescence intensity of individual Treg markers between ILD and controls, based on all samples in batches 1-3. Calculations of fold changes and adjusted p-values were done as described above (f). $P<0.05$ (*), $P<0.01$ (**), $P<0.001$ (***), $P<0.0001$ (****).

3.8f). Thus, our data show that patients who had LLN enlargement at the time of diagnosis accumulate more naïve T cells and less PD-1 expressing T cells in their LLNs by the end-stage of the disease.

As the frequency and etiology of hospitalizations are linked with survival in fibrosing ILD (Salonen et al., 2020), we tested whether ILD patients with history of hospitalization due to respiratory causes have different LLN immune profiles than other ILD patients. ILD patients with at least one hospitalization had significantly decreased T$\gamma\delta$ cells and ICOS+ CD4 T cells compared to ILD patients who had never been hospitalized (Figure 3.8g-i). These data suggest that T$\gamma\delta$ cell recruitment and ICOS+ CD4 T cells may be protective of respiratory health, which is consistent with our previous studies that established a protective role for ICOS during lung injury in mice (Hrusch et al., 2018), and an association of ICOS expression on circulating CD4 T cells with patient respiratory function and survival (Bonham et al., 2019).

IPF and immune-associated ILD patients' LLN T cells are similarly activated and expanded

The etiology of HP is known to be due to environmental exposures that induce immune responses, and CTD-ILD and IPAF are caused by, or associated with, autoimmune mechanisms. Therefore, the involvement of the LLNs in these immune-associated ILDs

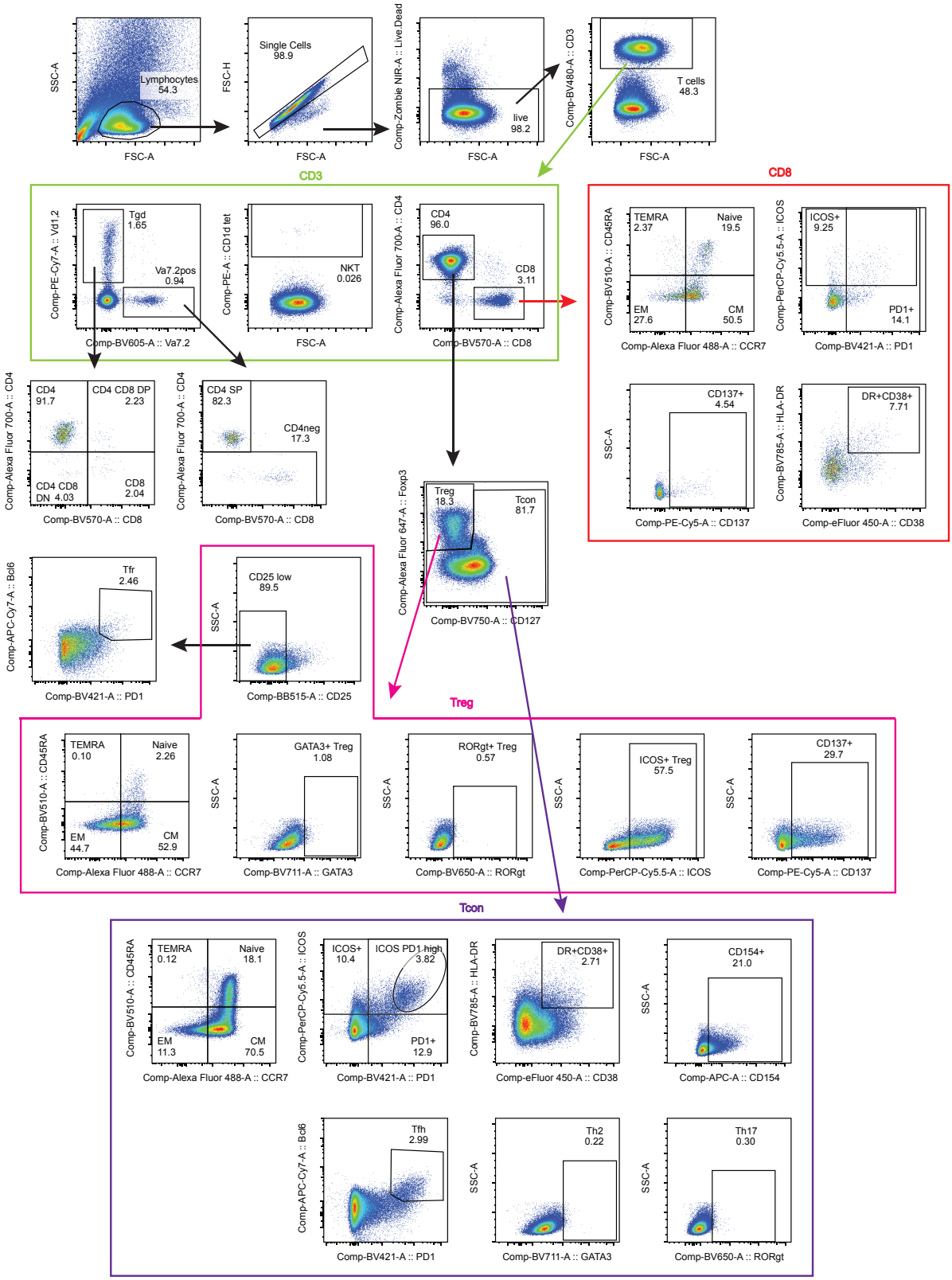

Figure 3.5: Gating strategies for T cell populations.

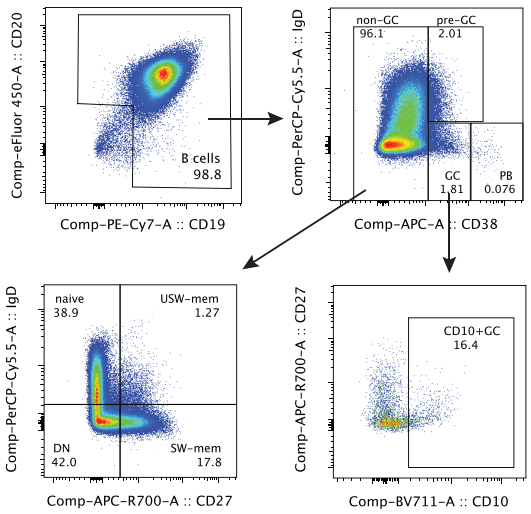

Figure 3.6: Gating strategies for B cell populations.

(immune-ILD) is not surprising. However, whether IPF specifically is associated with a dysregulated immune response, and whether the immune system plays any role in IPF etiology or pathology remains controversial. To test the hypothesis that IPF patients' LLNs have different immunophenotypes than immune-ILD patients, we compared different T cell population frequencies between IPF and immune-ILD groups, as well as donor controls. Surprisingly, CD4 T cells in both IPF and immune-ILD LLNs significantly upregulated CD154 compared control LLNs (Figure 3.9a,b). Similarly, CD137 was upregulated on CD8 T cells (Figure 3.9c,d) and Tregs (Figure 3.9e,f) of both ILD groups compared to non-diseased control LLN. CD154 and CD137 are known to be upregulated in response to recent antigen stimulation of T cell receptors (Frentsch et al., 2005; Wolfl et al., 2007). Thus, both CD4 and CD8 T cells in the IPF LLNs were activated similarly to the immune-ILD group, suggesting that T cell activation may be down-stream of antigen-specific responses.

We found that the majority of Tregs in ILD patients, both IPF and immune-ILD, have low expression of CD25 (Figure 3.9g,h). Low CD25 expression is a phenotype of T follicular regulatory cells (Tfr), which can inhibit low affinity interactions between Tfh and GC B cells

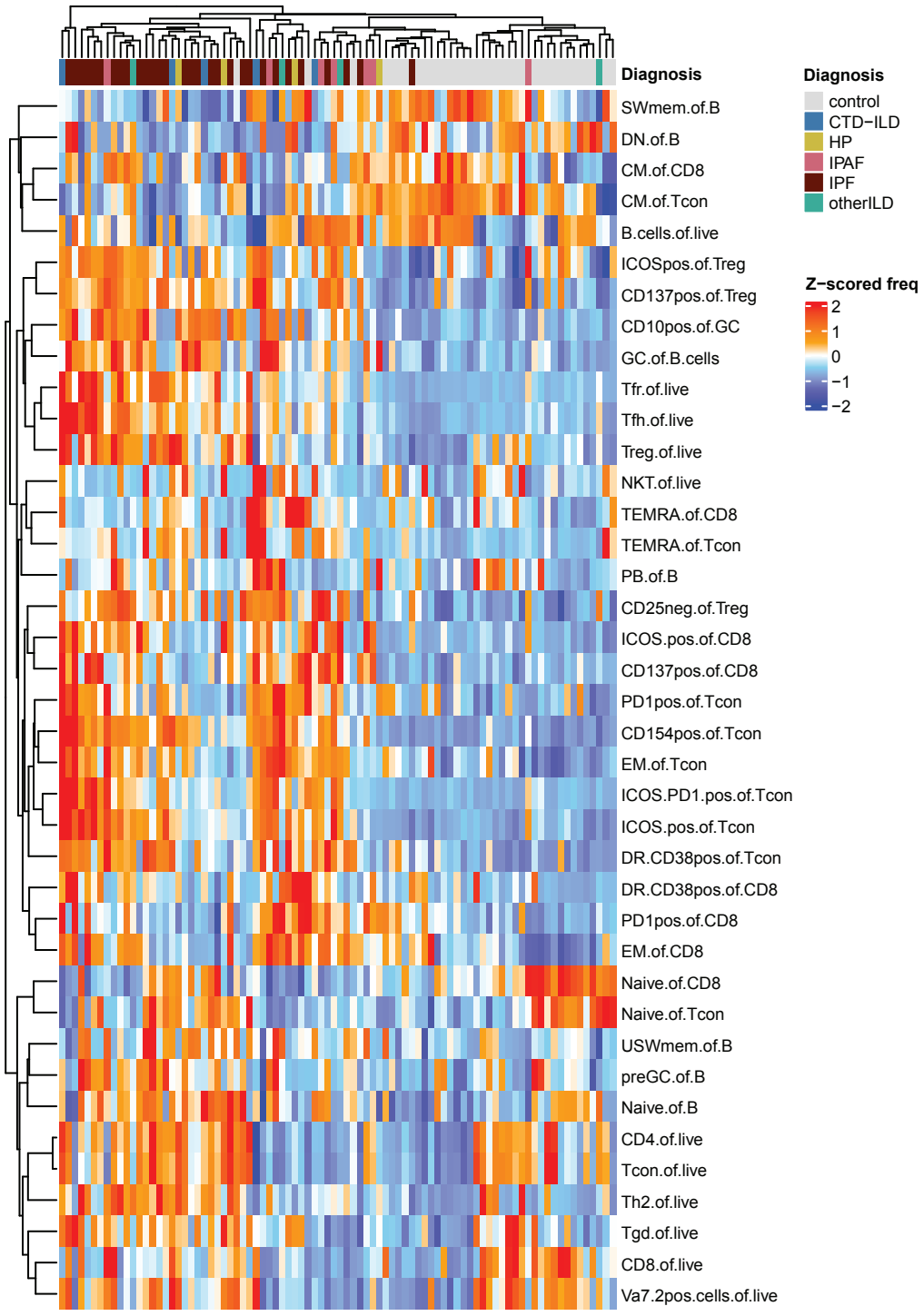

Figure 3.7: Heatmap with unsupervised clustering based on immune cell abundance. Heatmap visualizing a hierarchical clustering of control and ILD individuals based on z-scored frequencies of 39 immune cell populations.

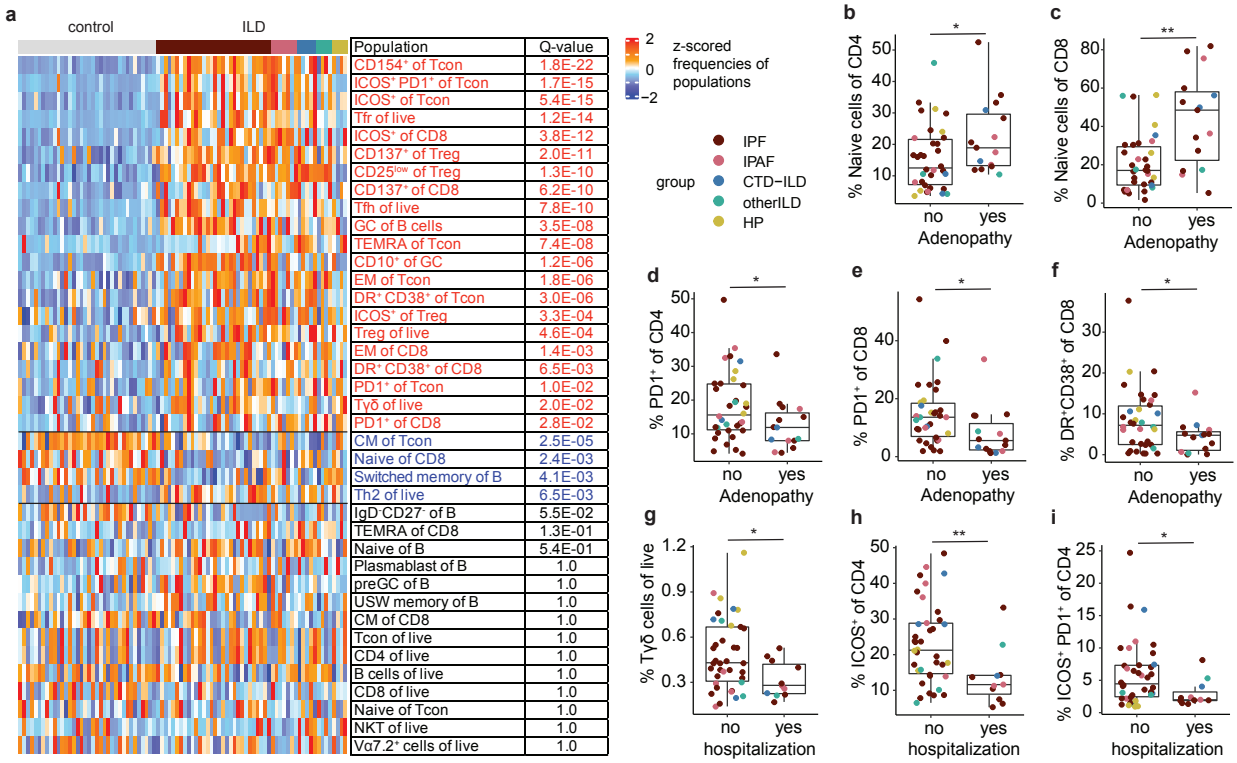

Figure 3.8: Cells in LLNs of ILD patients have significant adaptive immune activation signatures, some of which are associated with patients' clinical history. **a.** Heatmap visualizing batch-normalized z-scores of populational frequencies ranked in the order of statistical significance in difference between ILD and control. A total of 39 populations were quantified by flow cytometry using gating strategies shown in Figure 3.5, Figure 3.6. An associated with ILD was tested for each cellular population by a likelihood-ratio test on each linear regression coefficient. Q-values are adjusted p-values based on the Benjamini-Hochberg method. **b-f.** Quantifications of immune cell populations that are significantly different between ILD patients who had lymphadenopathy (yes) and ILD patients who did not have lymphadenopathy (no) based on chest CT scans obtained at diagnosis. **g-i.** Quantifications of immune cell populations that are significantly different between ILD patients who had history of hospitalization due to respiratory cause (yes) and ILD patients who had not been hospitalized prior to transplantation (no).

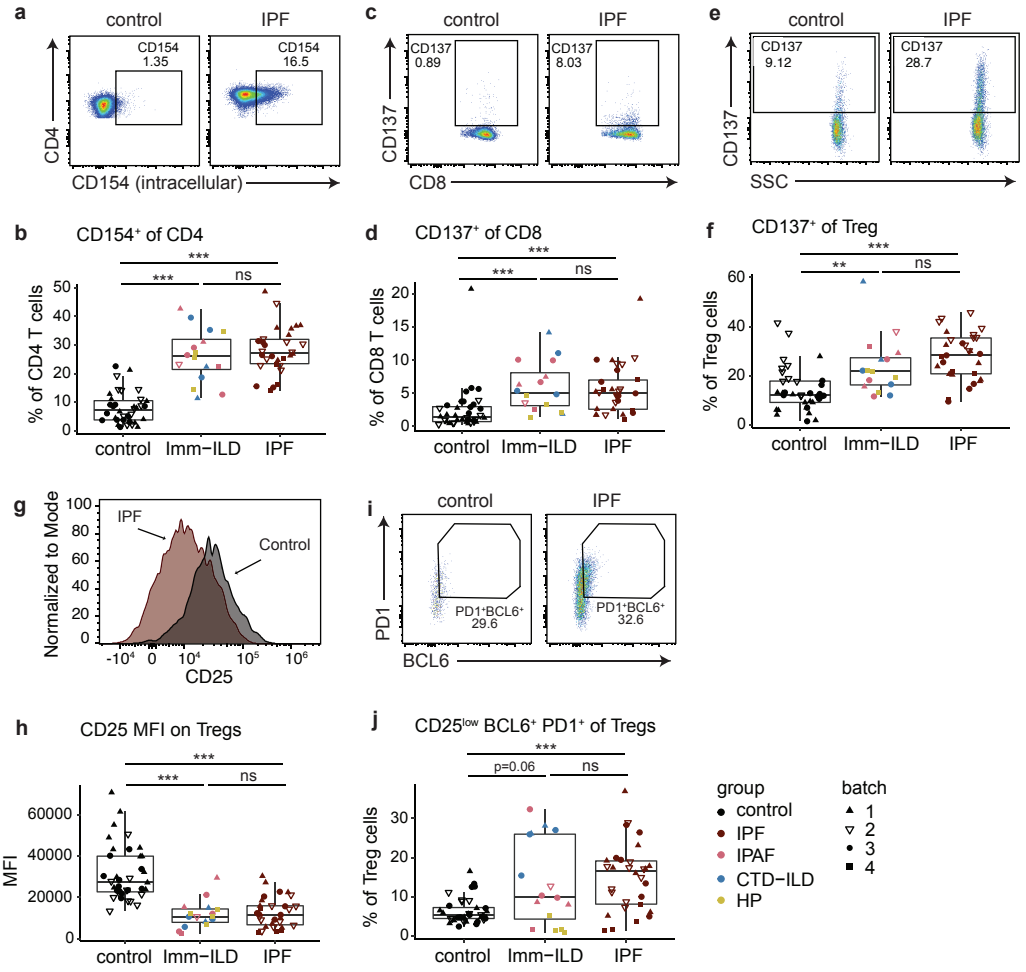

Figure 3.9: IPF and immune-mediated ILD patients have similar levels of enrichments for antigen-stimulated T cells and Treg cells in their LLNs. a-b. Gating strategies and quantification of frequencies of CD4 T cells expressing CD154(CD40L) in control, immune-associated ILD (Imm-ILD), and IPF LLNs. Imm-ILD group includes IPAF, CTD-ILD, and HP. **c-d.** Gating strategies and quantifications of frequencies of CD8 T cells expressing CD137(41BB). **e-f.** Gating strategies and quantifications of frequencies of Treg cells expressing CD137. **g-h.** Histograms and quantifications of median fluorescence intensity for CD25 on Treg cells. **i-j.** Gating strategies and quantifications of frequencies of Treg cells that have follicular regulatory phenotype (CD25low, BCL6+, PD1+). Statistical differences in each cell subset were tested between each ILD subtypes and control LLN, by one-way ANOVA followed by Wilcoxon rank sum tests. $P<0.05$ (*), $P<0.01$ (**), $P<0.001$ (***).

(Linterman et al., 2011) or prevent autoantibody production (Fu et al., 2018). Consistently, Tfr cells were significantly increased in both IPF and immune-ILD LLNs (Figure 3.9i,j), but Tfr cells accounted for only a small fraction of total Tregs. Altogether, these data suggest that enrichments of activated T cells and $CD25^{low}$ Treg cells may be common characteristics of all end-stage fibrotic ILD regardless of etiology.

Germinal center responses are activated and associated with respiratory decline in ILD patients

CD154, which is highly upregulated on ILD CD4 T cells, is essential for helping B cells make antibodies. We investigated whether T and B cells involved in GC response are also expanded in LLN of all ILD patients. Frequencies of Tfh cells and GC B cells were significantly increased in both IPF and immune-ILD LLNs compared to control LLNs, reflecting ongoing GC responses in all ILD patients (Figure 3.10a-d). Surprisingly, IPF patients had the highest amount of GC B cells, even more so than immune-ILD patients. We further interrogated GC B cells for the expression of CD10, as it has been used to define human GC B cells in lymph nodes (Clavarino et al., 2016). We found that CD10-expressing GC B cells are a significant subset of total B cells in IPF LLNs, compared to both immune-ILD patient and control LLNs (Figure 3.10e,f). Moreover, histology of IPF LLNs demonstrated the presence of many GC structures, while in donor control LLN, few GCs were identified (Figure 3.10g,h). Therefore, aberrant humoral immunity could be an important part of ILD pathology, especially for IPF.

Interestingly, variance in GC B cell enrichment was high among ILD patients. Indeed, some patients had almost no GC B cells while others had as much as 10% of total B cells in LLNs. We hypothesized that GC B cells could have functional impact and asked if there was a relationship between the presence of an active GC response and pulmonary function. Patients with CD10+ GC B cell accumulation greater than 1% in their LLNs experienced worse decline in lung function as measured by the overall change in forced vital capacity

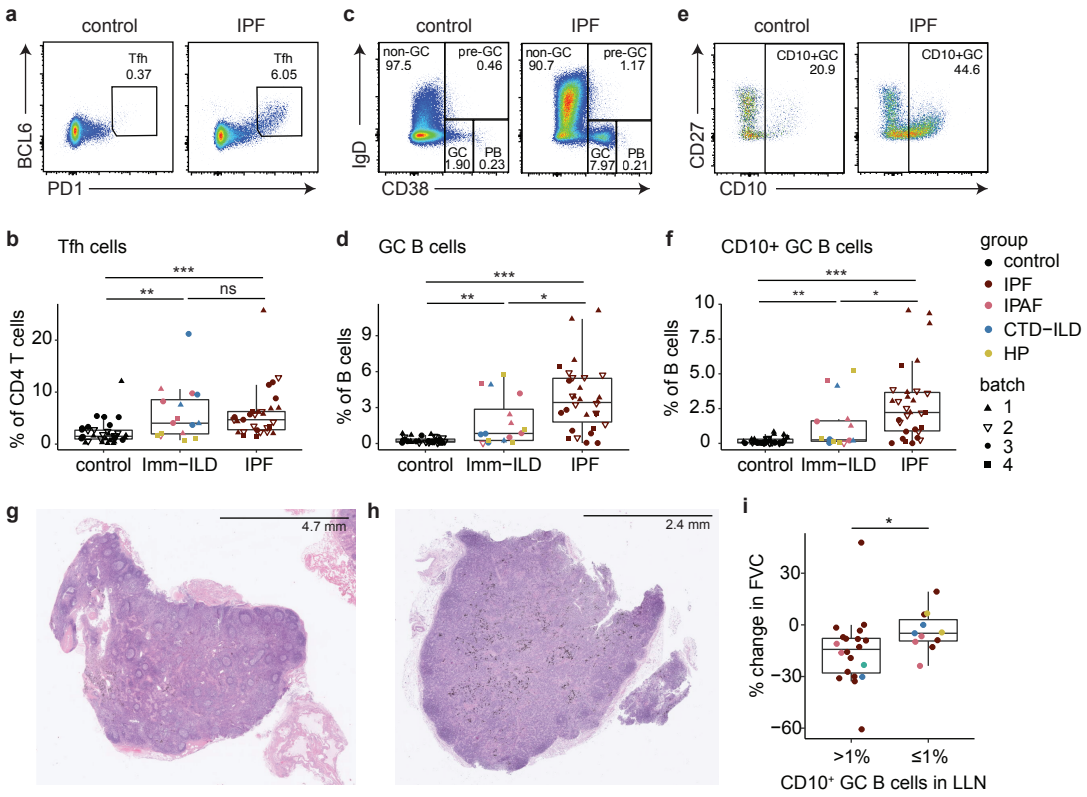

Figure 3.10: Germinal center response is activated and associated with respiratory decline in fibrotic ILD patients. a-b. Gating strategies and frequencies of Tfh cells in control, immune-associated ILD (Imm-ILD), and IPF LLNs. **c-d.** Gating strategies and frequencies of GC B cells. **e-f.** Gating strategies and frequencies of $CD10^+$ GC B cells. **g.** A representative H&E staining of LLN from end-stage IPF patients demonstrating the formation of germinal center structures, the scale bar is 4.7mm **h.** A representative H&E staining of LLN from organ donor controls, the scale bar is 2.4mm **i.** Comparisons of the overall percent change in forced vital capacity (FVC) over time between ILD patients who had $CD10^+$ GC B cells (>1%) and ILD patients who did not have those cells ($\leq$1%) at 1% cutoff in LLNs. P-values were obtained by Wilcoxon rank sum tests, and significance from one-way ANOVA was confirmed prior to multiple comparisons. P<0.05 (*), P<0.01 (**), P<0.001 (***).

```
Mixed-effects ML regression                     Number of obs     =        274
Group variable: sampleID                        Number of groups  =         31

                                                Obs per group:
                                                              min =          2
                                                              avg =        8.8
                                                              max =         37

                                                Wald chi2(3)      =      54.83
Log likelihood =  -972.3637                     Prob > chi2       =     0.0000

------------------------------------------------------------------------------
           fvc |      Coef.   Std. Err.      z    P>|z|     [95% Conf. Interval]
---------------+--------------------------------------------------------------
          year |  -1.453615   .3754472    -3.87   0.000    -2.189479   -.7177524
    GCB_status |   6.396411   5.580307     1.15   0.252     -4.54079    17.33361
      GCB*year |   -1.99864   .6660458    -3.00   0.003    -3.304066   -.6932146
         _cons |   55.72422   3.998668    13.94   0.000     47.88697    63.56146
------------------------------------------------------------------------------

------------------------------------------------------------------------------
  Random-effects Parameters  |   Estimate   Std. Err.     [95% Conf. Interval]
-----------------------------+------------------------------------------------
mrn: Identity                |
                  var(_cons) |   224.9574   59.48363      133.9751    377.7257
-----------------------------+------------------------------------------------
               var(Residual) |   47.42213   4.303841      39.69441    56.65427
------------------------------------------------------------------------------
LR test vs. linear model: chibar2(01) = 340.84        Prob >= chibar2 = 0.0000
```

Figure 3.11: Relationship between the lung function changes over time and GC B cell status in explanted LLNs. Mixed-effects regression modeling with a random intercept was used to analyze changes in forced vital capacity (FVC) over time (year) by germinal center B cell status (GCB_status) in explanted LLNs.

(FVC) over time (Figure 3.10i). The association between CD10+ GC B cells and lung function was further confirmed using the mixed effects regression model (Figure 3.11). The GC B cell status and time interaction coefficient suggests that patients with GC B cells experienced a further decline of FVC at about 2% per year compared to patients who did not have GC B cells (β -1.999, 95% CI -3.304 – (-0.693), $p < 0.003$). These data suggest that antibodies generated from activated GC responses may have negative impact on lung function in ILD patients.

Proteome-wide screening of circulating antibodies revealed novel ILD autoantigens

Given the significant activation of adaptive immune cells and GC formation in the majority of ILD patients, we tested a hypothesis that the lymphocyte activation is driven in part by endogenous antigens. To elucidate potential auto-antigens, we performed phage immunoprecipitation sequencing (PhIP-seq) using a library spanning the entire human proteome (Larman et al., 2011a; O'Donovan et al., 2020; Vazquez et al., 2020a) (Figure 3.11a). We screened serum and plasma samples collected in two medical centers, University of California San Francisco (UCSF) and University of Chicago, from 398 ILD patients at various stages of the disease, as well as 138 non-diseased control plasma samples from blood bank collections (Table 3.2). The most common type of ILD among this study cohort was IPF (27% of patients), followed by CTD-ILD (17%) and HP (17%). Other ILD types represented included undifferentiated CTD-ILD (UCTD), sarcoidosis, familial ILD, and unclassifiable ILD. From screening, we used a stringent threshold (z-score > 50) to identify antigens that are specific to ILD and not reactive in any control individual. We identified 17 novel antigens that have not been reported elsewhere in any ILD subtype. Around 25% (101/398) of all ILD patients had autoantibodies against at least one of the 17 shared ILD antigens (Figure 3.11b,c). Interestingly, each patient was positive for no more

Table 3.2: Demographics of the serum/plasma PhIP-seq study cohort

Diagnosis or Group		Subjects (n)	Samples (n)
Control (Blood Bank Samples)		138	150
Non-ILD[a]		46	46
Connective Tissue Disease-ILD		80	104
Hypersensitivity Pneumonitis		70	87
Idiopathic Pulmonary Fibrosis		102	136
Interstitial Lung Abnormality[b]		10	12
Other[c]		81	97
Unclassifiable		28	34
Unknown Connective Tissue Disease ILD		27	38
Total		**582**	**704**
Self-Identified Race/Ethnicity	**Sex**	**Subjects (n)**	**Age (mean ± s.d.)**
White	*Female*	137	63.3 ± 11.9
	Male	170	67.0 ± 11.6
Black	*Female*	42	61.4 ± 11.0
	Male	8	53.6 ± 15.1
LatinX[1]	*Female*	22	58.5 ± 13.3
	Male	14	66.2 ± 11.1
Unknown[2]	*Female*	3	70 ± 11.4
	Male	5	68.2 ± 9.8
	NA	9	82[2]
Asian	*Female*	16	59.4 ± 12.0
	Male	13	68.5 ± 9.8
American Indian	*Female*	1	77 ± NA
	Male	2	68 ± 0
American Indian/LatinX	*Male*	1	63 ± NA
Other Identity[3]	*Male*	1	63 ± NA

[a]Non-ILD group includes patients with rheumatoid arthritis who do not have ILD symptoms (n=15) and age-matched controls with no known lung disease (n=31 subjects) from University of Chicago. [b]Interstitial lung abnormality reflected a diagnosis where underlying lung abnormalities were present (e.g. broncheictasis or inflammation) though not felt to reflect ILD. [c]Other reflected a constellation of diagnoses not otherwise represented on this table and were a heterogeneous group of disorders (e.g. sarcoidosis, asbestosis etc.) [1]LatinX indicated individuals that did not self identify with race but identified with ethnicity as Hispanic or Latino at UCSF or Hispanic at University of Chicago. [2]Individuals without known race or ethnicity information were categorized as Unknown. One individual that did not specify Race/Ethnicity or Sex was documented as being 82 years old. Data on age not available for n=20 other members of this group. [3]One individual identified as other identity without further specification. Data on race or ethnicity was not available for 138 subjects used as the screening reference group.

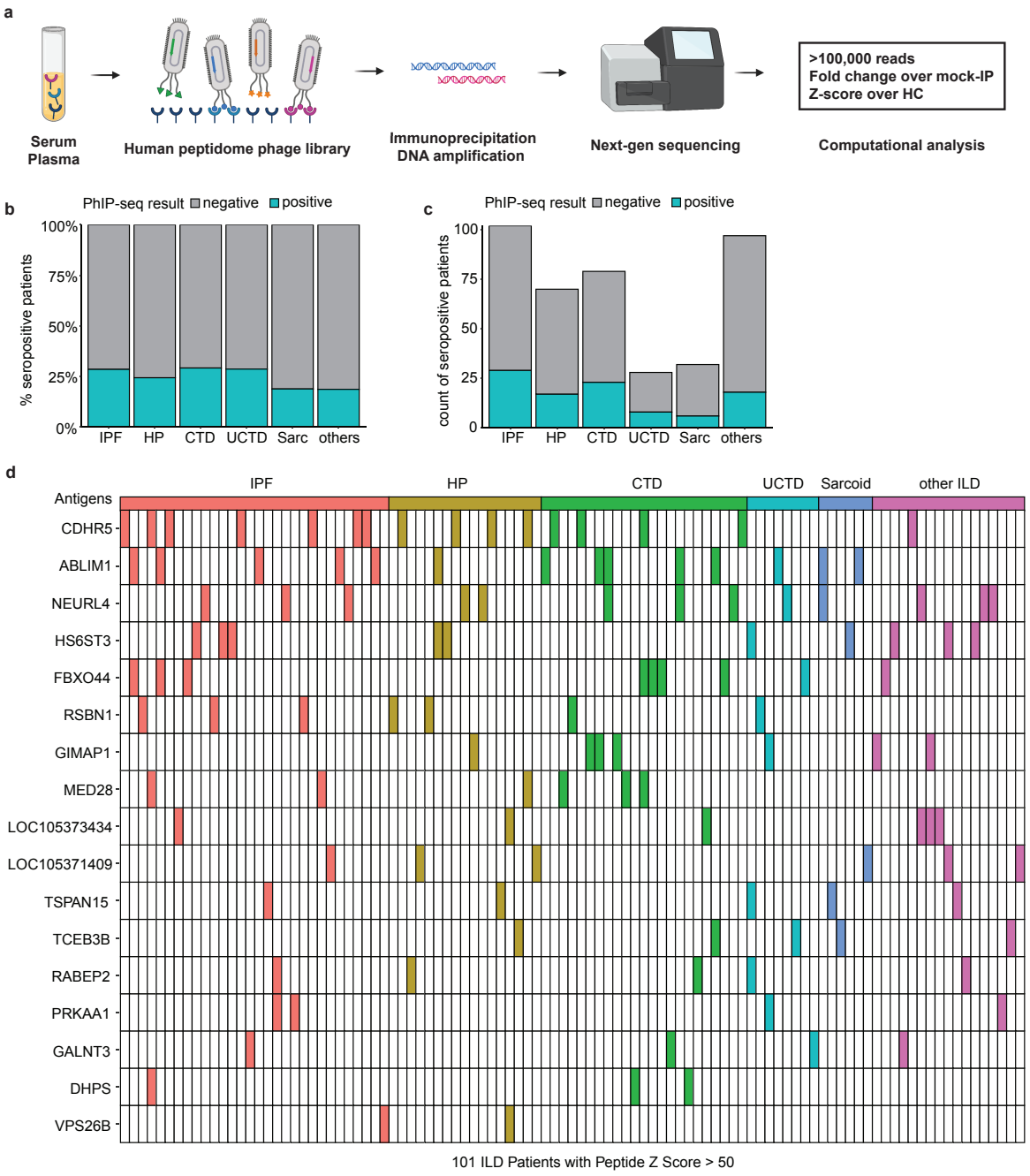

Figure 3.12: Phage-immunoprecipitation sequencing identifies novel and shared autoantigens for ILD. a. Using the phage library containing 700,000 unique phages, each displaying 49AA segments across the entire human proteome, a total of 398 ILD plasma/serum samples from University of Chicago and UCSF medical centers and 138 healthy control samples from the NY Blood Bank were screened. Shared autoantigens were determined where z-scores calculated relative to healthy control is above 50. *Caption continued on the next page*

Figure 3.12: **b-c.** Proportions of ILD patients who were seropositive for at least one of the shared antigens, plotted as percentage (b) and count (c). ILD individuals were grouped based on subtypes, IPF, HP, CTD-ILD (CTD), undifferentiated CTD-ILD (UCTD; includes IPAF), sarcoidosis (Sarcoid), and other ILDs. **d.** Distribution of ILD patients who were seropositive for shared ILD antigens, ranked in the order of prevalence from top to bottom. Each column is one of the 101 ILD individuals that tested positive. None of the healthy controls had positivity against these antigens.

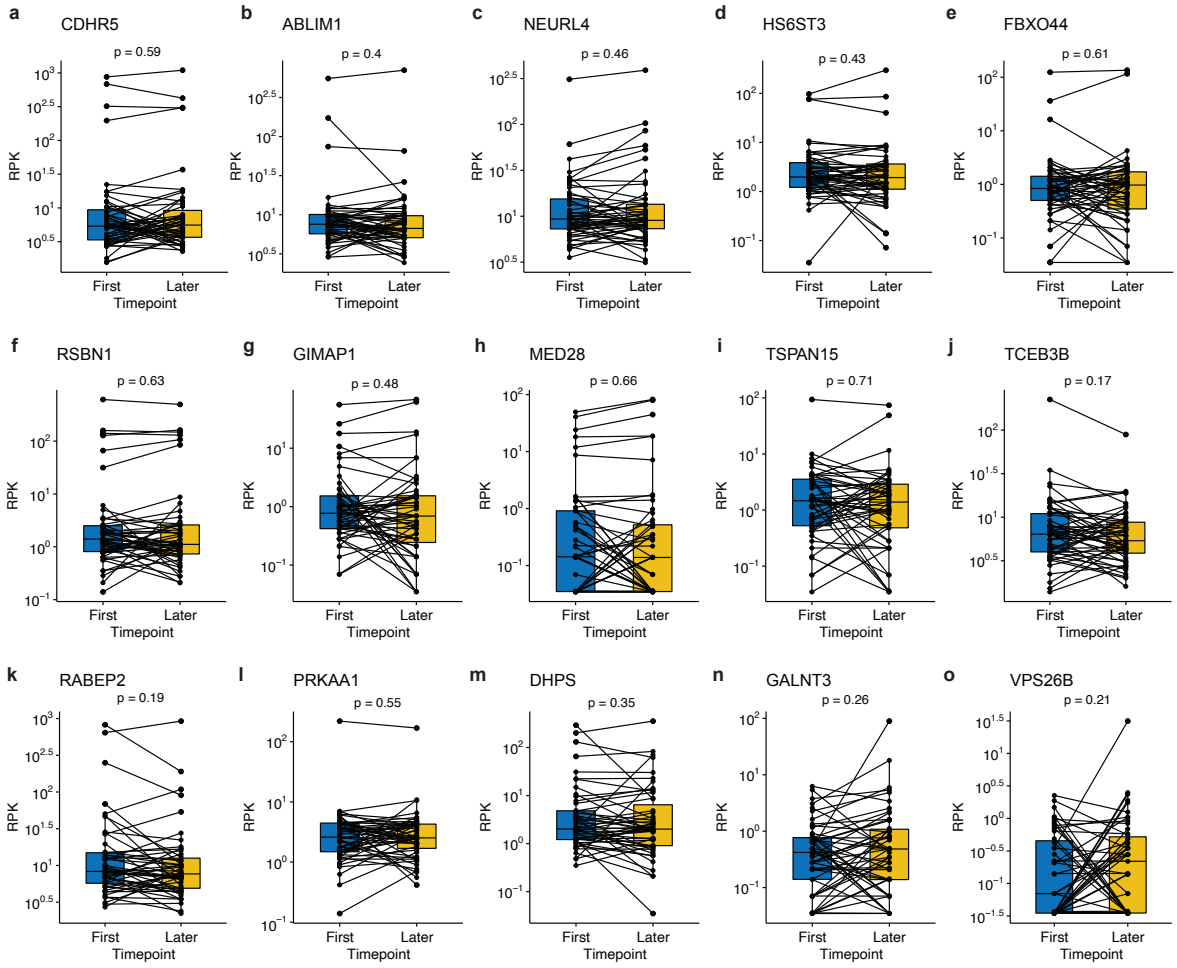

Figure 3.13: Longitudinal analysis of autoantibody amounts in ILD plasma. a-o. Autoantibody signals based on PhIP-seq results (RPK: reads per 100k) were compared between longitudinally paired plasma samples from ILD patients (n=51). Intervals between the first and later timepoints range between 98 to 2952 days. Paired Wilcoxon p-values are displayed for each of the 15 ILD antigens.

than three antigens, and the antigen specificity was heterogeneous with no apparent link to ILD subtypes (Figure 3.11d). Within the University of Chicago cohort, 51 patients were sampled more than once. We compared the first and last sample banked for each patient and found that there was no difference over time (Figure 3.13).

ABLIM1, a widely expressed cytoskeletal protein, is a target for auto-antibody responses in many ILD patients

We sought to investigate whether newly discovered antigens are expressed in lung tissues of ILD patients. Using publicly available single cell RNA sequencing data and protein data, we confirmed that many of the antigenic genes or proteins are detected in lungs, but none were exclusive to the lungs (not shown). Immunofluorescence staining of explanted IPF lungs revealed a large area of lungs positive for alpha-smooth muscle actin (α-SMA)-expressing fibroblasts (Shinde et al., 2017), and the presence of small airway architectures with strong cytokeratin-17 (KRT-17) expressions, which is consistent with the recently reported phenotype for dedifferentiated airway basal cells (Jaeger et al., 2022) (Figure 3.14a). Importantly, staining of IPF lungs showed strong ABLIM1 expression, which was present throughout the lungs with clear co-localization with KRT-17+ cells (Figure 3.14b). KRT-17 is a canonical basal cell marker, which becomes upregulated in fibrotic lungs due to the expression in aberrant basaloid cells. Indeed, interrogation of the publicly available scRNAseq data demonstrated that ABLIM1 is highly expressed in these aberrant cells of IPF patients' lungs (Neumark et al., 2020). Immunofluorescence staining of control lungs showed a different expression pattern where expression of α-SMA and KRT-17 were restricted to large airways, but ABLIM1 was still widely expressed (Figure 3.15).

Next, we validated the binding of circulating patient antibodies to the full-length ABLIM1 protein by radioligand binding assay (RLBA), in the University of Chicago

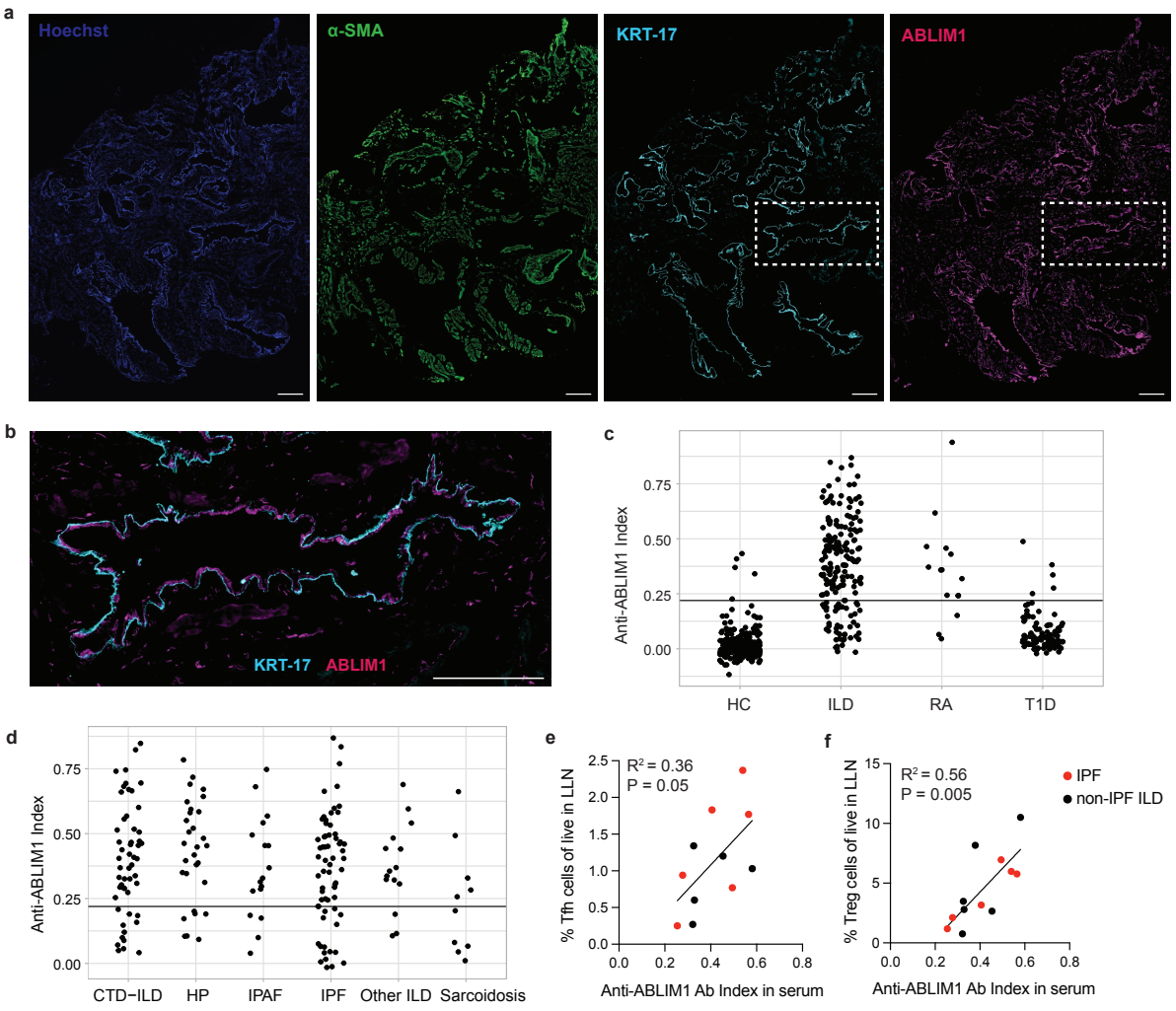

Figure 3.14: ABLIM1 is a common ILD autoantigen with high expression in fibrotic lungs. a. Representative immunofluorescence staining of explanted IPF lungs for Hoechst, alpha-smooth muscle actin (α-SMA), cytokeratin 17 (KRT-17), and ABLIM1. Images were taken with an 40x objective, and the scale bar is 100um. **b.** Close-up view of a region of IPF lung where there is the co-localization of ABLIM1+ cells and KRT-17+ de-differentiated airway basal cells. The scale bar is 100um. **c.** Quantification of plasma/serum antibody bindings to the full-length, radio labeled ABLIM1 protein. The horizontal line is placed at three standard deviations above the mean value for healthy controls (HC), which was used as a cutoff to determine positivity. Samples from rheumatoid arthritis (RA) patients with no symptoms of lung disease, and type 1 diabetes patients (T1D) were included as comparison groups, and healthy controls (HC) are samples donated through NY Blood Bank. **d.** Comparison of anti-ABLIM1 index among ILD subtypes. **e-f.** Linear regression between anti-ABLIM1 index in serum and Tfh cell (d) and Treg cell (e) proportions in ILD LLNs (n=11; 6 IPF and 5 non-IPF ILD).

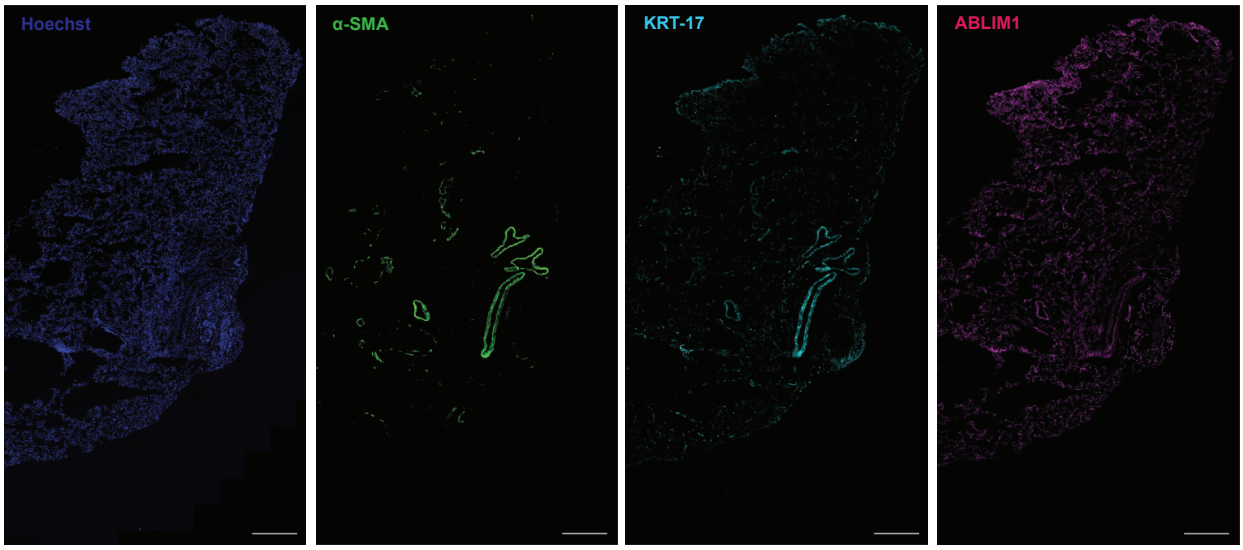

Figure 3.15: Immunofluorescence analysis of ABLIM1 in control lungs. Representative immunofluorescence staining of organ donor control lungs for Hoechst, alpha-smooth muscle actin (α-SMA), cytokeratin 17 (KRT-17), and ABLIM1. Images were taken with an 40x objective, and the scale bar is 100μm.

cohort. The majority of ILD patients (142/189), regardless of the disease subtype, tested positive for having anti-ABLIM1 antibodies in blood plasma (Figure 3.14c,d). To elucidate a potential immunodominant epitope on ALBIM1, we searched for hotspots based on multiple sequence alignment of the individually immunoprecipitated phage sequences. Since all known splicing isoforms were represented in our phage-displayed library, we used NCBI BLAST and determined that 21 out of 22 immunoprecipitated phage sequences aligned to either the ABLIM1 isoform a (NP_002304) or isoform j (NP_001309817) (Figure 3.16). Intriguingly, over 50% of the immunoprecipitated sequences aligned to a specific region of the isoform j (amino acid position 193 – 217), a proline-rich portion of the linker domain, suggesting that this could be an immunodominant epitope in ILD patents. To test whether the anti-ABLIM1 response was specific for ILD, we included a small cohort of rheumatoid arthritis (RA) patients who had no symptoms of lung disease (n=15), and type 1 diabetes patients (n=96) (Figure 3.14c). Interestingly, 80% of RA patients had anti-ABLIM1 autoreactivity, while only 5% of type 1

diabetes patients tested positive. Thus, we found reactivity in a systemic connective tissue disease, which often affects the lungs, but not in an organ-specific autoimmune disease.

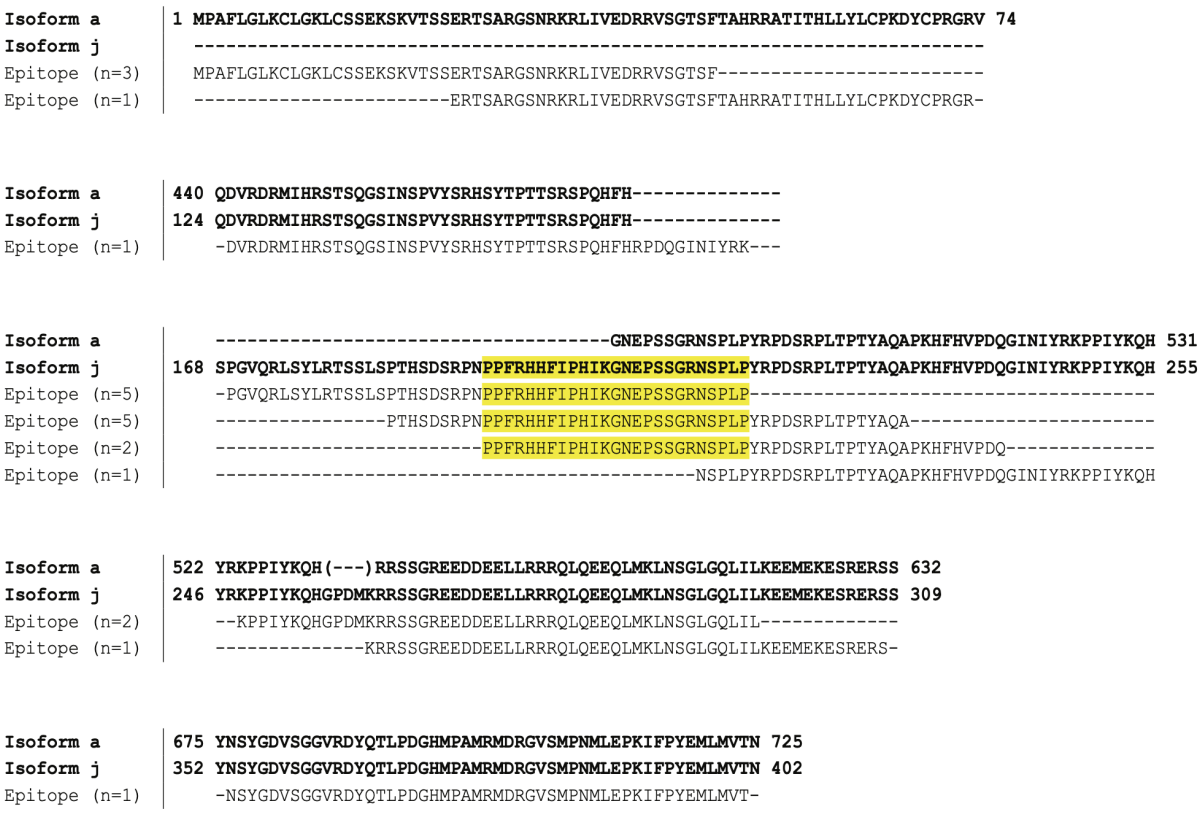

Figure 3.16: Immunodominant peptide epitopes on ABLIM1. Phage-displayed library sequences (epitope sequences) that were immunoprecipitated by ILD patient plasma antibodies were aligned to ABLIM1 isoform a (NP_002304) and isoform j (NP_001309817). Number of patients that had reactivity to each epitope sequence is indicated on the figure. Highlighted region indicates the proline-rich region, which is commonly represented in a total of 12 phage-immunoprecipitated sequencing hits.

Finally, we investigated whether the amount anti-ABLIM1 antibodies in blood correlated with GC response in LLNs. We had both plasma PhIP-seq and LLN flow cytometry data from 12 individuals. We measured whether there was a linear relationship between anti-ABLIM1 index and frequency of each of the cells involved in GC response in LLN. Although we did not find a correlation between GC B cell proportion in LLN and anti-ABLIM1 in plasma (p=0.72 and R2=0.013), we discovered a positive linear relationship between Tfh

cell proportion in LLN and anti-ABLIM1 index that was nearly significant (Figure 3.14e). Moreover, we tested whether accumulation of anti-ABLIM1 antibody is related to the Treg cell proportions since these regulatory cells are responsible for suppressing autoantibody production. Surprisingly, we found a strong correlation between Treg cell proportion in LLN and anti-ABLIM1 index (Figure 3.14f) suggesting that there may be unproductive suppression of GC response against ABLIM1 by Treg cells. Overall, antibody responses against common antigens expressed in fibrotic lungs suggest that these autoantigens may indeed drive adaptive immune activation that could lead to uncontrolled inflammation in lungs and lung lymph nodes.

3.1.4 Discussion

Our study provides, for the first time, comprehensive insight of the adaptive immune landscape in the LLNs of fibrotic ILD patients at the end-stage of disease. ILD patients' LLNs had increased GC response regardless of their diagnosis. Importantly, IPF patients had immune responses as robust as patients with immune-associated fibrotic ILD, and even had significantly more GC B cells, which displayed an association with reduced lung function. In this active LLN environment, we hypothesized that regulatory responses would be present at low levels; however, all ILD patients had increased percentages of total and activated Tregs. As LLN T cells in the ILD patients expressed markers of recent antigen activation, we investigated whether auto-antigen responses were present in these patients. We identified serum reactivity to a novel auto-antigen, ABLIM1, and determined that anti-ABLIM1 responses were associated with LLN frequencies of Tfh and Treg in ILD patients. Together, these data underscores the significance of prevalent immune responses in ILD and the potential roles in pathogenesis of disease.

Regardless of clinical subtypes, LLN cells from all ILD patients presented antigen-stimulated phenotypes characterized by upregulation of co-stimulatory molecules.

In previous work, we demonstrated that high expression of ICOS on peripheral CD4 T cells predicted favorable survival outcomes for IPF patients (Bonham et al., 2019). In this study, we further demonstrate the importance of high ICOS expression on T cells in the LLNs. ILD patients with history of hospitalization due to respiratory cause had significantly lower percent of ICOS-expressing CD4 T cells at the end-stage of disease in LLNs, compared to patients without a history of hospitalization. Thus, ICOS on T cells is not only predictive of survival but could also be a phenotype relevant for the clinical course of the disease such as acute exacerbation.

In the presence of active immune responses in the LLN of ILD patients, we hypothesized there would be lower, if not the same, frequency of Tregs compared to controls. Surprisingly, we found Tregs were elevated in all ILD patients. A significant aspect of this finding was distinguishing Tregs as $Foxp3^{+}CD127^{-}$. While previous studies on Tregs in IPF use CD25-high expression to designate Tregs, this strategy may have overlooked $CD25^{low}$ expressing Tregs (Adegunsoye et al., 2016; Galati et al., 2014; Hou et al., 2017; Kotsianidis et al., 2009). We identified that a subset of $CD25^{low}$ Tregs in ILD patients are Tfr cells, which regulate B cell responses by maintaining self-tolerance and downregulating ineffective GC B cell interactions (Fu et al., 2018; Linterman et al., 2011; Lu and Craft, 2021). However, Tfr responses do not seem sufficient to control auto-reactive GC B cells since we observed prevalent autoantibody responses in ILD patients. Interestingly, similar accumulation and clinical significance of $CD25^{low}$ $FOXP3^{+}$ T cells have been reported in the context of autoimmune diseases such as systemic lupus erythematosus (SLE) (Bonelli et al., 2009; El-Maraghy et al., 2018; Zhang et al., 2008), multiple sclerosis (Fransson et al., 2010), and rheumatoid arthritis (de Paz et al., 2012). It is possible that Tregs in ILD patients are playing a pro-fibrotic role via ICOS, CD137, or PD-1 dependent mechanisms. For example, PD-L1 ligation transforms fibroblasts into myofibroblast (Guo et al., 2022), thus PD-1 expressing Tregs may directly promote PD-L1

signaling. Thus, the origin(s) and function(s) of $CD25^{low}$ $FOXP3^{+}$ T cells in ILD remain to be explored in future studies.

Enrichment of GC B cells in LLNs was associated with respiratory decline in ILD patients, suggesting a potentially pathogenic role for the humoral immunity in pulmonary fibrosis. This is consistent with previous studies that showed a negative relationship between circulating IgA and lung function in IPF patients (Heukels et al., 2019) and the benefit of B cell and antibody depletions in IPF patients with acute exacerbation (Donahoe et al., 2015). Furthermore, anti-CD20 therapy using Rituximab has shown to be efficacious in preserving lung function in autoimmune disease-associated ILD patients (Atienza-Mateo et al., 2020). Our findings extend the B cell impact on lung function to other subtypes of ILD and could support potential therapeutic benefit for treating GC B cell-high ILD patients with B cell-targeted therapies such as rituximab and anti-CD19 CAR T therapy.

The presence of germinal center responses led us to determine whether ILD patients also had antibody responses. While there may be environmental reactivities in ILD patients, we focused on auto-antigen reactivities, as there is current literature that many IPF patients have detectable levels of circulating autoantibodies to various proteins and cellular extracts. (Feghali-Bostwick et al., 2007; Heukels et al., 2019). Despite IPF not being considered an autoimmune disease, approximately 35 percent of IPF patients are seropositive for autoantibodies without meeting the full diagnostic criteria for an autoimmune disease (Ghang et al., 2019; Oldham et al., 2016). In this study, we distinguished IPAF from IPF patients, yet still found that some autoantibodies are common across all ILD including IPF patients without any sign of autoimmune features. In a recent manuscript (Upadhyay, Yoon, et al. *manuscript submitted*), we performed the first PhIP-seq analysis on the serum and plasma of ILD patients and identified reactivity to 17 auto-proteins. We highlighted ABLIM1, a protein highly expressed in aberrant basaloid cells in fibrotic ILD lungs. Interestingly, we found that there was a break in B cell

tolerance to ABLIM1 in the majority of our ILD patients, although the impact of this autoimmune response in disease pathogenesis remains unknown.

ABLIM1, consists of an actin binding headpiece domain at carboxy-terminal and a zinc-binding LIM domain at amino-terminal, is an intracellular protein that mediates interactions between actin and cytoplasmic targets (Roof et al., 1997). While the protein is ubiquitously expressed across many tissues, some splicing isoforms have been linked to tissue-specific function or pathology of skeletal muscles (Ohsawa et al., 2015), retinal neurons (Lu et al., 2003), and osteoclasts (Narahara et al., 2018). In our PhIP-seq data, peptide epitopes for over 50% of anti-ABILM1+ ILD patients mapped to a region that only exists in the isoform j (NP_001309817), which is a shorter isoform (455AA) compared to others. Further study is needed to determine exon-splicing profiles of the ABLIM1 expressed in fibrotic lungs. Interestingly, we did not find a correlation between anti-ABLIM1 index and ILD subtypes, as distributions of ILD subtypes were nearly identical between the full cohort and the seropositive subset. This is consistent with our findings from the flow cytometry analysis of LLN, which revealed lymphocyte activation including germinal center response across all ILD types.

Antibodies to ABLIM1 were also detected in RA patients, but not in type 1 diabetes patients, suggesting that the break in tolerance against ABLIM1 might be due to some shared pathology between ILD and RA. In fact, pulmonary involvement is one of the common extra-articular manifestation of RA (Yunt and Solomon, 2015), and even patients without symptoms of lung disease can have radiographic lung abnormalities (Bilgici et al., 2005). Though investigation of a larger RA cohort is needed, it is possible that anti-ABLIM1 response are specific to lung pathologies. The lack of response in type 1 diabetes patients further supports that ILD-specific mechanisms rather than chronic inflammation likely contribute to autoantibody response.

While PhIP-seq screening covers the entire human proteome, this method is limited to

linear peptides which would exclude complex epitopes and post-translational modifications of an entire protein. In fact, the anti-ABLIM1 prevalence turned out to be greater when we performed RLBA using the full-length protein compared to PhIP-seq analysis, suggesting strong immunogenicity of 3-dimentional epitopes. In addition, we now know that smoking, a risk factor in ILD, also induces a post-translational modification called citrullination (Makrygiannakis et al., 2008). Citrullination can result in major structural changes including charge shift, hydrogen bond formation, and protein denaturation (Alghamdi et al., 2019). Thus, with PhIP-seq, we may have missed reactivity of citrullinated peptides. Studies on RA patients, demonstrate that presence anti-citrullinated protein antibodies in the sera resulted in susceptibility to ILD (Xie et al., 2021). These caveats of PhIP-seq may explain why we did not detect previously published auto-antigen reactivities.

The initial trigger leading to enlarged lymph nodes remains an outstanding question. Although we provide a compelling data on auto-antigen reactivities in ILD, it is entirely possible that there are also environmental antigens or even inhaled atmospheric particulate matter (Ural et al., 2022) participating in the activation of immune responses in the LLN. Further, acute exacerbations in ILD patients expedite decline of lung function in patients, thus infectious pathogens may also contribute to our findings. Finally, although we had a large number of explanted lung lymph node samples, we did not have enough power to include drug history as a variable. Thus, the relative increase in GC B cell enrichment in LLNs of IPF patients compared to immune-ILD patients could reflect differences in immunomodulatory treatments between the two groups.

Together, these data provide an interesting new avenue for research on human ILD. We provide evidence that there is an antigen response occurring in ILD patients and importantly, there is a commonality amongst IPF and immune-associated ILDs at end-stage of disease. With these data, we can hypothesize that auto-antigens may be driving germinal center responses and activation of lymphocytes that are contributing to pathogenesis of disease.

However, autoantibody production could be either a driver or byproduct of the disease. Although our analysis of paired samples nullified a hypothesis that there is an increasing autoantibody response over time, ILD patients become seropositive at various stages of the disease. In contrast to the view that end-stage fibrotic ILD is a burnt-out fibrosis, our work implies that autoimmunity remains ongoing even at the time of lung transplantation. This suggests that break in humoral tolerance is a widespread phenomenon and that there seems to be uncontrolled immune responses against common autoantigens in fibrotic ILDs, even in IPF patients who do not present autoimmune features. An autoantibody panel based on our study could be used as a molecular tool that informs clinical decisions. Future studies on clinical phenotype and prognosis of patients who are seropositive for ILD autoantigens could potentially define new endotypes that inform clinical decisions.

3.2 Gut microbiota modulates bleomycin-induced acute lung injury response in mice

3.2.1 Abstract

Airway instillation of bleomycin (BLM) in mice is a widely used, yet challenging, model for acute lung injury (ALI) with high variability in treatment scheme and animal outcomes among investigators. Whether the gut microbiota plays any role in the outcome of BLM-induced lung injury is currently unknown. To investigate ALI, intratracheal instillation of BLM into C57BL/6 mice was performed. Fecal microbiomes were analyzed by 16s rRNA amplicon and metagenomic sequencing. Germ-free mice conventionalization and fecal microbiota transfer between SPF mice were performed to determine dominant commensal species that are associated with more severe BLM response. Further, lungs and gut draining lymph nodes of the mice were analyzed by flow cytometry to define immunophenotypes associated with the BLM-sensitive microbiome. As a result, mice from

two SPF barrier facilities at the University of Chicago exhibited significantly different mortality and weight loss during BLM-induced lung injury. Conventionalizing germ-free mice with SPF microbiota from two different housing facilities recapitulated the respective donors' response to BLM. Fecal microbiota transfer from the facility where the mice had worse mortality into the mice in the facility with more survival rendered recipient mice more susceptible to BLM-induced weight loss in a dominant negative manner. BLM-sensitive phenotype was associated with the presence of *Helicobacter* and *Desulfovibrio* in the gut, decreased Th17-neutrophil axis during steady state, and augmented lung neutrophil accumulation during the acute phase of the injury response. Overall, we demonstrated that the composition of gut microbiota has significant impact on BLM-induced wasting and death suggesting a role of the lung-gut axis in lung injury.

3.2.2 Introduction

Increasing evidence based on both clinical and experimental studies suggest that the microbiome plays an essential role in inflammatory pulmonary conditions such as acute lung injury (ALI) and acute respiratory distress syndrome (ARDS). Characterized by acute and diffuse lung inflammation, ARDS development is most often associated with respiratory infection induced-pneumonia, non-pulmonary sepsis, aspiration of gastric and/or esophageal contents, and major trauma (Force et al., 2012; Johnson and Matthay, 2010; Matthay et al., 2019). In recent studies, the enrichment of specific commensal species in the lung microbiome community was shown to be closely linked to development and outcome of ARDS among critically ill patients (Dickson et al., 2020, 2016; O'Dwyer et al., 2019). Enteric bacteria *Enterobacteriaceae* were found in lungs of ARDS patients even in the absence of systemic bacterial infection, suggesting that translocation of commensal bacteria from gut to lung can alter the lung microbiota and affect lung health (Dickson et al., 2016; Panzer et al., 2018). Furthermore, anaerobic gut commensals including

Bacteroides and *Enterococcus faecalis* were abundantly found in lungs and correlated with survival in an experimental sepsis model (Dickson et al., 2016). Therefore, understanding the effect of microbiome on lung injury and inflammation could lead to improved prediction and treatment strategies for ARDS patients.

Intratracheal instillation of bleomycin (BLM) in mice is a commonly used model of lung injury and fibrosis. Unlike systemic bacterial infection, BLM model induces sterile injury without the use of any infectious agent or bacterial components. BLM is an anticancer antibiotic, which was originally isolated from the actinomycete Streptomyces verticillus (Matute-Bello et al., 2008). It induces cell death by generating reactive oxygen species and double-stranded DNA breaks, which primarily leads to epithelial injury (Burger et al., 1981; Matute-Bello et al., 2008; Millar et al., 2016). The response to intratracheal administration of BLM in animals is characterized by two phases, acute and fibrosis. Neutrophilic alveolitis and increased lung permeability take place during the first 7 to 11 days of the acute phase after injury, followed by a fibrotic phase with the contraction of inflammation (Aeffner et al., 2015; Hrusch et al., 2018; Matute-Bello et al., 2008). Even though the BLM model has been refined over the years, the BLM dosage used to induce pathology in animals varies widely among investigators (Scotton and Chambers, 2010). The need for a varying amount of BLM even for the same strain of mice suggests that some environmental factors, such as diet and microbiome, may contribute to the susceptibility to BLM-induced lung injury.

Previous studies showed that germ-free animals are protected from BLM-induced mortality, suggesting that the microbiome plays a pivotal role in the BLM model (O'Dwyer et al., 2019; Todd et al., 2013). However, in the context of BLM challenge, the effect of the spontaneous difference in the composition of commensal microbes in specific pathogen-free (SPF) environments remains unknown. Herein, we investigated the hypothesis that spontaneous differences in gut microbial communities between genetically similar animals

could contribute to variability in response to BLM challenge. Our findings suggest that the presence of specific gut commensal microbes may be a risk factor for having more severe inflammatory lung diseases and additionally highlight the need for defining microbial environments in laboratories for improving the reproducibility of experimental lung injury studies.

3.2.3 Results

C57BL/6 mice housed in two SPF animal facilities respond differently to BLM-induced lung injury

Previous work from our group has shown that intratracheal administration of BLM induces lung injury, including weight loss, lung edema, and neutrophilia, in C57BL/6 mice (Hrusch et al., 2018). We found that C57BL/6 mice and wild-type (WT) littermates of the B6.ICOS$^{-/-}$ strain survived BLM challenge at a dose of 1 U/kg when the experiments were performed in one of our University of Chicago animal housing facilities (Facility A). However, WT littermates from multiple strains on a C57BL/6 background (B6.PHIL and B6.PLZF$^{-/-}$ strains) died at a significantly higher rate when we performed experiments in a different housing facility (Facility B) (Figure 3.17A). Both facilities are maintained at the SPF Barrier I level by the same Animal Resource Center of the University. To ensure the exclusion of certain pathogens, these facilities are equipped with directional airflow and provided with irradiated diets and autoclaved caging and bedding. Since both facilities are at the same barrier level, the transfer of animals between the two facilities are allowed, and researchers can enter these facilities in any sequence. Therefore, it was surprising to observe vastly different survival in animals between the facilities. The different colonies of WT littermates on the C57BL/6 background were all born and raised in the respective rooms where the animals were BLM challenged and subsequently monitored. The BLM

model is sensitive to the sex and age of the mice and the source of BLM (Lamichhane et al., 2022; Redente et al., 2011). For example, male mice are significantly more susceptible to weight loss, pro-inflammatory response, and fibrosis in the BLM model (Lamichhane et al., 2022; Voltz et al., 2008). Consistent with this known phenomenon, the facility-dependent difference in BLM susceptibility was prominent in adult male mice while female mice rarely died in both facilities during the present study. Next, we used the same BLM stock and personnel to challenge age- and sex-matched male C57BL/6 mice in both facilities on the same day. Again, we observed a striking difference in survival among matched mice between the two facilities (Figure 3.17B). Furthermore, the differential susceptibility to lung injury between mice in the two facilities was observed in a second lung injury model using LPS (Figure 3.18). These data suggest that the phenomenon we observed is relevant for some common pathways induced during lung injury.

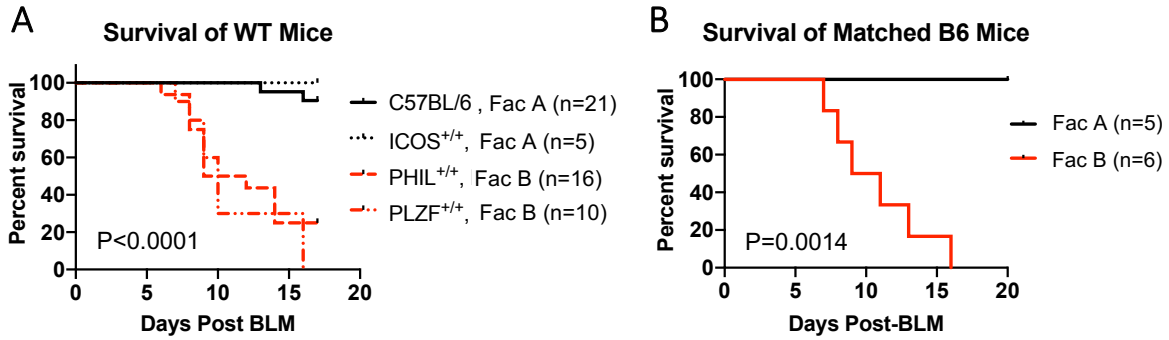

Figure 3.17: WT mice housed in two SPF housing facilities exhibit differential survival in response to lung injury. The response to bleomycin was measured in WT mice that are all on a C57BL/6 background but born and raised in separate SPF animal housing facilities at the University of Chicago. Mice received 1.0U/kg bleomycin intratracheally and were monitored daily for weight loss and survival. Mice were euthanized if they lost 25% or more of the original weight. (A) Survival data compiled from multiple experiments. (B) Survival of age matched male B6 mice in two facilities after being challenged with the same stock of BLM on the same day. P-values were obtained from log-rank test.

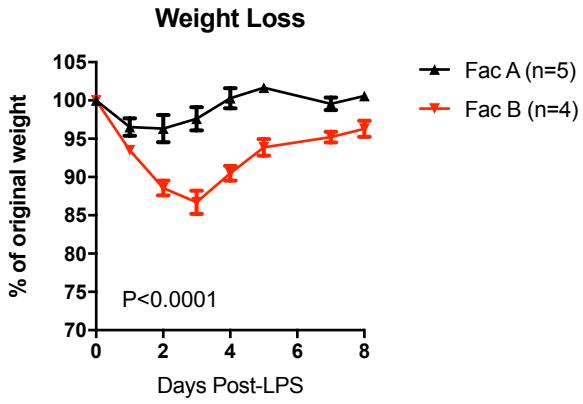

Figure 3.18: Intratracheal LPS-induced ALI responses in mice housed in the two facilities. Mice were challenged with 1mg/kg LPS. 2-way ANOVA was performed to assess statistical significance.

Conventionalizing germ-free mice recapitulates the respective donors' responses to BLM challenge.

We hypothesized that the difference in microbiota in our two animal housing facilities could be responsible for the difference in susceptibility to the BLM challenge. To test this hypothesis, germ-free (GF) C57BL/6 male littermates were conventionalized in either of the two facilities by adding dirty bedding and feces from neighboring cages housing WT SPF mice in respective facilities twice a week. The mice were conventionalized for 2 weeks according to a published study design that demonstrated that the horizontal transfer of bacteria and differentiation of host immune cells are achieved after 2 weeks of cohousing of animals (Ivanov et al., 2008).

The conventionalized ex-GF mice were challenged with BLM (Figure 3.19A). We monitored body weight as an indicator for the degree of lung injury since there is a significant correlation between body weight loss and lung injury for the BLM model (Cowley et al., 2019). Mice that lost 25% or more of their starting weight were euthanized even if the mice had sufficiently high wellness scores. Similar to the response of SPF mice, only one of the ex-GF mice in Facility A succumbed to BLM-induced lung injury (10%

mortality), while 5 out of 11 (45%) succumbed in Facility B (Figure 3.19B). Furthermore, the mice had already lost significantly more weight in Facility B by day 3, suggesting that the early response to lung injury was affected. Weight loss was significantly different throughout the experiment (Figure 3.19C). A limitation of our findings in Figure 3.17 was that while all the mice were of the C57BL/6 background, the origin of each strain was unknown, thus there could have been some genetic differences in mice. However, these results from conventionalized ex-GF C57BL/6 mice suggest that the weight loss during BLM-induced lung injury is influenced by the microbiota, independent of genetics of the mice.

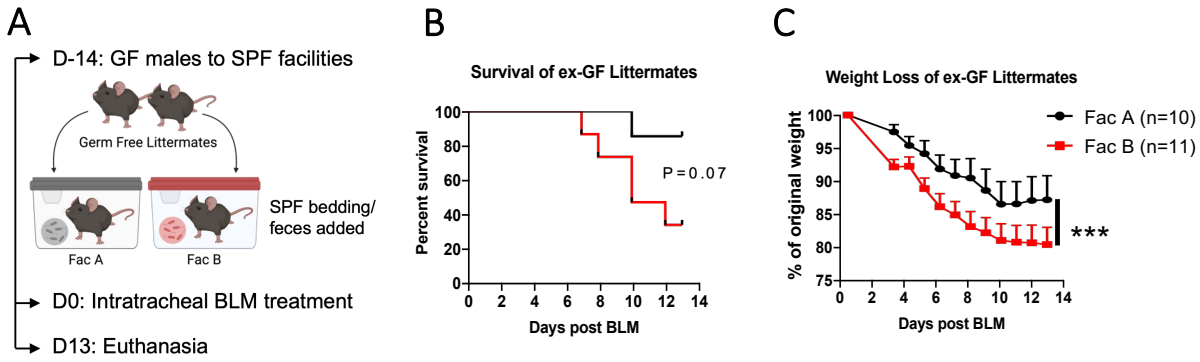

Figure 3.19: Conventionalizing germ-free littermates in two SPF facilities modulate the severity of lung injury response. (A) Germ-free C57Bl/6 male littermates were transferred into either of the two SPF facilities and conventionalized for 14 days by adding dirty bedding and feces from neighboring cages twice a week. Conventionalized ex-GF mice were treated with 1.0U/kg intratracheal bleomycin and monitored daily for survival and weight loss. (B) Survival and (C) weight loss of conventionalized ex-GF mice after bleomycin challenge. P-values were obtained from log-rank test and 2-way ANOVA, respectively, and depicted as $P<0.05$ (*), $P<0.01$(**), $P<0.001$(***).

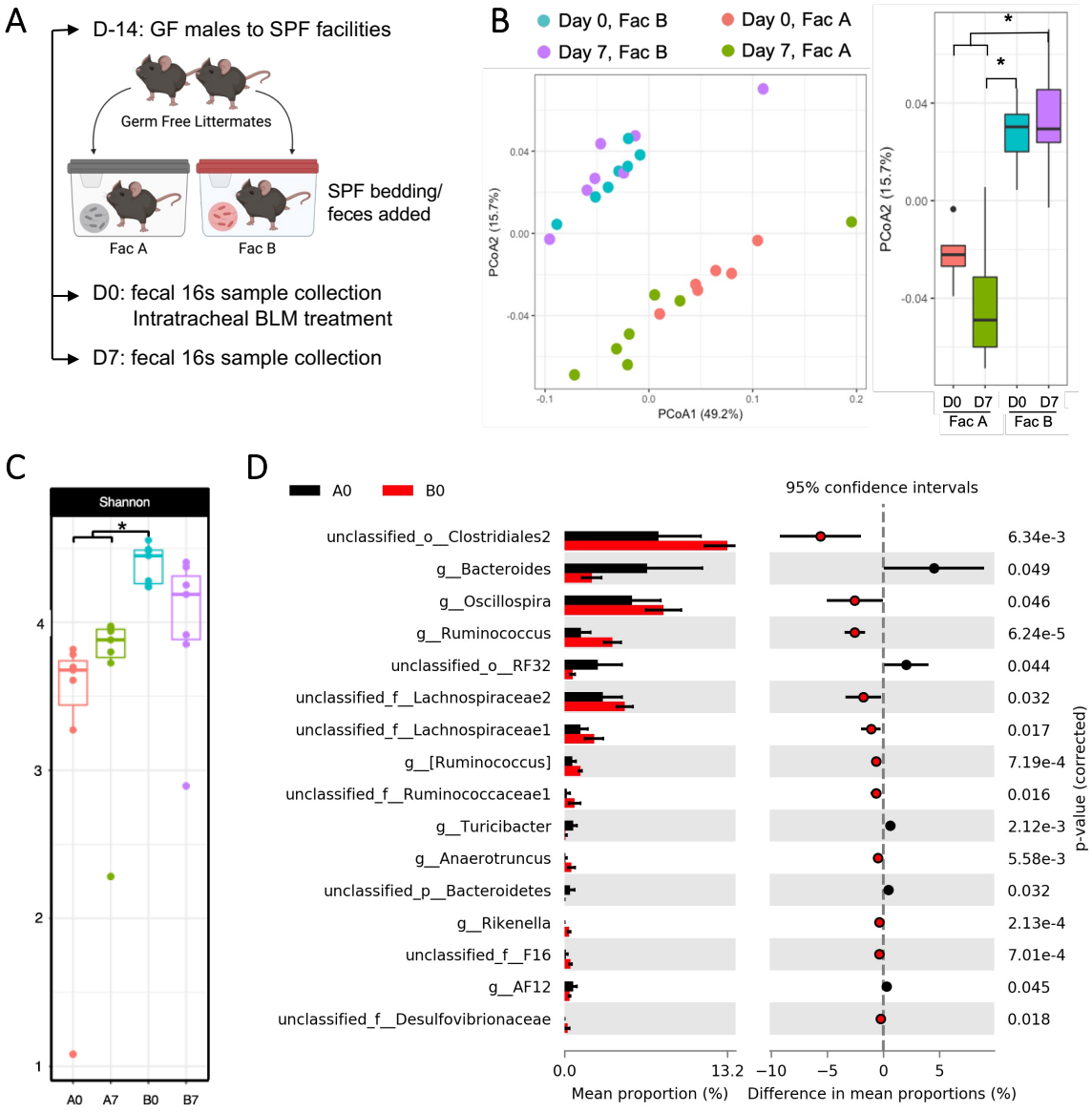

Figure 3.20: Gut microbial community structures are different between the two SPF facilities. (A) Following the 14-day conventionalization, fecal samples were collected from ex-GF mice at before (D0) and after (D7) bleomycin challenge (n=7 per condition). Gut microbial structures were analyzed by 16S rRNA gene (V4 region) sequencing of the fecal samples. (B) Weighted UniFrac analysis of similarity coefficients were calculated from 16S rRNA gene sequences of each mouse. Permutational multivariate analysis of variance was done to analyze paired statistical differences in beta diversity.

Figure 3.20: continued. (C) The within-sample richness and evenness (alpha diversity) were measured by Shannon diversity index (A0 vs. B0 (p-value = 0.0003); A7 vs. B0 (p-value = 0.0267)). (D) Differential abundance of microbial taxa between the two facilities at D0 was analyzed using the Statistical Analysis of Metagenomic Profiles (STAMP) package. P-value of 0.05 was used as a cutoff.

Conventionalized ex-GF mice in two SPF housing facilities harbor unique fecal microbiomes

To investigate whether the difference in BLM susceptibility among conventionalized ex-GF mice in the two SPF facilities can be attributed to microbial communities, we performed 16S rRNA gene amplicon sequencing of fecal samples obtained either at the time of (A0 and B0) or 7 days after (A7 and B7) the BLM challenge (Figure 3.20A). Weighted UniFrac analysis of the amplicon sequence variants (ASV) showed that there was a significant difference in community structures of the fecal microbiomes in animals in the two facilities (Figure 3.20B). The difference in weighted UniFrac distance between the two facilities was evident on the second principal component (PCoA2), independent of BLM challenge. Shannon index, which is a measure of total ASV number and the abundance of each ASV, was significantly higher in the samples from Facility B mice at baseline compared to that from Facility A mice at both baseline and 7 days after BLM challenge (Figure 3.20C). These data suggest that not only are the overall structures of microbial communities different, but also the species diversity is greater in the microbial community in Facility B mice compared to Facility A mice.

To investigate whether specific taxa drive the difference in gut microbial diversity and structure, we compared the relative abundance of ASV by performing statistical analysis of metagenomic profiles (STAMP) on data from unperturbed animals. We found that members of *Ruminococcaceae* (family), *Lachnospiraceae* (family), *Oscillospira* (genus), *Rikenella* (genus), and *Desulfovibrionaceae* (family) were significantly more abundant in Facility B, whereas *Bacteroides* (genus) and *Turicibacter* (genus) were significantly

enriched in Facility A (Figure 3.20D). Three taxa with relatively high abundance in Facility B mice at baseline, including *Ruminococcaceae*, *Lachnospiraceae* and *Oscillospira*, are all members of the order *Clostridiales*. Additionally, some unclassified members of *Clostridiales2* were among the most differentially enriched taxa in Facility B mice.

Interestingly, we observed a shift in the abundance of *Clostridiales* after BLM treatment. Analyses of samples collected on day 7 after the BLM challenge revealed that the abundance of *Clostridiales2* was no longer significantly different, whereas some unclassified members of *Clostridiales1* (order) became significantly less abundant in Facility B mice compared to Facility A mice (Figure 3.21). Furthermore, there was enrichment of *Bifidobacterium* (genus), *Adlercreutzia* (genus), and *Turicibacter* (genus) in Facility A mice after BLM challenge. Interestingly, the significant enrichment of some members of *bacterium F16* (family) and *Desulfovibrionaceae* (family) among mice in Facility B was maintained even after BLM treatment (Figure 3.21). Overall, our analyses of the 16S rRNA gene sequence showed that the community structures and relative abundance of specific taxa are significantly different between genetically similar littermate mice that are conventionalized in two different facilities.

Transfer of fecal microbiota between SPF mice in one housing facility to another modulates susceptibility to intratracheal BLM

Given that unique microbiomes are maintained in each housing facility, we sought to determine whether each facility's microbiome is associated with the promotion or prevention of lung injury. Although the differential BLM susceptibility phenomenon was initially observed throughout multiple inbred mouse strains in our animal facilities, some heterogeneity in the microbial community even in the same facility is inevitable due to the vertical transmission of mammalian gut microbiota from different ancestral origins (Moeller et al., 2018). To control for a possible impact of the ancestral microbiome, the progeny of

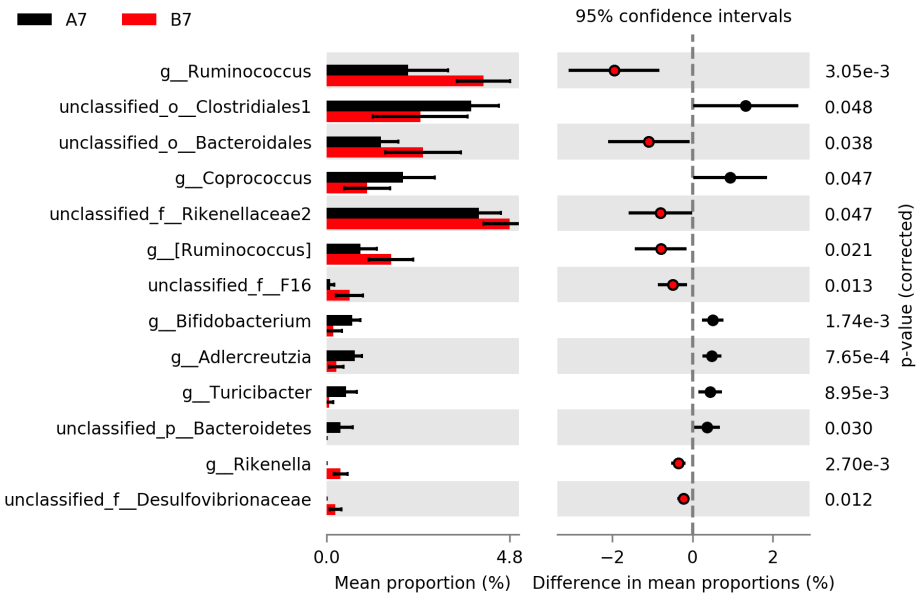

Figure 3.21: 16S rRNA sequencing of conventionalized ex-GF mice on D7 after BLM challenge. Differential abundance of fecal microbial taxa between animals in the two facilities at 7-days post BLM treatment was analyzed using the Statistical Analysis of Metagenomic Profiles (STAMP). P-value of 0.05 was used as a cutoff.

conventionalized ex-GF littermates in each animal facility were maintained as stable SPF colonies for multiple generations and used for all following experiments in this study. To investigate whether the transfer of fecal microbiota from mice in one facility into mice housed in another facility can modulate susceptibility to BLM-induced lung injury, we performed fecal microbiota transfer (FMT) in these SPF mice. Without prior manipulation of the endogenous microbiome, SPF littermates in both facilities received FMT from animals in either the same facility or another facility via oral gavage 3 times, and then the mice were challenged with BLM. Strikingly, introducing the Facility B microbiota was sufficient to increase the weight loss of SPF animals in Facility A, compared to their littermate controls, in response to the BLM challenge (Figure 3.22A). However, the Facility A microbiota did not change the BLM-induced weight loss of animals in Facility B (Figure 3.22B). These data suggest that some components of Facility B microbiota are responsible for worsening the BLM-induced weight loss in mice in a dominant-negative

manner.

Colonization of *Helicobacter* and *Desulfovibrio* species are associated with increased weight loss during ALI response

To ensure the colonization of transplanted microbiome, we characterized fecal microbiomes of the mice at both baseline and after FMT by 16S rRNA gene amplicon sequencing. Alpha-diversities of the microbiome in FMT recipient animals were comparable to those of control animals, despite the introduction of additional microbial species (Figure 3.22C). Unweighted UniFrac analysis revealed that the microbial community structures of mice from the two facilities were distinct at baseline, but they became more similar to the respective donor microbiomes after FMT (Figure 3.22D). Facility B microbiota recipients (Fac B→A FMT), which showed the most significant change in lung injury response, had the greatest shift in PCoA1 of their fecal microbiomes. Since UniFrac takes the phylogenetic distance into account (Lozupone and Knight, 2005), the drastic difference in the beta diversity could be driven by the engraftment of some phylogenetically distant lineages by FMT.

Using 16S rRNA gene analysis, we investigated whether the Facility B donor-specific taxa can successfully colonize the FMT recipients in Facility A. Based on the percent sequence reads, we found that two members of *proteobacteria*, *Helicobacter* and *Desulfovibrionaceae*, were among the most consistently colonized genera (Figure 3.22E and Figure 3.23) across biological replicates. Importantly, several donor-specific taxa also showed successful engraftment in the Facility A microbiota recipients (Fac A→B FMT) despite driving a small shift in PCoA1. The newly introduced microbes from Facility A were assigned to multiple phyla, including *Vampirovibrio*, *Ruminococcus*, *Alloprevotella*, *Allobaculum*, and *Akkermansia* (Figure 3.24). These findings suggest that the Facility A microbiota is unable to suppress the negative effect of pre-existing microbiota in Facility B mice, but Facility B microbiota can dominantly worsen the BLM-induced weight loss in

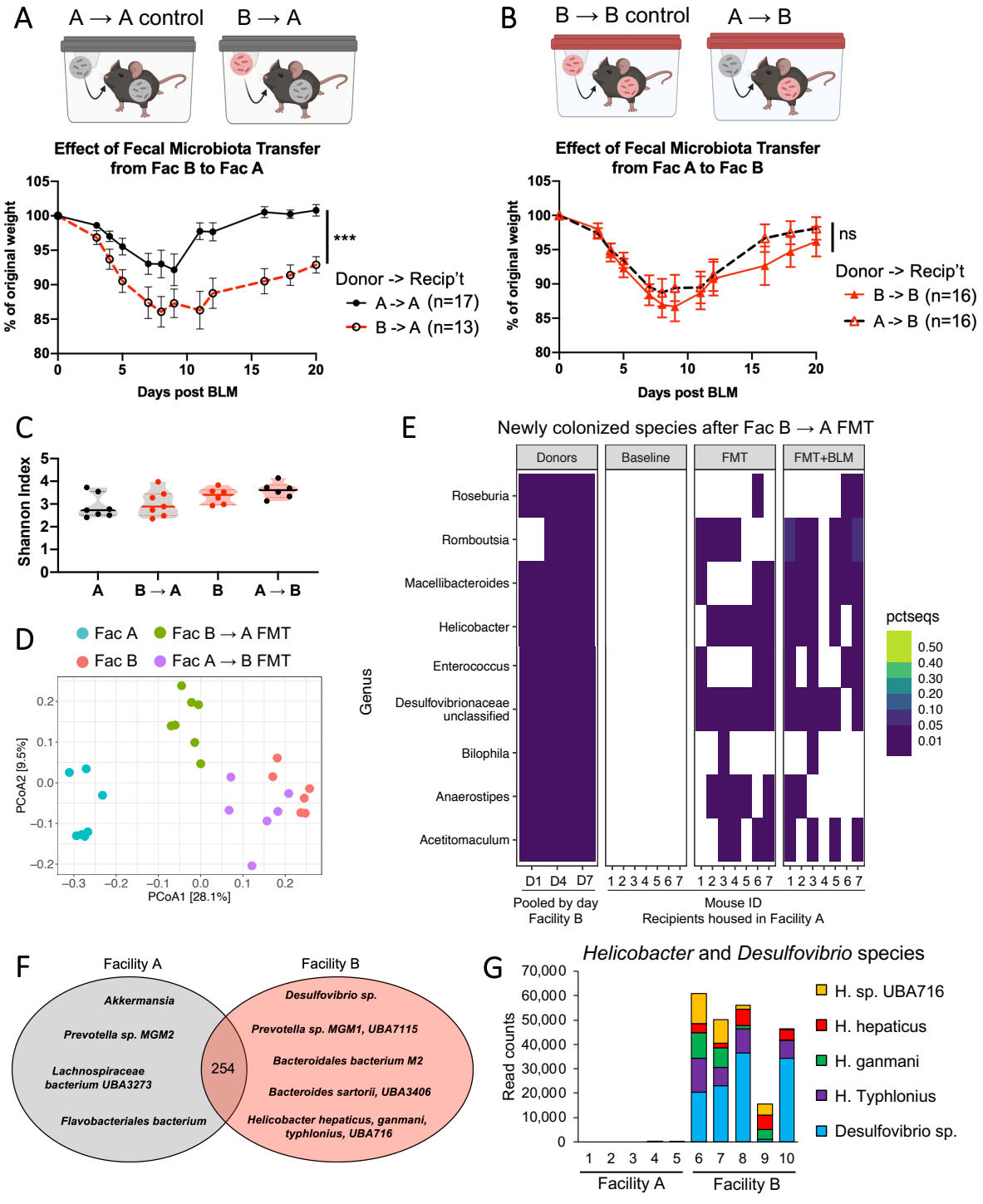

Figure 3.22: Additive fecal microbiota transfer from Facility B to A renders the recipients more susceptible to the lung injury response.

Figure 3.22: continued. (A-B) Littermate progenies of the conventionalized ex-GF founders that were born and raised in each SPF facility were separated into two cages. One cage of mice received the pooled fecal slurry from themselves (A→A or B→B), and another cage of mice received the pooled fecal slurry from mice housed in different facility (A→B or B→A), via 3 oral gavages in a week. 10-days after the first dose of gavage, the mice were challenged with 1 U/kg of intratracheal bleomycin. Weight curves showing the effect of fecal microbiota transfer from the Facility B to A (A), and from the Facility A to B (B). Overall, around 70% of the mice from all groups survived with no statistically significant difference, and datapoints were censored upon death. P-values were obtained from the mixed-effects analysis of the data and depicted as $P<0.001$ (***) or non-significant (ns). (C-E) Fecal samples collected from FMT recipients at before and after gavaging were sequenced for 16S rRNA genes (V4-V5 region). (C) The within-sample richness and evenness (alpha diversity) were measured by Shannon index. Four groups are A: samples were collected from Facility A mice prior to FMT (n=7), B→A: samples were collected from Facility A mice at 10 days after the first dose of Facility B microbiota transplant (n=7), B: samples were collected from Facility B mice prior to FMT (n=6), A→B: samples were collected from Facility B mice at 10 days after the first dose of Facility A microbiota transplant (n=6). (D) Unweighted UniFrac analysis of similarity coefficients were calculated from 16S rRNA gene sequences of each mouse. (E) Heatmap of the percent sequence amplicons measured from a list of commensal taxa that were present in donor mice in Facility B but absent in recipient mice in Facility A at baseline. Fecal samples from donor mice were pooled and sampled on days of gavage treatment. Fecal samples from 7 recipient mice were collected longitudinally at baseline, 10-days after the first dose of gavage (FMT), and 7-days after bleomycin challenge (FMT+BLM). (F-G) Shallow shotgun metagenomics analysis of fecal samples from progenies of the conventionalized ex-GF founder mice in the two facilities. The samples were collected from naïve mice without any treatment. Total 268 unique taxa were identified using k-mer based classification on One Codex databse (Transnetyx), (F) Venn diagram showing the taxa that were exclusively present in each facility. (G) Read counts for species within *Helicobacter* and *Desulfovibrio* genera in 10 mice sampled for metagenomic sequencing analysis.

Facility A mice.

To further elucidate the microbes that may be responsible for promoting severe weight loss in Facility B mice, we performed shotgun metagenomic sequencing of fecal microbiota from naïve mice in the two facilities. A total of 268 taxa were identified from fecal sample sequences. The normalized reads for virus, fungi, archaea, and protists were less than 0.005%, and there was no observable difference in compositions of these non-bacterial taxa between animals from the two facilities. Similar to the results of differentially colonized taxa in FMT recipients, we found members of both *Desulfovibrio* and *Helicobacter* genera to be

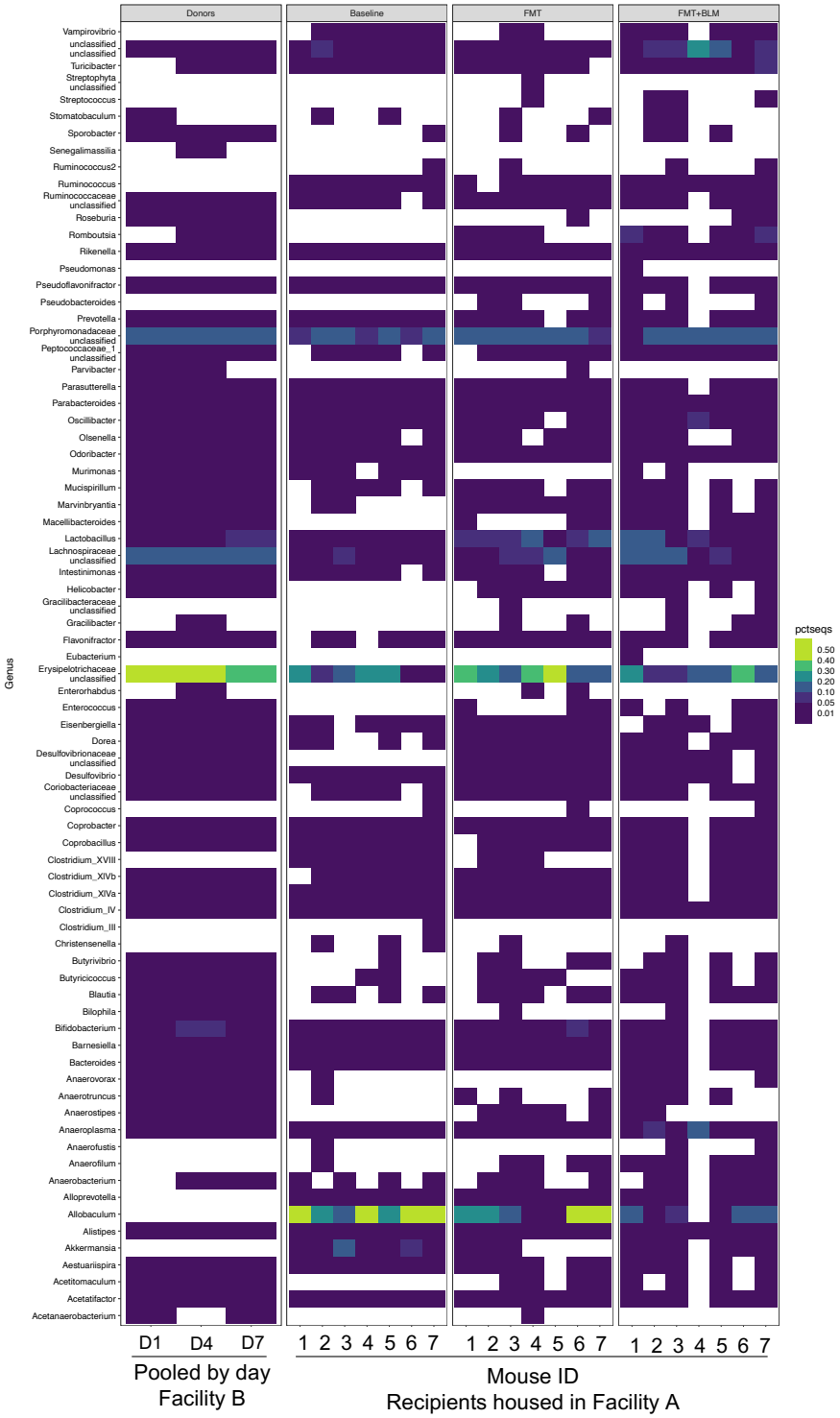

Figure 3.23: Full list of taxa resolved from fecal samples from donor and recipient mice in the Facility B-to-A FMT experiment.

Figure 3.23: continued. Heatmap visualizing percent sequences of all the taxa resolved to genus level. Fecal samples from donor mice of Facility B microbiota were pooled and sampled on each day of gavage treatment. Fecal samples from 7 recipient mice in Facility A were collected longitudinally at baseline, 10-days after the first dose of gavage (FMT), and 7-days after bleomycin challenge (FMT+BLM).

exclusively present in Facility B microbiota at baseline (Figure 3.22F). With the greater resolution provided by metagenomic sequencing, we were able to identify candidate microbes at the species level. The microbial species associated with severe weight loss in Facility B included *Desulfovibrio sp.* (Tax ID 885), *Helicobacter hepaticus* (Tax ID 32025), *H. ganmani* (Tax ID 60246), *H. typhlonius* (Tax ID 76936), and *H. UBA716* (Tax ID 1946589), all of which were absent in the Facility A microbiota (Figure 3.22G). Thus, our results from both 16S rRNA gene and metagenomic sequencing suggest that *Desulfovibrio* and *Helicobacter* species are candidate microbes that modulate the degree of weight loss during BLM-induced lung injury.

Naïve SPF mice housed in Facility A and Facility B have unique immunophenotypes

The gut microbiota plays an essential role in the development and maintenance of the host's immune system, which can determine the health of not only the gut, but also distant organs including the lungs. To test the hypothesis that SPF mice housed in the two facilities have distinct baseline immunophenotypes, we designed comprehensive flow cytometry panels for T cells, dendritic cells, B cells, innate immune cells, and innate-like lymphocytes and analyzed gut-draining lymph nodes (gLN), spleens, and lungs of age- and sex-matched naïve animals from the two facilities. First, we focused on investigating phenotypes of T cells in the gLN as some commensal microbes in our housing facilities are known to regulate T helper cell differentiation. As *H. hepaticus* is a pathobiont, WT mice have adapted a tolerance mechanism, which is induction of RORγt$^+$Foxp3$^+$ regulatory T (Treg) cells that suppress

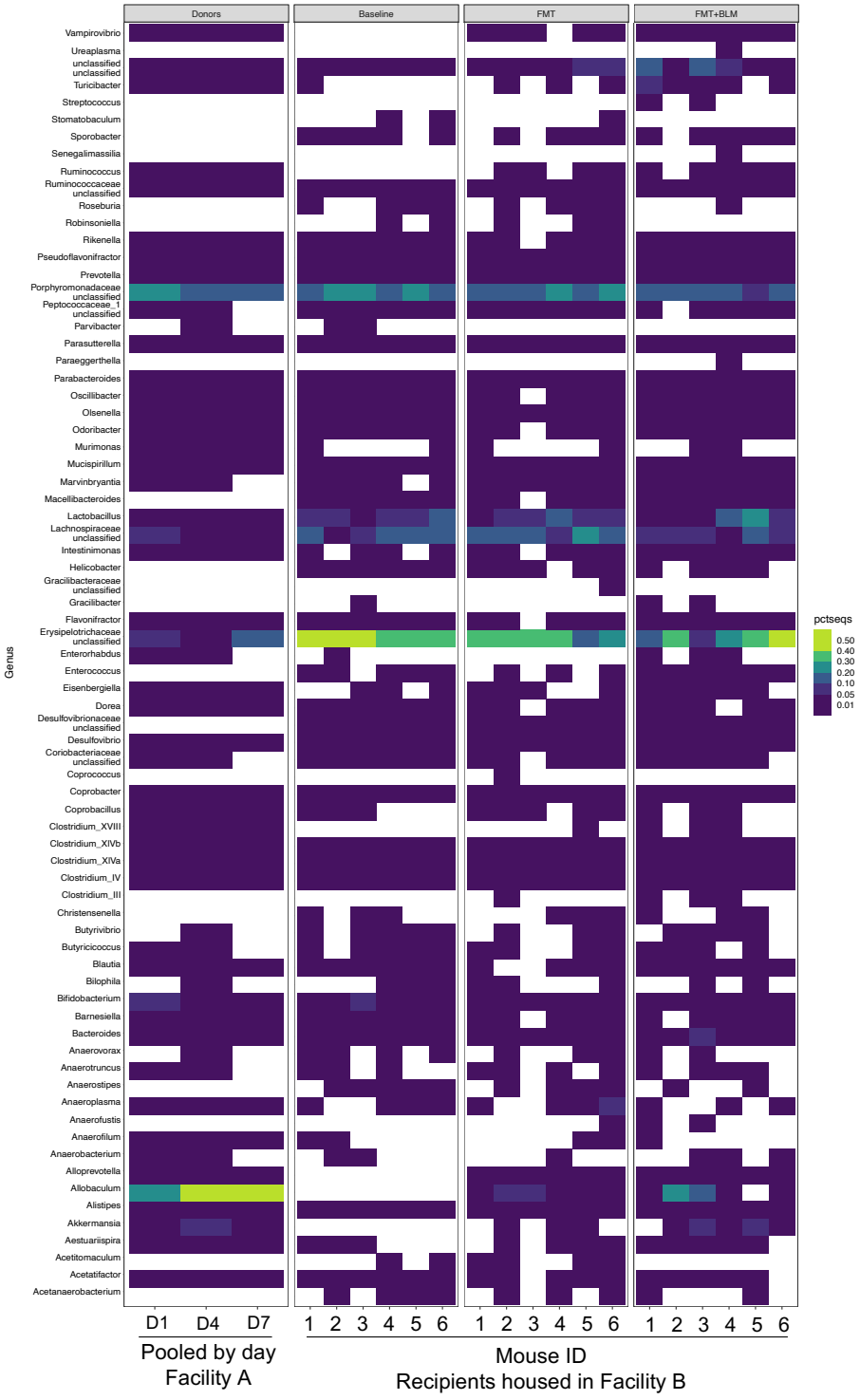

Figure 3.24: Unchanged lung injury outcome in Fac A microbiome recipients is not due to the lack of colonization of additional species.

Figure 3.24: continued. Heatmap visualizing percent sequences of all the taxa resolved to genus level. Fecal samples from donor mice of Facility A microbiota were pooled and sampled on each day of gavage treatment. Fecal samples from 6 recipient mice in Facility B were collected longitudinally at baseline, 10-days after the first dose of gavage (FMT), and 7-days after bleomycin challenge (FMT+BLM).

pro-inflammatory T helper 17 (Th17) cells (Kullberg et al., 1998; Xu et al., 2018). Consistent with this, we found that RORγt$^+$ Treg cells were increased and Th17 cells were decreased in gLN of the *H. hepaticus*-harboring mice in Facility B compared to the Facility A mice at baseline (Figure 3.25A-B, Figure 3.26A). However, compositions of adaptive immune cells in the lungs were comparable between naïve mice in the two housing facilities (Table 3.3).

Next, we performed FlowSOM clustering analysis to compare overall landscapes of the innate immune cells in the lungs of naïve mice in the two facilities. We found that FlowSOM population 8 was increased, and population 9 was decreased in Facility B mice compared to Facility A mice (Figure 3.25C). Cells in population 8 expressed markers consistent with NK cells, and neutrophil markers were expressed in population 9 (Figure 3.25D). Based on the manual gating, we confirmed that the proportion of NK cells was increased, and neutrophils were decreased in the lungs of Facility B mice (Figure 3.25E-F, Figure 3.26B-C). Interestingly, the frequency of neutrophils was also lower in the spleens of Facility B mice, further corroborating our results (Figure 3.26D). This suggests that granulopoiesis during homeostasis might be differentially regulated in these SPF mice with distinct gut microbiota. Overall, our data demonstrate that mice housed in the two facilities have distinct immunophenotypes, such that the gut lymph node Th17 cells and systemic neutrophils are downregulated in Facility B mice at baseline.

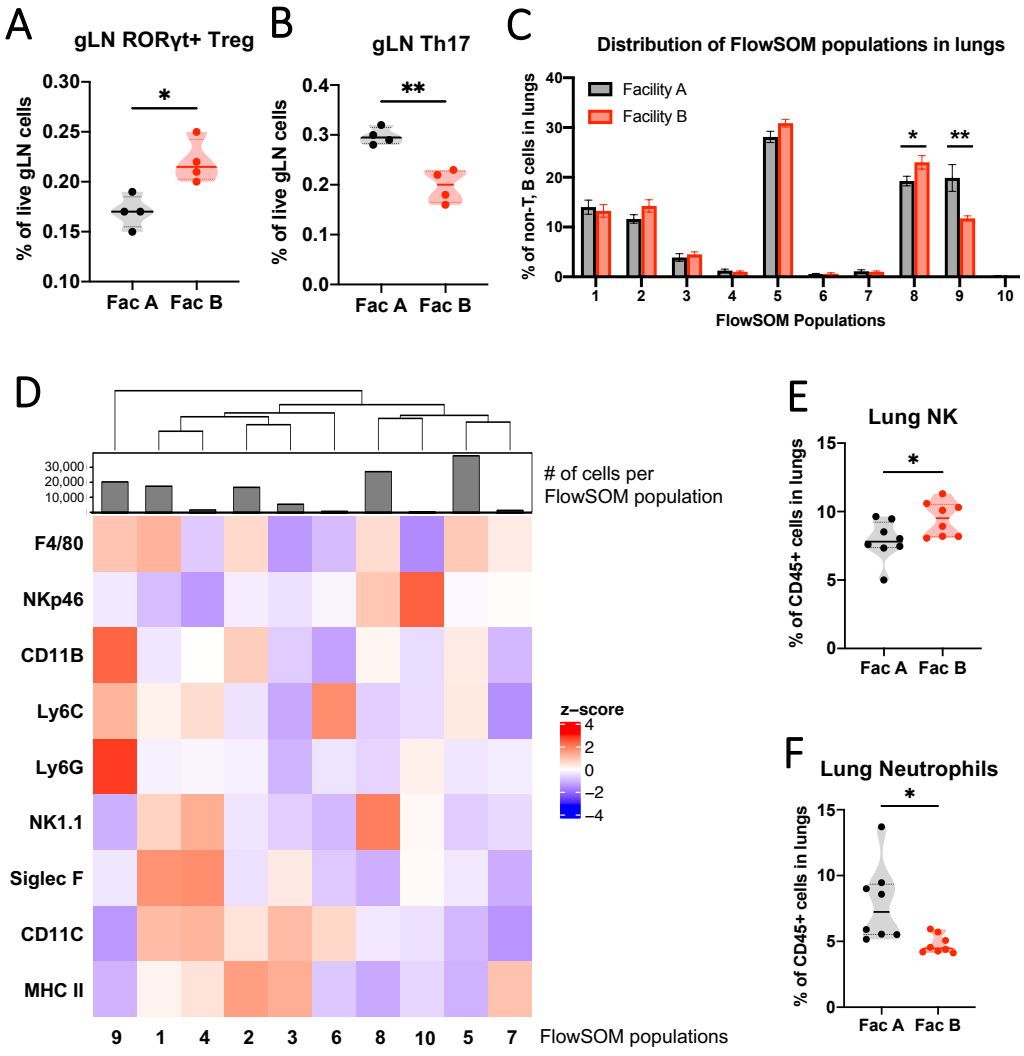

Figure 3.25: Differential colonization of commensal species corresponds with specific immunolandscapes of the lungs in naïve animals. Gut-draining LN and lungs of unperturbed progenies of the conventionalized ex-GF founders were immunophenotyped. (A) Frequencies of RORγt$^+$ Treg (CD25$^+$ Foxp3$^+$) cells in gLN. (B) Frequencies of Th17 (RORγt$^+$ Foxp3$^-$) cells in gLN. (C-D) Non-adaptive immune cell population (CD45$^+$ CD3$^-$ CD19$^-$) in the lungs were analyzed using the FlowSOM clustering algorithm. Total 128,000 cells were analyzed from n=8 mice from each facility (Down sampled to 8,000 cells per mouse). FlowSOM generated 10 clusters with unique phenotypes. (C) Proportion of cells in each cluster is compared between mice in the two facilities. Multiple unpaired t-tests using the two-stage step-up method were performed for statistical analysis. (D) Heatmap of expressions of 9 markers in each cluster. (E) Frequencies of NK cells in the lungs based on manual gating (NK1.1$^+$ lineage$^-$). (F) Frequencies of neutrophils in the lungs (Ly6G$^+$ CD11b$^+$ lineage$^-$). P-values were obtained from student t-tests and depicted as P<0.05 (*), P<0.01(**), P<0.001(***).

Table 3.3: Frequencies of immune cell populations in the lungs of unperturbed mice raised in the two SPF housing facilities. (n=8 per facility, 15-17 weeks of age, values are the percent of $CD45^+$ cells (± standard deviation), and p-values are from t-test.)

Lung immunophenotypes at baseline. Values as percent of CD45+ (± standard deviation)			
Cell population	Fac A	Fac B	P-value
Neutrophils	7.86 (±2.94)	4.78 (±0.71)	0.01
Eosinophils	2.87 (±0.66)	3.39 (±1.17)	0.29
DC	5.13 (±1.45)	6.46 (±1.47)	0.09
Monocyte	12.07 (±1.86)	13.76 (±0.97)	0.04
NK cells	7.88 (±1.46)	9.46 (±1.27)	0.04
B cells	36.45 (±7.57)	36.04 (±4.27)	0.90
$T_{\gamma\delta}$ cells	5.16 (±0.75)	5.33 (±0.54)	0.62
$T_{\alpha\beta}$ cells	19.58 (±4.06)	20.04 (±2.26)	0.78
CD8 T cells	4.14 (±0.49)	4.78 (±1.01)	0.13
CD4 T cells	10.06 (±2.64)	9.23 (±1.19)	0.43
T_{conv}	8.60 (±2.32)	7.85 (±1.17)	0.43
Th1	1.29 (±0.53)	1.40 (±0.60)	0.69
Th2	0.42 (±0.23)	0.42 (±0.17)	0.93
Th17	0.53 (±0.47)	0.23 (±0.07)	0.10
T_{reg} (all Foxp3+)	1.41 (±0.36)	1.31 (±0.22)	0.53
TBET+ T_{reg}	0.13 (±0.04)	0.15 (±0.09)	0.52
GATA3+ T_{reg}	0.17 (±0.09)	0.18 (±0.07)	0.79
RORγt+ T_{reg}	0.07 (±0.04)	0.07 (±0.03)	0.91
CD25+ T_{reg}	0.65 (±0.18)	0.60 (±0.11)	0.52
TBET+ CD25+ T_{reg}	0.04 (±0.02)	0.05 (±0.06)	0.49
GATA3+ CD25+ T_{reg}	0.08 (±0.05)	0.08 (±0.04)	0.83
RORγt+ CD25+ T_{reg}	0.03 (±0.02)	0.04 (±0.02)	0.29

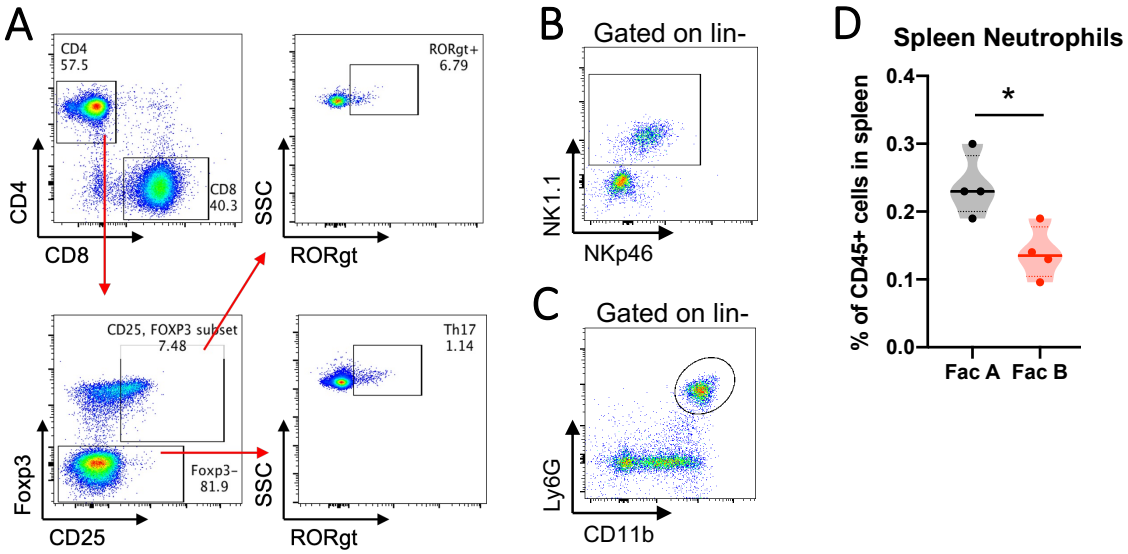

Figure 3.26: Examples of flow cytometry gating strategies and frequencies of spleen neutrophils in naïve animals. (A) Gating strategies for RORγt$^+$ CD25$^+$ Treg and Th17 populations, using gLN cells as representative. (B) Gating strategy for NK cells in lungs. Cells were pre-gated on CD45$^+$, TCRb$^-$, CD19$^-$, non-AM, non-neutrophil, non-Eosinophil, non-DC population. (C) Gating strategy for neutrophils in lungs. Cells were pre-gated on CD45$^+$, TCRb$^-$, CD19$^-$, non-AM population. (D) Frequency of neutrophils in spleens of unperturbed animals housed in the two facilities. T-test was done to obtain the p-value.

Neutrophil recruitment to the lungs is more robust in Facility B mice during BLM-induced lung injury response

To investigate whether the cellular responses during BLM are different between animals housed in the two facilities, we immunophenotyped lungs of mice at 3 days post-BLM administration. Facility B mice were more sensitive to BLM treatment and recruited more neutrophils to the lungs during the acute phase of injury, even though control PBS treated mice in Facility B maintained neutrophils at lower levels than Facility A control mice (Figure 3.27A). On day 3 after BLM treatment, lung neutrophils were increased by over 1.5-fold after BLM treatment in Facility B mice, compared to little change in Facility A mice (Figure 3.27B). By day 6 post-BLM, neutrophils were recruited at similar levels in

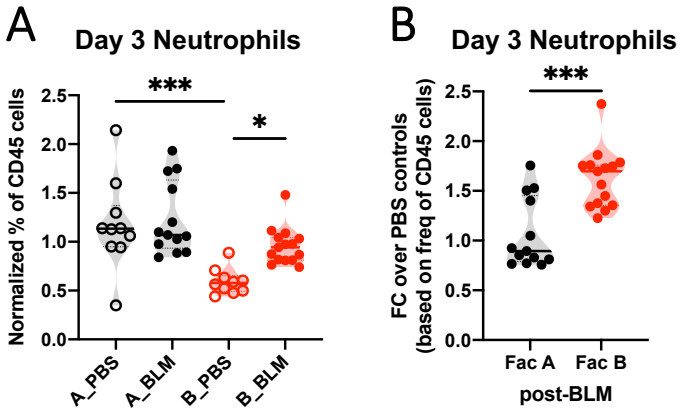

Figure 3.27: Relatively increased neutrophil recruitment to the lungs during lung injury coincides with worse weight loss in mice in Facility B. Lungs were harvested from progenies of the conventionalized ex-GF founders in the two facilities after bleomycin (1U/kg) or PBS (vehicle control) challenge. (A) Normalized frequencies of neutrophils in the lungs on day 3 post-BLM. Data from three independent experiments were combined, and experimental values were normalized by the group variance for each experiment. The cells were gated based on Ly6G$^+$ CD11b$^+$ lineage$^-$ as shown in Figure 3.26C. P-values were obtained from Sidak's multiple comparisons test after confirming $P<0.05$ from one-way ANOVA. (B) Fold change of neutrophil accumulations in lungs on 3 days after bleomycin challenge compared to PBS treatment in each facility. P-values are depicted as $P<0.05$ (*), $P<0.01$(**), $P<0.001$(***).

lungs of mice in both housing facilities (data not shown). Histopathological analysis of lung sections showed that BLM-treated lungs of mice in both facilities have similar patterns of patchy neutrophilic alveolitis as previously described (Matute-Bello et al., 2008) (Figure 3.28). Therefore, increased neutrophil numbers at homeostasis may confer protection from BLM-induced weight loss, while a rapid fold increase in neutrophils during BLM response is detrimental.

3.2.4 Discussion

Our study demonstrates that the composition of commensal fecal microbiota impacts the severity of BLM-induced weight loss in C57BL/6 mice. Using various mouse strains that we maintain in two animal housing facilities on campus, we observed that BLM-challenged WT

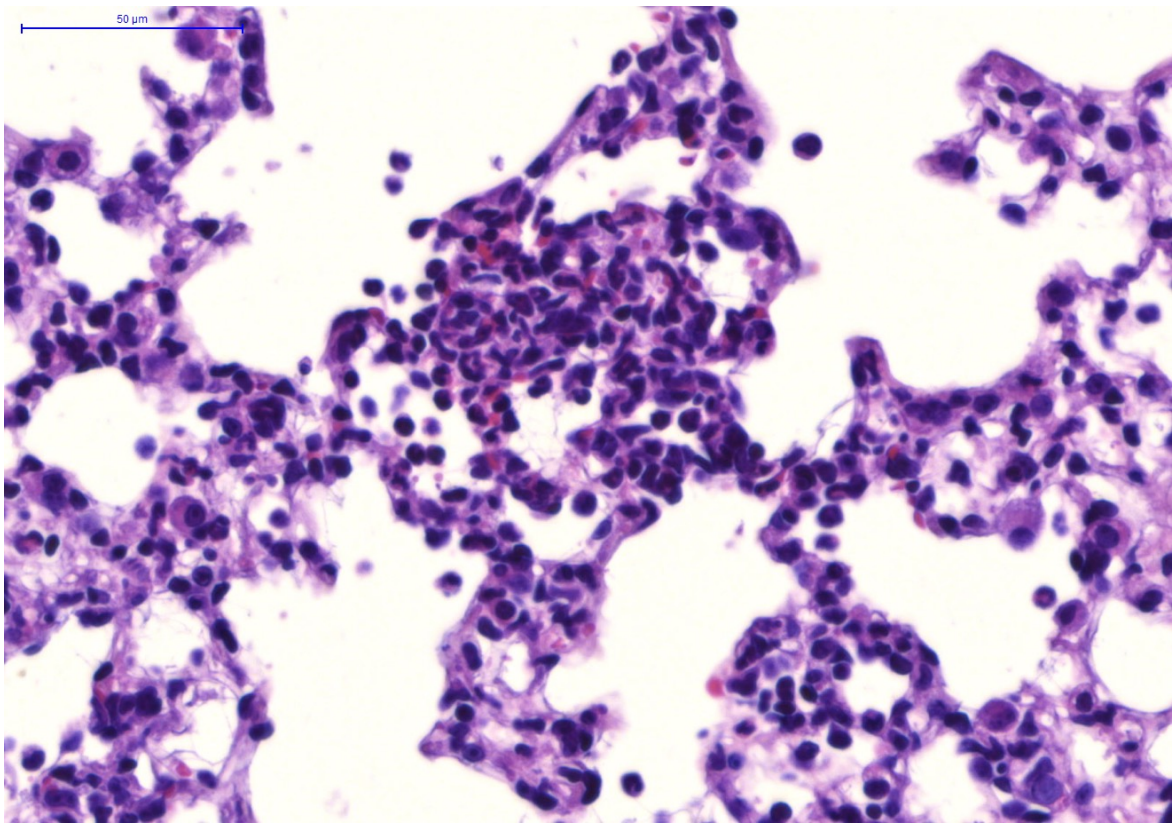

Figure 3.28: Hematoxylin and eosin (H&E) staining of a mouse lung section on day 3 post-BLM challenge. An example of patchy neutrophilic alveolitis that are found in BLM-treated mice in both housing facilities. The image shown here is from a Fac B mouse, but a similar histopathological pattern was observed in Fac A mice. For staining, left lungs harvested from mice on day 3 post-BLM treatment were formalin fixed and paraffine embedded. Lung blocks were sectioned at 5µm thick and stained with H&E. Slides were imaged with a 40x objective using the CRi Pannoramic SCAN. The scale bar is 50µm long.

littermate control mice have strikingly high mortality in one facility (Facility B), compared to the mice in another facility (Facility A). We determined that WT mice maintain distinct gut microbial communities based on housing facilities in which the mice were born and raised, despite both facilities having the same SPF protocols. Further, unperturbed WT mice in Facility B had lower Th17 and neutrophil levels compared to Facility A mice. During the BLM challenge, Facility B mice responded with a greater fold increase in lung neutrophils, indicating a more severe inflammatory response. We demonstrate that the BLM-highly-susceptible phenotype is transferrable by the fecal microbiota. When the two microbial

communities are combined, the Facility B-associated microbiota exerts a dominant-negative effect. We identify members of *Helicobacter* and *Desulfovibrio* genera as candidate microbes that contribute to the increased susceptibility to BLM-induced weight loss.

While the initial observation was on survival difference between various B6 strains housed in the two facilities, the effect of the microbiota on genetically identical animals and their progenies became largely evident by the degree of weight loss rather than survival. Weight loss and survival are directly linked because animal death in our survival study was mostly due to excessive weight loss. The less dramatic phenotypes in conventionalized GF mice and their SPF progenies are likely attributable to changes in microbiota compositions over the years of this study. Both facilities are maintained as level I barriers, which require constant monitoring for pathogens, personal protective equipment, and biosafety cabinet usage. Since there is no hierarchical entry restriction for these facilities, the relative abundance of some taxa could have been shifted over time. Therefore, we defined candidate microbes for body weight modulation during BLM-challenge by identifying the consistent differences between the two facilities in three independent sets of fecal microbiome sequencing data, which were collected at three different time periods. Notably, *Desulfovibrio* and *Helicobacter* always remained excluded from Facility A, and their presence in Facility B consistently correlated with aggravated weight loss following BLM during the past several years of the study period.

Our data suggest potential pro-inflammatory roles for *Desulfovibrio sp.* and some *Helicobacter* species during the lung injury response. *Desulfovibrio sp.* is an unknown species of the *Desulfovibrio* genus, which is a group of sulfate-reducing bacteria found in the gastrointestinal tracts of many animals including humans (Fox et al., 1994; Gibson et al., 1988). Little is known about this commensal species, but other related species of *Desulfovibrio* have recently been discovered to be associated with rare cases of bacteremia (Goldstein et al., 2003; Hagiya et al., 2018; Nasreddine et al., 2019). On the other hand, the immune impact of *H. hepaticus* has been well-documented in the context of gut health

and disease. *H. hepaticus* is a pathobiont, which can cause colitis in IL10-deficient mice only in specific microbial environments (Kullberg et al., 2001, 1998; Whary et al., 2011; Yang et al., 2013). Interestingly, gut colonization with *H. hepaticus* has been shown to promote persistent lung injury after Mycobacterium tuberculosis infection in mice (Majlessi et al., 2017), suggesting that crosstalk between *H. hepaticus* and the host immune system can modulate immune responses in the lungs. In support of this idea, we found that the proportion of RORγt$^+$ Treg cells is increased in gLN of naïve mice in Facility B, where *Helicobacter* species are present. Furthermore, the relative proportion of neutrophils is decreased in both lungs and spleens of BLM-highly-susceptible animals at baseline. IL-17A signaling via G-CSF is a key mediator of granulopoiesis and neutrophil recruitment (Schwarzenberger et al., 2000, 1998), and RORγt$^+$ Treg cells can specifically suppress Th17 cells, which secrete IL-17A Xu et al. (2018). Therefore, the systemic decrease in neutrophils that we observed in BLM-highly-susceptible animals at homeostasis could be explained by the expansion of Th17-specific immunoregulatory cells.

The implication of a decreased Th17-neutrophil axis at homeostasis in BLM-highly-susceptible mice is puzzling. Activated neutrophils during ALI play pathogenic roles by releasing proinflammatory cytokines and cytotoxic products, including granular enzymes, reactive oxygen species, and neutrophil extracellular traps (Albaiceta et al., 2010; Hayashi et al., 2002; Kellner et al., 2017; Lefrancais et al., 2018). Our finding that the Facility A mice showed no increase in lung neutrophils, while Facility B mice had over 1.5-fold increase in lung neutrophils in only 3 days after the BLM challenge is consistent with the known role of neutrophils in lung injury. However, the Facility B mice had relatively smaller proportions of neutrophils in the lungs at both baseline and during intratracheal PBS vehicle treatment. We postulate that increased neutrophils at homeostasis might be protective, and the gut microbiota may modulate neutrophils at homeostasis. It has been shown that the level of granulopoiesis during steady state is

influenced by the microbiota (Balmer et al., 2014; Tada et al., 1996). Further, some gut commensals can promote change in lung neutrophil phenotypes to provide protection from lung infection (Deshmukh et al., 2014; Felix et al., 2018). Thus, while mechanisms involved in the potentially protective role of neutrophils remain unclear, it's possible that the gut microbiota modulate granulopoiesis and neutrophil functions.

The effect of fecal microbiota transplant on lungs could be both systemic and lung specific. Since we transferred entire fecal contents, the effect may be systemic partially due to some metabolites and other secretory factors present in the slurry. For example, bacterial metabolites called short-chain fatty acids are known to maintain epithelial barrier integrity and protect against allergic inflammation in the lung (Trompette et al., 2014). Further, the level of fecal secretory IgA, which can be regulated by members of Sutterella genus microbes in the gut, determines the severity of dextran sodium sulphate-induced intestinal injury (Moon et al., 2015). These secretory factors in circulation could impact health of structural cells throughout the body, including the lungs. On the other hand, perturbation of the gut microbiota could affect the lungs via the gut-lung axis. Correlations observed between gut microbiome composition and respiratory disease development support the idea of crosstalk between the two organs (Budden et al., 2017; Huffnagle, 2010). Microbial communities in the gut and lungs have shown to be interconnected from the time of embryonic developmental in both health and disease (Grier et al., 2018; Madan et al., 2012). Furthermore, some gut microbes are abundantly found in the lungs and correlated with severity or development of ALI/ARDS in experimental models of sepsis and studies of mechanically-ventilated patients, respectively (Dickson et al., 2016; Panzer et al., 2018). Finally, while we delivered the fecal microbiota directly into the gut by oral gavage, we cannot eliminate the possibility that we also introduced gut microbes to the lungs through translocation and aspiration of the donor microbiota.

One factor that may explain the difference in the overall microbial community

structures between the two housing facilities is that the mice were on different standard chow diets. This difference in diets were already in place prior to the present study, and hence, could be contributing to our findings. BLM-highly-susceptible mice in Facility B were on Teklad Global 18% Protein Rodent Diet (2918, Harlan-Envigo) throughout their lifetime including during fetal development. However, breeders in Facility A were on a high-fat diet, and all other mice were given NIH-31 Modified Open Formula (7913, Harlan-Envigo) after weaning. Both standard non-high fat diets 2918 and 7913 consist of similar macronutrient compositions and are irradiated. Differences between the two diets are that the 7913 diet (Facility A) contains ground oats, fish meal, and dehydrated alfalfa meal, whereas the 2918 diet (Facility B) contains L-lysine and DL-methionine. While diets would not be the source of new commensal species, the subtle differences in ingredients could select for specific taxa and contribute to maintaining the unique microbial communities between the two facilities.

Our results support the role for microbiota in controlling the BLM-induced injury response. Of note, the impact of gut microbiota on response to BLM challenge seems to be most significant during the acute phase of BLM treatment, while a previous work has shown that the gut-specific depletion of microbiome has a negligible impact on development of BLM-induced pulmonary fibrosis (Todd et al., 2013). We demonstrate the need for controlling the presence of *Proteobacteria* in mice microbiota during the study of lung injury response. Notably, *H. hepaticus* and *Desulfovibrio* are not among the excluded pathobionts in specific pathogen-free facilities and vendors unless specifically requested. Our study highlights a need for reporting the composition of commensal microbiomes in laboratory animals, in order to improve reproducibility in research using the BLM model across institutions. Our data also impacts the potential use of BLM in cancer patients as it is a chemotherapy that is effective but less-often used due to infrequent, but serious side effects including lung pneumonitis and fibrosis. As the development of lung complications

is also unpredictable in cancer patients, understanding whether the microbiome of each patient affects their chances of developing pneumonitis may influence clinical decision-making.

CHAPTER 4

CONCLUSION AND FUTURE DIRECTION

4.0.1 Discussion

In the first chapter, I established that antigen-driven adaptive immune activation could be a critical immunopathology for all fibrotic ILD subtypes by the end-stage of the disease (Figure 4.1). We found that uncontrolled humoral immunity against self-antigens is a main immune pathway active in fibrotic ILD patients, and we discovered 17 novel autoantigens to which ILD patients were commonly reactive. Furthermore, auto-antibody response was accompanied by the accumulation of Treg cells that express $CD25^{low}$ phenotype in ILD patients' lung-draining lymph nodes, suggesting a potential dysregulation of self-reactive T and B cells in fibrotic ILD. Importantly, our findings support the notion that adaptive immune activation, including auto-antibody response, may contribute to the progression of not only immune-associated ILDs but also IPF. In the second chapter, I demonstrated that the composition of gut microbiota has significant impact on wasting and death of animals during the lung injury response (Figure 4.2). I identified that members of *Proteobacteria*, such as *Helicobacter* and *Desulfovibrio*, are the gut microbes associated with an increased sensitivity to the bleomycin-induced lung injury. These data support the role for the gut-lung axis in lung injury. Taken together, my work elucidates characteristics and specificities of immune responses during lung injury and fibrosis, and it brings novel insight into human immunology in fibrotic lung diseases.

Our work inspires the reevaluation of how the autoimmune feature is assessed in ILD patients. The American Thoracic Society guidelines recommend routine testing for circulating autoantibodies via anti-nuclear antibody, rheumatoid factor, anti-cyclic citrullinated peptide antibodies, and anti-myositis panels. Based on these panels, autoantibody positivity has been reported in up to 40% of IPF patients, and IPAF

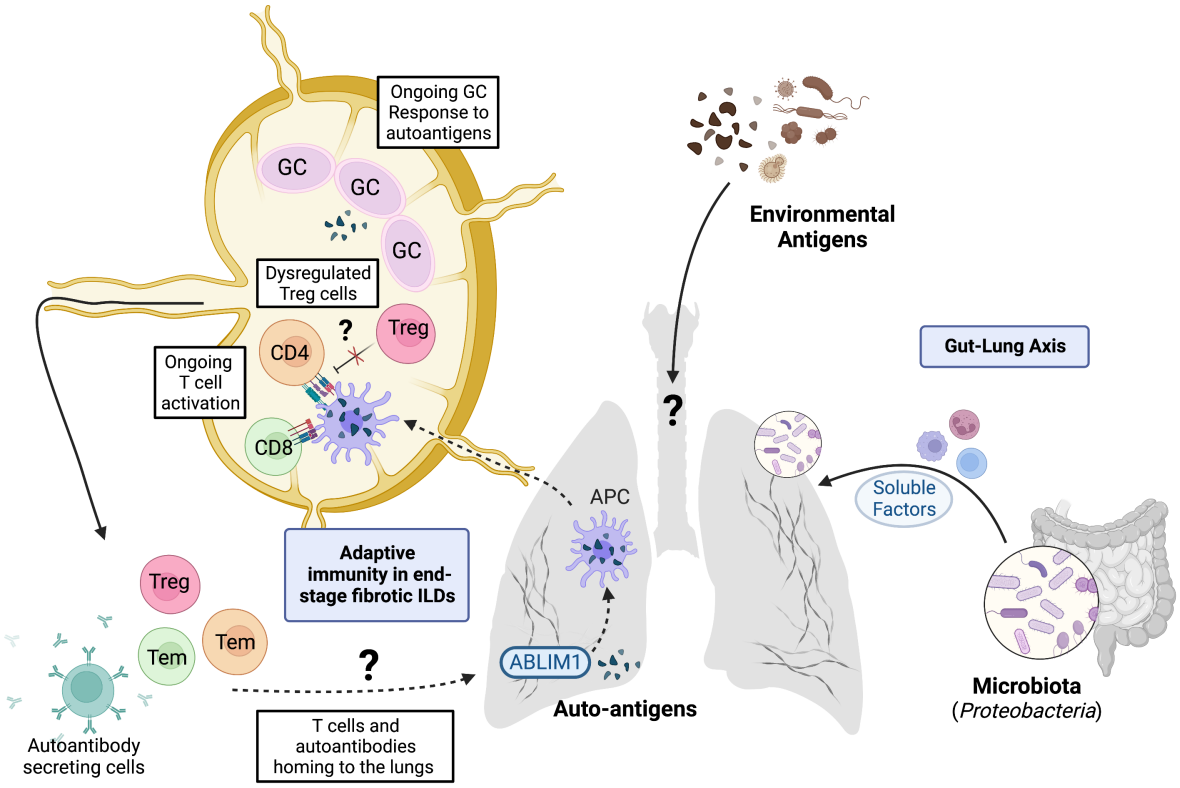

Figure 4.1: **A model of common antigen-driven immune activation in human fibrotic ILDs.** Fibrotic ILD patients have ongoing activation of T cells and GC responses at the end-stage disease, regardless of etiology. Break in tolerance against an endogenous protein, ABLIM1, could be an underlying immunopathology common to fibrotic ILDs. Exposure to specific microbes from the environmental and commensal sources contribute to modulating lung injury and fibrosis, but their involvement in antigen responses is yet to be established.

designates a group of patients with distinct clinical characteristics but without a consensus on diagnosis and treatment guidelines (Mackintosh et al., 2021). Based on the anti-ABLIM1 index, we now know that autoantibody production in ILD patients is likely more extensive than previously reported. Although the presence of autoantibodies may not be sufficient to indicate an autoimmune response, it has been suggested that autoantibodies have clinical significance in fibrotic ILD patients (Ghang et al., 2019; Kirgou et al., 2022). Our discovery of ILD autoantigens can contribute to improving the current autoantibody panels, which will further our understanding of the effect of

autoantibodies in ILD progression and treatment. To begin with, we need to understand how ABLIM1-seropositive patients differ from ABLIM1-seronegative patients. Future studies can aim to test whether there are genetic, molecular, or inhalational factors that underly anti-ABLIM1 responses across many ILD subtypes.

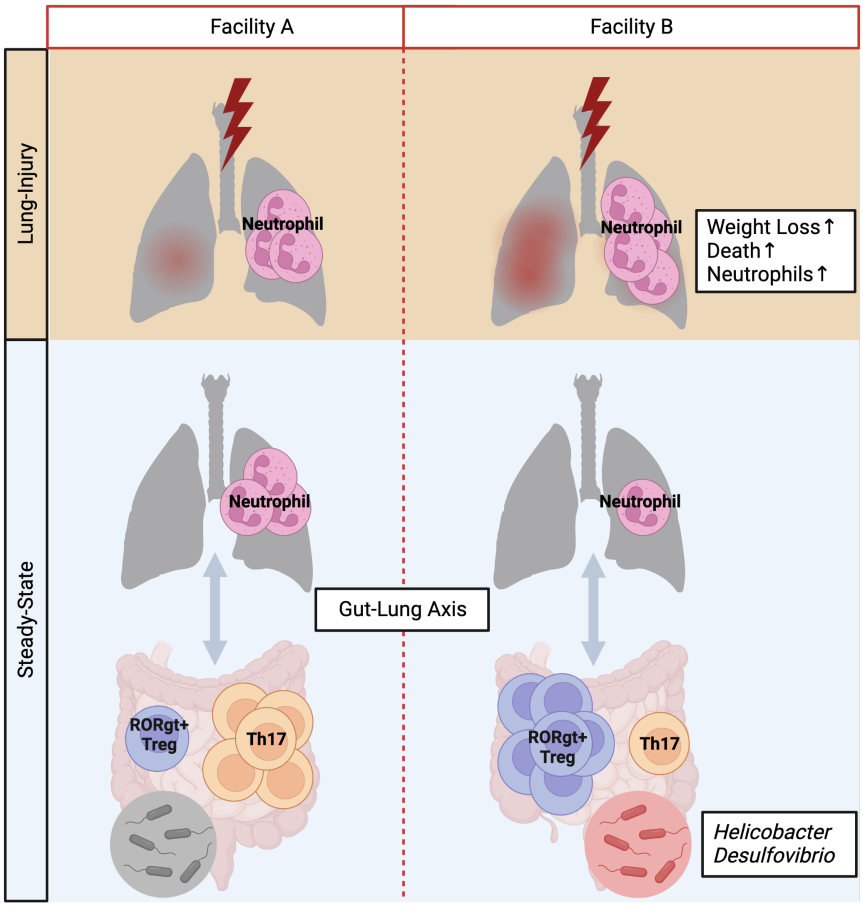

Figure 4.2: **Gut microbiome modulates the severity of bleomycin-induced lung injury response in mice.** Mice housed in two different SPF facilities had different gut microbiome compositions. Presence of *Helicobacter* and *Desulfovibrio* in the gut microbiome (Facility B) was associated with more severe lung injury response characterized by wasting and death. Compared to mice in Facility A, bleomycin-highly-susceptible mice in Facility B showed relatively diminished Th17-neutrophil axis at steady state, but an increase in lung neutrophil infiltration upon intratracheal bleomycin challenge.

Even though most ILD subtypes are not considered autoimmune conditions, our fibrotic ILD patient data revealed an interesting parallel to an autoimmune disease regarding

$CD25^{low}$ $FOXP3^{+}$ T cells in that these cells are overrepresented and correlated with anti-ABLIM1 titers in ILD patients. Accumulation of $CD25^{low}$ $FOXP3^{+}$ T cells have been reported in the context of autoimmune disease such as systemic lupus erythematosus (SLE) (Bonelli et al., 2009; Todd et al., 2013), multiple sclerosis (Fransson et al., 2010), and rheumatoid arthritis patients (de Paz et al., 2012). In the case of SLE, the level of $CD25^{-}$ $FOXP3^{+}$ T cells is directly associated with disease severities including renal function and anti-dsDNA antibody titer (El-Maraghy et al., 2018; Zhang et al., 2008). CD25, which is the alpha chain of the high-affinity IL-2 receptor complex, is critical for the immunoregulatory function of Treg cells. For instance, a specific ablation or disruption of CD25 function is sufficient to trigger autoimmunity in mice or to increase susceptibility to autoimmune diseases in humans, respectively (Goudy et al., 2013; Matesanz et al., 2007; Willerford et al., 1995).

The origin and function of $CD25^{low}$ $FOXP3^{+}$ T cells in ILD remain to be determined. A possible origin of $CD25^{low}$ $FOXP3^{+}$ T cells in ILD patients is the T effector lineage, since activation of T effector cells induces de novo Foxp3 expression without acquiring immunoregulatory function (Allan et al., 2007; Kmieciak et al., 2009). Alternatively, these cells may originate from a stable Treg lineage and downregulate CD25 due to some dysregulation. An approach to test this possibility is investigating demethylation status of a region on FOXP3 called the Treg-specific demethylated region, which is associated with stable FOXP3 expression (Polansky et al., 2008). Moreover, human FOXP3 encodes two major isoforms, and the shorter FOXP3 isoform, which is only present in humans but not mice, lacks the exon 2 and is the dominant isoform expressed in Tregs of patients with some autoimmune diseases including antineutrophil cytoplasmic antibody-associated vasculitis (Free et al., 2013) and celiac disease (Serena et al., 2017). A recent study showed that the specific deletion of Foxp3 exon 2 in mice results in lower CD25 expression on Treg cells, as well as increased Tfh and GC B cell responses with dsDNA and anti-nuclear

autoantibody production (Du et al., 2022). This data could support a possibility that $CD25^{low}$ $FOXP3^{+}$ T cells in ILD patients are instable Tregs that accord to increased germinal center and autoantibody production in ILD.

In our flow cytometry study, we used the antibody clone 2A3 to assess CD25 expression. The monoclonal 2A3 binds to an epitope on the p55 subunit at or near the IL-2 binding site (Watson et al., 1988). Given that activated T cells are a potent source of IL-2, ILD LLN would be an IL-2-rich environment. Hence, it is possible that IL-2 molecules preoccupy the antibody binding sites and result in a lower detection efficiency for CD25. However, this possibility is only valid if IL-2 protein can stay stably bound to CD25 throughout the cryopreservation and thawing of LLN cells. Such assumption seems unlikely, but further experiments need to be done to distinguish the two possibilities.

Though we had hypothesized that ILD patients' autoantibody levels would change over time and correspond to specific disease phases at which break-in-tolerance might take place, we found a high degree of variability in autoantibody trajectories during the analysis of paired plasma samples. Autoantibody levels increased, decreased, or unchanged over time, and the trajectory did not depend on the length of interval between blood draws. This data reflects the complexity of the pathobiology, including varying etiology, exposure history, and importantly treatment strategies. We were unable to include the medication as a variable in the present study, but it is possible that the downward trend in autoantibody trajectory observed in a few ILD patients is driven by immunomodulatory drugs or steroids.

Surprisingly, anti-ABLIM1 antibodies were readily detected in ILD plasma samples even from the earliest timepoints after the study enrollment. Due to the complexity of diagnosis, many patients have delayed access to a tertiary care center, thereby the exact onset of the disease is difficult to examine in our patient cohort. Nonetheless, we observed anti-ABLIM1 responses in patient samples obtained years before the lung transplantation, suggesting that GC response is active during not only the end-stage but also the early-stage of the disease.

Since ABLIM1 is an intracellular protein, the initiation of the response would likely require a release of antigens through necrotic cell deaths. Interestingly, anti-ABLIM1 responses were observed in both ILD and RA patients without symptoms of a lung disease. Since RA patients often develop ILD or radiographic lung abnormalities (Bilgici et al., 2005; Yunt and Solomon, 2015), it would be interesting to test whether anti-ABLIM1 production precedes lung function decline by comparing the autoantibody serology and lung radiopathology in RA patients. Furthermore, controlled future study investigating autoantibodies throughout the full course of ILD would help addressing unanswered questions. For instance, at which point in fibrotic process do immune activation and autoantibody production become common to all ILD?

Post-translational modifications can have dramatic impact on structural and immunological properties of proteins. Citrullination, the enzymatic conversion of arginine into citrulline, is a prime example. Citrullination can turn innocuous proteins into autoantigens through modifying proteolytic cleavage for antigen presentation (Curran et al., 2023). Conversion of antigen repertoire and induction of autoimmune response are considered key mechanisms by which citrullination is involved in the pathogenesis of RA. Furthermore, the citrullination pathway is shown to be upregulated in ILD patients (Samara et al., 2017) and is induced by cigarette smoking, a risk factor for lung fibrosis (Margaritopoulos et al., 2015). A recent study showed that soluble citrullinated vimentin can directly induce collagen and α-SMA expression in lung fibroblasts via TLR4 dependent mechanisms (Li et al., 2021). Therefore, citrullination may promote fibrosis directly by modulating fibroblasts and indirectly by modulating the adaptive immunity.

While most adaptive immune responses are initiated and sustained in lymph nodes, understanding of an immunopathology is not complete without the study of lung tissues. Explanted lungs from ILD patients have been extensively investigated using both scRNA sequencing and CYTOF methods by several groups, and these data are complementary to

our work. Single cell analysis identified multiple populations that are uniquely present in fibrotic lungs such as an alveolar macrophage subset expressing high SPP1 and MERTK, a phenotype with profibrotic and proliferative properties (Morse et al., 2019; Reyfman et al., 2019). Another cell population consistently found in fibrotic lungs is aberrant structural cells that express markers for both epithelial and basal cells, KRT5, KRT17 and KRT15, along with senescence phenotypes (Adams et al., 2020; Habermann et al., 2020). Furthermore, a recent study demonstrated that IPF patient lungs were enriched with memory T cells subsets, both effector memory and resident memory cells, as well as antigen processing dendritic cells that show immune activation transcription profiles (Serezani et al., 2022). This could support a notion that expanded and activated T cells found in the draining lymph nodes are in fact targeting the lungs.

Our work in an animal lung fibrosis model highlights the effect of the gut microbiome in modulating the severity of lung injury response. This result supports the gut-lung axis, a phenomenon of the gut microbial environment having a long-reaching effect on lung health, which is observed in both acute and chronic lung conditions for years. Excitingly, a group at Vanderbilt University recently reported a similar finding, in which mice housed in animal biosafety level (ABSL)2 developed more severe lung fibrosis after the bleomycin injury compared to mice housed in ABSL1 with enhanced STAT3/IL17-A signaling in lung T cells of ABSL2 mice (Chioma et al., 2022). Association between IL-17A and increased lung fibrosis severity is in line with the phenotype we observed where bleomycin-highly-susceptible mice had increased neutrophil recruitment during lung injury compared to less susceptible mice, since IL-17A induces neutrophil recruitment (Miyamoto et al., 2003). However, there was a difference in the fibrosis phenotype since Chioma et al. observed increased lung fibrosis in ABSL2 mice compared to ABLS1 mice while we did not find conclusive effects on lung fibrosis. In fact, we noticed a slight shift in the microbial composition over years, which coincided with the loss of effect in fibrosis. Due to the lack

of historic samples, we were unable to determine which factors caused such difference, but comparing the 16s rRNA sequencing data from the two institutions could lead to new insight in this front.

Impact of the lung microbiome in human ILD is increasingly recognized. For many years, lungs were considered sterile, but recent studies proved otherwise with significant advances in sequencing techniques. Although much lower in biomass than the gut (10^3–10^5 bacteria per gram of lung tissue (Mathieu et al., 2018) versus 10^{11}–10^{12} bacteria per gram of gut tissue (Guarner and Malagelada, 2003)), it has been demonstrated that the lung microbiome is established during the postnatal period (Pattaroni et al., 2018) and maintained heterogeneously based on the local environment of different anatomical spaces within the lungs (Dickson et al., 2015). Although antimicrobial therapy using co-trimoxazole or doxycycline do not improve morbidity or mortality of IPF patients, lung dysbiosis has been linked to ILD (Martinez et al., 2021). For example, both the overall microbial burden and the presence of specific microbes in the lungs are associated with IPF patient survival (Molyneaux et al., 2014; Han et al., 2014). Moreover, the bacterial burden of IPF patients undergoing acute exacerbation was four times higher than that of stable IPF patients, with *Proteobacteria sp.* being one of the microbes present at relatively higher abundance in exacerbated IPF patients (Molyneaux et al., 2017). Therefore, specific microbiomes may contribute to the disease pathogenesis through modulating epithelial and immune cell function or through being antigenic sources for adaptive immune activation in the lungs of ILD patients.

4.0.2 Future Direction

Given that antigen-experienced T cells are overrepresented in lungs and lymph nodes of fibrotic ILD patients, future ILD studies can focus on three main areas: 1) investigating antigen targets of activated T cells in patients through understanding the clonal diversity,

2) further identifying classes of antigens such as environmental antigens to improve our mechanistic understanding of the disease, and 3) developing an understanding of whether auto-antibodies or Tregs in fibrotic ILD are pathogenic. Moreover, to better understand the impact of the microbiome, future mouse studies can focus on mechanistic understanding of the role of specific gut microbes in modulating lung injury and fibrosis.

We found that T cells are one of the main cell types activated and/or dysregulated in fibrotic ILD. Determining antigens that drive T cell activation can be tackled using two-pronged approaches: *ex vivo* antigen stimulation and T cell receptor (TCR) sequencing. First, leveraging the information we have produced on novel auto-antigens, the response of LLN cells to antigen stimulation can be studied using an *ex vivo* culture system (Wagar et al., 2021). Candidate antigens based on PhIP-seq data could be translated and purified as endotoxin-free proteins and then used to stimulate ILD patients' LLN cells, which include endogenous antigen presenting cells and T cells. Antigen-responding T cells can be identified based on the surface expression of CD154 or the intracellular expression of Nur77, both of which are known to be upregulated in response to TCR stimulation. Challenges to this approach are that many T cells from ILD patients' LLNs already upregulate CD154 and that antigen presenting cells from LLNs may continue to present antigens from the reservoir established in the patient's body prior to explantation. Therefore, the cells may require a resting period in culture prior to the antigen stimulation. A non-stimulated control should be included for each patient sample and used as a benchmark when determining whether there are antigen-specific T cells after the *ex vivo* stimulation.

A secondary approach to investigate antigen-specific T cell responses is to perform TCR repertoire sequencing of activated T cells. Unlike the first approach, both LLN and lung T cells can be investigated by TCR sequencing. T cells of interest, including $CD154^{+}$ CD4 T cells and $CD25^{low}$ Treg cells in LLNs and memory T cells in the lungs, would be flow sorted and single-cell sequenced. Clonal diversity would be investigated based on V

gene usage, distribution of CDR3 lengths, and paired TCR alpha and TCR beta sequences. Furthermore, individuals' HLA types should be accounted for when determining public T cell clones with shared antigen reactivities because HLA molecules shape the antigen repertoire and directly interact with the TCR during an antigen recognition (Francis et al., 2022). As a reference group, human T cells from known HLA backgrounds can be stimulated with candidate antigens in the *ex vivo* culture system using tonsil or other secondary lymphoid organs, and antigen-specific T cells can be isolated based on surface CD154 expression and TCR sequenced. TCR sequences from these reference controls would be compared to TCR sequences of ILD patients to test whether they match. Computational tools such as the Immune Epitope Database (https://www.iedb.org/) can be used as an additional reference to investigate TCR specificities. Expected findings are that there would be common antigen specificity between lung and LLN T cells within an individual. Public T cell clones could be discovered based on shared TCR motifs if a group of ILD patients have the same HLA types. In the case of having distinct HLA types in the patient cohort, a common antigen reactivity would be determined based on matched TCR sequence to the antigen stimulated reference TCR. I anticipate that a significant portion of patients would have shared T cell reactivity to candidate antigens.

Furthermore, comparing TCR repertoires of Tcon, $CD25^{+}$ Treg, and $CD25^{low}$ Treg cells in LLN of each individual would provide information on the lineage of $CD25^{low}$ $FOXP3^{+}$ cells in ILD patients. The presence of overlapping TCR clones in either Tcon or $CD25^{+}$ Treg populations would indicate that $CD25^{low}$ $FOXP3^{+}$ cells originate from either the activated Tcon cells or dysregulated Treg cells. It is possible that the TCR repertoire of $CD25^{low}$ $FOXP3^{+}$ cells would be either completely unique or shared with both Tcon and $CD25^{+}$ Treg TCR repertoires. A unique TCR repertoire would suggest that $CD25^{low}$ $FOXP3^{+}$ cells differentiate via an antigen-independent mechanism. The latter outcome could also support an antigen-independent differentiation of $CD25^{low}$ $FOXP3^{+}$ T cells.

Continued future effort in identifying disease-promoting antigens is critical. While my work significantly improved the understanding of self-antigen repertoire in ILD patients, the immunological impact of inhaled antigens remains to be an important area of investigation. A recent multicenter study reports that over 60% of all fibrotic ILDs have history of inhalational exposures relating to mold, bird, asbestos, silica, and other inorganic dust (Lee et al., 2022). While the existence of a relationship between exposures and patient outcomes supports the implication of the identified exposure sources in pulmonary fibrosis, it remains to be established whether certain exposure histories are overrepresented in ILD compared to matched non-diseased controls. Given that inhaled particles build up in lung-associated LN over time and interfere with immune function even in individuals without lung disease (Ural et al., 2022), it is imperative to include age-matched controls in future studies investigating non-self antigens.

Exposure sources for ILD patients are often broken down to two categories: organic and inorganic. Organic exposures, such as molds, bacteria, and bird droppings, contain proteins, which can be processed as both T cell and B cell antigens. In contrary, inorganic particles cannot be recognized by T cell receptors but instead may act as haptens, which elicit immune responses in the presence of carrier proteins. The established PhIP-seq platform can be extended to elucidate environmental antigens. In future studies, new phage-display libraries can be designed using sequences of candidate environmental immunogens and used to screen patient serum antibodies. Since remediating antigen exposures is increasingly recognized as an effective intervention to improve pulmonary function and survival in fibrotic ILD patients (Fernandez Perez et al., 2013; Lee et al., 2021a), completing the knowledge of antigens beyond autoantigens will ensure the full benefit of such intervention.

An inevitable limitation of human studies is that we are unable to establish the causal relationship between the adaptive immune activation and pulmonary fibrosis. While the use of animal models allows experimental interventions and definitive evidence, currently

available mouse models, such as the bleomycin model, do not faithfully recapitulate the disease. Bleomycin causes direct oxidative damage to the lungs, which leads to acute inflammation and subsequent fibrosis of the tissues near airways instead of the parenchyma. New animal models can be tested based on findings from our human study. I propose to generate monoclonal antibodies against ILD autoantigens in mice and test whether the infusion of these autoantibodies is sufficient to induce lung fibrosis. Additional studies using Foxp3 exon2 mutant mice (Du et al., 2022) combined with the monoclonal injection might accelerate the lung pathology if dysregulated Treg cells contribute to disease pathogenesis.

Understanding the role of Treg cells, including $CD25^{low}$ $FOXP3^{+}$ cells, in fibrotic ILD is an important goal for future studies. I hypothesize that $CD25^{low}$ $FOXP3^{+}$ cells have unique molecular pathways compared to both $CD25^{+}$ Treg cells and Tcon cells and function to promote lung fibrosis via failing to suppress auto-reactivity and/or secreting cytokines that activate lung myofibroblasts. First, whether there are $CD25^{low}$ $FOXP3^{+}$ cells in the lungs of fibrotic ILD patients could be investigated utilizing publicly available lung scRNA sequencing data. If present in the lungs, the proposed analysis can be done for both lung and LLN cells. $CD25^{low/+}$ $FOXP3^{+}$ T cells and Tcon cells from patients' LLNs would be scRNA sequenced. I would propose a paired scRNA sequencing of T cells from LLNs to get information on both gene expression and TCR repertoire as discussed above. Differentially expressed genes (DEG) can be determined between $CD25^{low}$ $FOXP3^{+}$ cells and $CD25^{+}$ Treg cells, and between $CD25^{low}$ $FOXP3^{+}$ cells and Tcon cells from patient samples. Molecular pathways specifically upregulated or downregulated in $CD25^{low}$ $FOXP3^{+}$ cells can be identified by finding the overlapping DEGs from the two comparison sets. In addition, DEG between Tregs of ILD patients and Tregs of non-diseased controls could be determined. Since $CD25^{low}$ Tregs are rarely found in control LLNs, the comparison between ILD and controls can be made at the total $FOXP3^{+}$ cell level. The focus of analysis would be to identify the overall

pathways that are differentially regulated, as well as to determine whether pro-fibrotic genes are upregulated in $CD25^{low}$ $FOXP3^{+}$ cells.

Using the 16s rRNA sequencing and computational approaches, I identified candidate commensal bacteria that are associated with excessive weight loss and death in bleomycin lung injury model. Future studies can address whether the presence of specific *Proteobacteria* is sufficient to worsen the lung injury response in mice. Several strains of *Helicobacter* and *Desulfovibrio* genera are candidates that could be tested by mono-association studies. With access to a gnotobiotic facility where the microbial composition can be maintained without any contamination, specific pathogen free mice from a vendor or Altered Schaedler Flora mice could be colonized with one candidate strain at a time and tested for their response to bleomycin in comparison to mock colonized controls. Some candidate bacteria such as *Helicobacter hepaticus* are available from other laboratories and others would require the isolation and development of specific culture conditions using an anaerobic chamber.

However, the effect of the microbiome is likely imparted through complex interactions among multiple bacteria and their products. In that case, a mono-association of individual bacterial species may not be sufficient to elicit a phenotype. A process of elimination can be used instead by first establishing a bacterial consortium based on the core members of the microbiome in bleomycin-highly-susceptible mice. After confirming that the colonization of germ-free mice with the consortium can recapitulate the response of the highly susceptible mice, the effect of removing one strain at a time can be tested by colonizing fresh germ-free mice with modified consortia and treating with bleomycin. I anticipate that the mice will become less susceptible to bleomycin when the culprit strain is lost. Whether the disease-promoting property of specific commensal bacteria in bleomycin model is also applicable to other models of lung injury and fibrosis could be tested. Therefore, the exact microbial contents need to be carefully monitored and reported even in specific pathogen free conditions when developing and studying animal models of pulmonary fibrosis.

4.0.3 Conclusion

Overall, I propose a model of common antigen-driven immune activation in human fibrotic ILDs. Though clinical and mechanistic significance of the adaptive immune response requires further examination, our work offers important new insight to the current understanding of the disease. We demonstrate that despite having a distinct ILD diagnosis, which is largely instructed by radiologic patterns and inhalational exposure history, many fibrotic ILD patients present common phenotypes of activated T cell and GC responses. Strikingly, the immune activation and autoantibody production are ongoing even at the time of lung transplantation in fibrotic ILD patients. Adaptive immune activation is driven, in part, by auto-antigens expressed in the lungs. Furthermore, specific gut microbiomes can have dominant negative effect on the morbidity of lung injury and fibrosis as we demonstrated in a mouse model. While the impact of the microbiome in lung health may be through shaping the baseline immunity via soluble factors, the commensals could elicit antigenic responses that are relevant for lung fibrosis in both mice and humans. Importantly, our model that antigen-driven immune responses are common features of fibrotic ILDs and are ongoing even in the end-stage diseases challenges the current paradigm of the ILD. Our data could support a potential benefit of specific immunomodulatory therapies such as B cell targeted medication in a broader subset of fibrotic ILD patients regardless of etiology. However, there were individual variations in the degree of GC responses among ILD patients, which correlated with lung function, suggesting that GCs or antibody responses could inform a new grouping of ILD patients. Establishing biologically meaningful endotypes would pave the way for the development of mechanistic studies and effective treatment.

REFERENCES

T. S. Adams, J. C. Schupp, S. Poli, E. A. Ayaub, N. Neumark, F. Ahangari, S. G. Chu, B. A. Raby, G. DeIuliis, M. Januszyk, Q. Duan, H. A. Arnett, A. Siddiqui, G. R. Washko, R. Homer, X. Yan, I. O. Rosas, and N. Kaminski. Single-cell rna-seq reveals ectopic and aberrant lung-resident cell populations in idiopathic pulmonary fibrosis. *Sci Adv*, 6(28): eaba1983, 2020. doi:10.1126/sciadv.aba1983.

A. Adegunsoye, C. L. Hrusch, C. A. Bonham, M. R. Jaffery, K. M. Blaine, M. Sullivan, M. M. Churpek, M. E. Strek, I. Noth, and A. I. Sperling. Skewed lung ccr4 to ccr6 cd4(+) t cell ratio in idiopathic pulmonary fibrosis is associated with pulmonary function. *Front Immunol*, 7:516, 2016. doi:10.3389/fimmu.2016.00516.

A. Adegunsoye, J. M. Oldham, C. Bonham, C. Hrusch, P. Nolan, W. Klejch, S. Bellam, U. Mehta, K. Thakrar, J. V. Pugashetti, A. N. Husain, S. M. Montner, C. M. Straus, R. Vij, A. I. Sperling, I. Noth, M. E. Strek, and J. H. Chung. Prognosticating outcomes in interstitial lung disease by mediastinal lymph node assessment. an observational cohort study with independent validation. *Am J Respir Crit Care Med*, 199(6):747–759, 2019. doi:10.1164/rccm.201804-0761OC.

F. Aeffner, B. Bolon, and I. C. Davis. Mouse models of acute respiratory distress syndrome: A review of analytical approaches, pathologic features, and common measurements. *Toxicol Pathol*, 43(8):1074–92, 2015. doi:10.1177/0192623315598399.

G. M. Albaiceta, A. Gutierrez-Fernandez, E. Garcia-Prieto, X. S. Puente, D. Parra, A. Astudillo, C. Campestre, S. Cabrera, A. Gonzalez-Lopez, A. Fueyo, F. Taboada, and C. Lopez-Otin. Absence or inhibition of matrix metalloproteinase-8 decreases ventilator-induced lung injury. *Am J Respir Cell Mol Biol*, 43(5):555–63, 2010. doi:10.1165/rcmb.2009-0034OC.

M. Alghamdi, D. Alasmari, A. Assiri, E. Mattar, A. A. Aljaddawi, S. G. Alattas, and E. M. Redwan. An overview of the intrinsic role of citrullination in autoimmune disorders. *J Immunol Res*, 2019:7592851, 2019. doi:10.1155/2019/7592851.

S. E. Allan, S. Q. Crome, N. K. Crellin, L. Passerini, T. S. Steiner, R. Bacchetta, M. G. Roncarolo, and M. K. Levings. Activation-induced foxp3 in human t effector cells does not suppress proliferation or cytokine production. *Int Immunol*, 19(4):345–54, 2007. doi:10.1093/intimm/dxm014.

S. Ames, J. E. Allen, D. A. Hysom, G. S. Lloyd, and M. B. Gokhale. Design and optimization of a metagenomics analysis workflow for nvram. *2014 IEEE International Parallel & Distributed Processing Symposium Workshops*, pages 556–565, 2014. doi:10.1109/IPDPSW.2014.200.

S. K. Ames, D. A. Hysom, S. N. Gardner, G. S. Lloyd, M. B. Gokhale, and J. E. Allen. Scalable metagenomic taxonomy classification using a reference genome database. *Bioinformatics*, 29(18):2253–60, 2013. doi:10.1093/bioinformatics/btt389.

A. Ananda Rao and S. Johncy. Tennis courts in the human body: A review of the misleading metaphor in medical literature. *Cureus*, 14(1):e21474, 2022. doi:10.7759/cureus.21474.

M. J. Anderson. A new method for non-parametric multivariate analysis of variance. *Austral Ecology*, 26(1):32–46, 2001. doi:DOI 10.1046/j.1442-9993.2001.01070.x.

V. C. Ardi, T. A. Kupriyanova, E. I. Deryugina, and J. P. Quigley. Human neutrophils uniquely release timp-free mmp-9 to provide a potent catalytic stimulator of angiogenesis. *Proc Natl Acad Sci U S A*, 104(51):20262–7, 2007. doi:10.1073/pnas.0706438104.

B. Atienza-Mateo, S. Remuzgo-Martinez, D. Prieto-Pena, V. M. Mora Cuesta, D. Iturbe-Fernandez, J. Llorca, L. Sanchez-Bilbao, A. Corrales, G. Blanco Rodriguez, J. J. Gomez-Roman, J. M. Cifrian, and M. A. Gonzalez-Gay. Rituximab in the treatment of interstitial lung disease associated with autoimmune diseases: Experience from a single referral center and literature review. *J Clin Med*, 9(10), 2020. doi:10.3390/jcm9103070.

M. L. Balmer, C. M. Schurch, Y. Saito, M. B. Geuking, H. Li, M. Cuenca, L. V. Kovtonyuk, K. D. McCoy, S. Hapfelmeier, A. F. Ochsenbein, M. G. Manz, E. Slack, and A. J. Macpherson. Microbiota-derived compounds drive steady-state granulopoiesis via myd88/ticam signaling. *J Immunol*, 193(10):5273–83, 2014. doi:10.4049/jimmunol.1400762.

P. Bankhead, M. B. Loughrey, J. A. Fernández, Y. Dombrowski, D. G. McArt, P. D. Dunne, S. McQuaid, R. T. Gray, L. J. Murray, H. G. Coleman, et al. Qupath: Open source software for digital pathology image analysis. *Scientific reports*, 7(1):1–7, 2017. doi:10.1038/s41598-017-17204-5.

O. Bannard, R. M. Horton, C. D. C. Allen, J. An, T. Nagasawa, and J. G. Cyster. Germinal center centroblasts transition to a centrocyte phenotype according to a timed program and depend on the dark zone for effective selection. *Immunity*, 39(5):912–924, 2013. doi:10.1016/j.immuni.2013.08.038.

A. Bilgici, H. Ulusoy, O. Kuru, C. Celenk, M. Unsal, and M. Danaci. Pulmonary involvement in rheumatoid arthritis. *Rheumatol Int*, 25(6):429–35, 2005. doi:10.1007/s00296-004-0472-y.

S. Z. Birjandi, V. Palchevskiy, Y. Y. Xue, S. Nunez, R. Kern, S. S. Weigt, 3rd Lynch, J. P., T. A. Chatila, and J. A. Belperio. Cd4(+)cd25(hi)foxp3(+) cells exacerbate bleomycin-induced pulmonary fibrosis. *Am J Pathol*, 186(8):2008–2020, 2016. doi:10.1016/j.ajpath.2016.03.020.

M. Bonelli, A. Savitskaya, C. W. Steiner, E. Rath, J. S. Smolen, and C. Scheinecker. Phenotypic and functional analysis of cd4+ cd25- foxp3+ t cells in patients with systemic lupus erythematosus. *J Immunol*, 182(3):1689–95, 2009. doi:10.4049/jimmunol.182.3.1689.

C. A. Bonham, C. L. Hrusch, K. M. Blaine, S. T. Manns, R. Vij, J. M. Oldham, M. M. Churpek, M. E. Strek, I. Noth, and A. I. Sperling. T cell co-stimulatory molecules

icos and cd28 stratify idiopathic pulmonary fibrosis survival. *Respir Med X*, 1, 2019. doi:10.1016/j.yrmex.2019.100002.

K. F. Budden, S. L. Gellatly, D. L. Wood, M. A. Cooper, M. Morrison, P. Hugenholtz, and P. M. Hansbro. Emerging pathogenic links between microbiota and the gut-lung axis. *Nat Rev Microbiol*, 15(1):55–63, 2017. doi:10.1038/nrmicro.2016.142.

R. M. Burger, J. Peisach, and S. B. Horwitz. Activated bleomycin. a transient complex of drug, iron, and oxygen that degrades dna. *J Biol Chem*, 256(22):11636–44, 1981.

B. J. Callahan, P. J. McMurdie, M. J. Rosen, A. W. Han, A. J. Johnson, and S. P. Holmes. Dada2: High-resolution sample inference from illumina amplicon data. *Nat Methods*, 13 (7):581–3, 2016. doi:10.1038/nmeth.3869.

S. M. Caucheteux, J. Hu-Li, R. N. Mohammed, A. Ager, and W. E. Paul. Cytokine regulation of lung th17 response to airway immunization using lps adjuvant. *Mucosal Immunol*, 10 (2):361–372, 2017. doi:10.1038/mi.2016.54.

O. S. Chioma, E. K. Mallott, A. Chapman, J. C. Van Amburg, H. Wu, B. Shah-Gandhi, N. Dey, M. E. Kirkland, M. Blanca Piazuelo, J. Johnson, G. R. Bernard, S. R. Bodduluri, S. Davison, B. Haribabu, S. R. Bordenstein, and W. P. Drake. Gut microbiota modulates lung fibrosis severity following acute lung injury in mice. *Commun Biol*, 5(1):1401, 2022. doi:10.1038/s42003-022-04357-x.

L. Chiu, T. Bazin, M. E. Truchetet, T. Schaeverbeke, L. Delhaes, and T. Pradeu. Protective microbiota: From localized to long-reaching co-immunity. *Front Immunol*, 8:1678, 2017. doi:10.3389/fimmu.2017.01678.

Y. Chung, S. Tanaka, F. Chu, R. I. Nurieva, G. J. Martinez, S. Rawal, Y. H. Wang, H. Lim, J. M. Reynolds, X. H. Zhou, H. M. Fan, Z. M. Liu, S. S. Neelapu, and C. Dong. Follicular regulatory t cells expressing foxp3 and bcl-6 suppress germinal center reactions. *Nat Med*, 17(8):983–8, 2011. doi:10.1038/nm.2426.

G. Clavarino, N. Delouche, C. Vettier, D. Laurin, M. Pernollet, T. Raskovalova, J. Y. Cesbron, C. Dumestre-Perard, and M. C. Jacob. Novel strategy for phenotypic characterization of human b lymphocytes from precursors to effector cells by flow cytometry. *PLoS One*, 11(9):e0162209, 2016. doi:10.1371/journal.pone.0162209.

M. Corbel, J. Lanchou, N. Germain, Y. Malledant, E. Boichot, and V. Lagente. Modulation of airway remodeling-associated mediators by the antifibrotic compound, pirfenidone, and the matrix metalloproteinase inhibitor, batimastat, during acute lung injury in mice. *Eur J Pharmacol*, 426(1-2):113–21, 2001. doi:10.1016/s0014-2999(01)01209-2.

V. Cottin, N. A. Hirani, D. L. Hotchkin, A. M. Nambiar, T. Ogura, M. Otaola, D. Skowasch, J. S. Park, H. K. Poonyagariyagorn, W. Wuyts, and A. U. Wells. Presentation, diagnosis and clinical course of the spectrum of progressive-fibrosing interstitial lung diseases. *Eur Respir Rev*, 27(150), 2018. doi:10.1183/16000617.0076-2018.

P. M. Cowley, C. R. Roberts, and A. J. Baker. Monitoring the health status of mice with bleomycin-induced lung injury by using body condition scoring. *Comp Med*, 69(2):95–102, 2019. doi:10.30802/AALAS-CM-18-000060.

L. M. Crosby and C. M. Waters. Epithelial repair mechanisms in the lung. *Am J Physiol Lung Cell Mol Physiol*, 298(6):L715–31, 2010. doi:10.1152/ajplung.00361.2009.

M. Cundall, Y. Sun, C. Miranda, J. B. Trudeau, S. Barnes, and S. E. Wenzel. Neutrophil-derived matrix metalloproteinase-9 is increased in severe asthma and poorly inhibited by glucocorticoids. *J Allergy Clin Immunol*, 112(6):1064–71, 2003. doi:10.1016/j.jaci.2003.08.013.

A. M. Curran, A. A. Girgis, Y. Jang, J. D. Crawford, M. A. Thomas, R. Kawalerski, J. Coller, 3rd Bingham, C. O., C. H. Na, and E. Darrah. Citrullination modulates antigen processing and presentation by revealing cryptic epitopes in rheumatoid arthritis. *Nat Commun*, 14 (1):1061, 2023. doi:10.1038/s41467-023-36620-y.

Z. Daniil, P. Kitsanta, G. Kapotsis, M. Mathioudaki, A. Kollintza, M. Karatza, J. Milic-Emili, C. Roussos, and S. A. Papiris. Cd8+ t lymphocytes in lung tissue from patients with idiopathic pulmonary fibrosis. *Respir Res*, 6:81, 2005. doi:10.1186/1465-9921-6-81.

B. de Paz, C. Prado, M. Alperi-Lopez, F. J. Ballina-Garcia, J. Rodriguez-Carrio, P. Lopez, and A. Suarez. Effects of glucocorticoid treatment on cd25(-)foxp3(+) population and cytokine-producing cells in rheumatoid arthritis. *Rheumatology (Oxford)*, 51(7):1198–207, 2012. doi:10.1093/rheumatology/kes039.

D. J. DePianto, S. Chandriani, A. R. Abbas, G. Jia, E. N. N'Diaye, P. Caplazi, S. E. Kauder, S. Biswas, S. K. Karnik, C. Ha, Z. Modrusan, M. A. Matthay, J. Kukreja, H. R. Collard, J. G. Egen, P. J. Wolters, and J. R. Arron. Heterogeneous gene expression signatures correspond to distinct lung pathologies and biomarkers of disease severity in idiopathic pulmonary fibrosis. *Thorax*, 70(1):48–56, 2015. doi:10.1136/thoraxjnl-2013-204596.

H. S. Deshmukh, Y. Liu, O. R. Menkiti, J. Mei, N. Dai, C. E. O'Leary, P. M. Oliver, J. K. Kolls, J. N. Weiser, and G. S. Worthen. The microbiota regulates neutrophil homeostasis and host resistance to escherichia coli k1 sepsis in neonatal mice. *Nat Med*, 20(5):524–30, 2014. doi:10.1038/nm.3542.

R. P. Dickson, J. R. Erb-Downward, C. M. Freeman, L. McCloskey, J. M. Beck, G. B. Huffnagle, and J. L. Curtis. Spatial variation in the healthy human lung microbiome and the adapted island model of lung biogeography. *Ann Am Thorac Soc*, 12(6):821–30, 2015. doi:10.1513/AnnalsATS.201501-029OC.

R. P. Dickson, B. H. Singer, M. W. Newstead, N. R. Falkowski, J. R. Erb-Downward, T. J. Standiford, and G. B. Huffnagle. Enrichment of the lung microbiome with gut bacteria in sepsis and the acute respiratory distress syndrome. *Nat Microbiol*, 1(10):16113, 2016. doi:10.1038/nmicrobiol.2016.113.

R. P. Dickson, M. J. Schultz, T. van der Poll, L. R. Schouten, N. R. Falkowski, J. E. Luth, M. W. Sjoding, C. A. Brown, R. Chanderraj, G. B. Huffnagle, L. D. J. Bos, and I. C. U. Patients Consortium Biomarker Analysis in Septic. Lung microbiota predict clinical outcomes in critically ill patients. *Am J Respir Crit Care Med*, 201(5):555–563, 2020. doi:10.1164/rccm.201907-1487OC.

F. do Valle Duraes, A. Lafont, M. Beibel, K. Martin, K. Darribat, R. Cuttat, A. Waldt, U. Naumann, G. Wieczorek, S. Gaulis, S. Pfister, K. D. Mertz, J. Li, G. Roma, and M. Warncke. Immune cell landscaping reveals a protective role for regulatory t cells during kidney injury and fibrosis. *JCI Insight*, 5(3), 2020. doi:10.1172/jci.insight.130651.

M. Donahoe, V. G. Valentine, N. Chien, K. F. Gibson, J. S. Raval, M. Saul, J. Xue, Y. Zhang, and S. R. Duncan. Autoantibody-targeted treatments for acute exacerbations of idiopathic pulmonary fibrosis. *PLoS One*, 10(6):e0127771, 2015. doi:10.1371/journal.pone.0127771.

W. W. Douglas, J. H. Ryu, and D. R. Schroeder. Idiopathic pulmonary fibrosis: Impact of oxygen and colchicine, prednisone, or no therapy on survival. *Am J Respir Crit Care Med*, 161(4 Pt 1):1172–8, 2000. doi:10.1164/ajrccm.161.4.9907002.

J. Du, Q. Wang, S. Yang, S. Chen, Y. Fu, S. Spath, P. Domeier, D. Hagin, S. Anover-Sombke, M. Haouili, S. Liu, J. Wan, L. Han, J. Liu, L. Yang, N. Sangani, Y. Li, X. Lu, S. C. Janga, M. H. Kaplan, T. R. Torgerson, S. F. Ziegler, and B. Zhou. Foxp3 exon 2 controls t(reg) stability and autoimmunity. *Sci Immunol*, 7(72):eabo5407, 2022. doi:10.1126/sciimmunol.abo5407.

N. El-Maraghy, M. S. Ghaly, O. Dessouki, S. I. Nasef, and L. Metwally. Cd4+cd25-foxp3+ t cells as a marker of disease activity and organ damage in systemic lupus erythematosus patients. *Arch Med Sci*, 14(5):1033–1040, 2018. doi:10.5114/aoms.2016.63597.

D. C. Fajgenbaum and C. H. June. Cytokine storm. *N Engl J Med*, 383(23):2255–2273, 2020. doi:10.1056/NEJMra2026131.

R. Falfan-Valencia, A. Camarena, A. Juarez, C. Becerril, M. Montano, J. Cisneros, F. Mendoza, J. Granados, A. Pardo, and M. Selman. Major histocompatibility complex and alveolar epithelial apoptosis in idiopathic pulmonary fibrosis. *Hum Genet*, 118(2): 235–44, 2005. doi:10.1007/s00439-005-0035-7.

C. A. Feghali-Bostwick, C. G. Tsai, V. G. Valentine, S. Kantrow, M. W. Stoner, J. M. Pilewski, A. Gadgil, M. P. George, K. F. Gibson, A. M. Choi, N. Kaminski, Y. Zhang, and S. R. Duncan. Cellular and humoral autoreactivity in idiopathic pulmonary fibrosis. *J Immunol*, 179(4):2592–9, 2007. doi:10.4049/jimmunol.179.4.2592.

K. M. Felix, I. A. Jaimez, T. V. Nguyen, H. Ma, W. A. Raslan, C. N. Klinger, K. P. Doyle, and H. J. Wu. Gut microbiota contributes to resistance against pneumococcal pneumonia in immunodeficient rag(-/-) mice. *Front Cell Infect Microbiol*, 8:118, 2018. doi:10.3389/fcimb.2018.00118.

E. R. Fernandez Perez, J. J. Swigris, A. V. Forssen, O. Tourin, J. J. Solomon, T. J. Huie, A. L. Olson, and K. K. Brown. Identifying an inciting antigen is associated with improved survival in patients with chronic hypersensitivity pneumonitis. *Chest*, 144(5):1644–1651, 2013. doi:10.1378/chest.12-2685.

T. E. Fingerlin, W. Zhang, I. V. Yang, H. C. Ainsworth, P. H. Russell, R. Z. Blumhagen, M. I. Schwarz, K. K. Brown, M. P. Steele, J. E. Loyd, G. P. Cosgrove, D. A. Lynch, S. Groshong, H. R. Collard, P. J. Wolters, W. Z. Bradford, K. Kossen, S. D. Seiwert, R. M. du Bois, C. K. Garcia, M. S. Devine, G. Gudmundsson, H. J. Isaksson, N. Kaminski, Y. Zhang, K. F. Gibson, L. H. Lancaster, T. M. Maher, P. L. Molyneaux, A. U. Wells, M. F. Moffatt, M. Selman, A. Pardo, D. S. Kim, J. D. Crapo, B. J. Make, E. A. Regan, D. S. Walek, J. J. Daniel, Y. Kamatani, D. Zelenika, E. Murphy, K. Smith, D. McKean, B. S. Pedersen, J. Talbert, J. Powers, C. R. Markin, K. B. Beckman, M. Lathrop, B. Freed, C. D. Langefeld, and D. A. Schwartz. Genome-wide imputation study identifies novel hla locus for pulmonary fibrosis and potential role for auto-immunity in fibrotic idiopathic interstitial pneumonia. *BMC Genet*, 17(1):74, 2016. doi:10.1186/s12863-016-0377-2.

A. Fischer, K. M. Antoniou, K. K. Brown, J. Cadranel, T. J. Corte, R. M. du Bois, J. S. Lee, K. O. Leslie, D. A. Lynch, E. L. Matteson, M. Mosca, I. Noth, L. Richeldi, M. E. Strek, J. J. Swigris, A. U. Wells, S. G. West, H. R. Collard, V. Cottin, and Ers Ats Task Force on Undifferentiated Forms of CTD-ILD. An official european respiratory society/american thoracic society research statement: interstitial pneumonia with autoimmune features. *Eur Respir J*, 46(4):976–87, 2015. doi:10.1183/13993003.00150-2015.

M. Fisher, S. D. Nathan, C. Hill, J. Marshall, F. Dejonckheere, P. O. Thuresson, and T. M. Maher. Predicting life expectancy for pirfenidone in idiopathic pulmonary fibrosis. *J Manag Care Spec Pharm*, 23(3-b Suppl):S17–S24, 2017. doi:10.18553/jmcp.2017.23.3-b.s17.

Ards Definition Task Force, V. M. Ranieri, G. D. Rubenfeld, B. T. Thompson, N. D. Ferguson, E. Caldwell, E. Fan, L. Camporota, and A. S. Slutsky. Acute respiratory distress syndrome: the berlin definition. *JAMA*, 307(23):2526–33, 2012. doi:10.1001/jama.2012.5669.

J. G. Fox, F. E. Dewhirst, G. J. Fraser, B. J. Paster, B. Shames, and J. C. Murphy. Intracellular campylobacter-like organism from ferrets and hamsters with proliferative bowel disease is a desulfovibrio sp. *J Clin Microbiol*, 32(5):1229–37, 1994. doi:10.1128/jcm.32.5.1229-1237.1994.

J. M. Francis, D. Leistritz-Edwards, A. Dunn, C. Tarr, J. Lehman, C. Dempsey, A. Hamel, V. Rayon, G. Liu, Y. Wang, M. Wille, M. Durkin, K. Hadley, A. Sheena, B. Roscoe, M. Ng, G. Rockwell, M. Manto, E. Gienger, J. Nickerson, Mgh Covid Collection, Team Processing, A. Moarefi, M. Noble, T. Malia, P. D. Bardwell, W. Gordon, J. Swain, M. Skoberne, K. Sauer, T. Harris, A. W. Goldrath, A. K. Shalek, A. J. Coyle, C. Benoist, and D. C. Pregibon. Allelic variation in class i hla determines cd8(+) t cell repertoire

shape and cross-reactive memory responses to sars-cov-2. *Sci Immunol*, 7(67):eabk3070, 2022. doi:10.1126/sciimmunol.abk3070.

M. Fransson, J. Burman, C. Lindqvist, C. Atterby, J. Fagius, and A. Loskog. T regulatory cells lacking cd25 are increased in ms during relapse. *Autoimmunity*, 43(8):590–7, 2010. doi:10.3109/08916930903541190.

M. E. Free, D. O. Bunch, J. A. McGregor, B. E. Jones, E. A. Berg, S. L. Hogan, Y. Hu, G. A. Preston, J. C. Jennette, R. J. Falk, and M. A. Su. Patients with antineutrophil cytoplasmic antibody-associated vasculitis have defective treg cell function exacerbated by the presence of a suppression-resistant effector cell population. *Arthritis Rheum*, 65(7): 1922–33, 2013. doi:10.1002/art.37959.

M. Frentsch, O. Arbach, D. Kirchhoff, B. Moewes, M. Worm, M. Rothe, A. Scheffold, and A. Thiel. Direct access to cd4+ t cells specific for defined antigens according to cd154 expression. *Nat Med*, 11(10):1118–24, 2005. doi:10.1038/nm1292.

W. Fu, X. Liu, X. Lin, H. Feng, L. Sun, S. Li, H. Chen, H. Tang, L. Lu, W. Jin, and C. Dong. Deficiency in t follicular regulatory cells promotes autoimmunity. *J Exp Med*, 215(3):815–825, 2018. doi:10.1084/jem.20170901.

D. Galati, M. De Martino, A. Trotta, G. Rea, D. Bruzzese, G. Cicchitto, A. A. Stanziola, M. Napolitano, A. Sanduzzi, and M. Bocchino. Peripheral depletion of nk cells and imbalance of the treg/th17 axis in idiopathic pulmonary fibrosis patients. *Cytokine*, 66(2): 119–26, 2014. doi:10.1016/j.cyto.2013.12.003.

B. Ghang, J. Lee, O. Chan Kwon, S. M. Ahn, J. S. Oh, S. Hong, Y. G. Kim, B. Yoo, W. S. Jeong, J. Kim, and C. K. Lee. Clinical significance of autoantibody positivity in idiopathic pulmonary fibrosis. *Respir Med*, 155:43–48, 2019. doi:10.1016/j.rmed.2019.07.001.

G. R. Gibson, G. T. Macfarlane, and J. H. Cummings. Occurrence of sulphate-reducing bacteria in human faeces and the relationship of dissimilatory sulphate reduction to methanogenesis in the large gut. *J Appl Bacteriol*, 65(2):103–11, 1988. doi:10.1111/j.1365-2672.1988.tb01498.x.

E. J. Goldstein, D. M. Citron, V. A. Peraino, and S. A. Cross. Desulfovibrio desulfuricans bacteremia and review of human desulfovibrio infections. *J Clin Microbiol*, 41(6):2752–4, 2003. doi:10.1128/JCM.41.6.2752-2754.2003.

K. L. Good-Jacobson, C. G. Szumilas, L. Chen, A. H. Sharpe, M. M. Tomayko, and M. J. Shlomchik. Pd-1 regulates germinal center b cell survival and the formation and affinity of long-lived plasma cells. *Nat Immunol*, 11(6):535–42, 2010. doi:10.1038/ni.1877.

K. Goudy, D. Aydin, F. Barzaghi, E. Gambineri, M. Vignoli, S. Ciullini Mannurita, C. Doglioni, M. Ponzoni, M. P. Cicalese, A. Assanelli, A. Tommasini, I. Brigida, R. M. Dellepiane, S. Martino, S. Olek, A. Aiuti, F. Ciceri, M. G. Roncarolo, and R. Bacchetta. Human il2ra null mutation mediates immunodeficiency with lymphoproliferation and autoimmunity. *Clin Immunol*, 146(3):248–61, 2013. doi:10.1016/j.clim.2013.01.004.

A. Grier, A. McDavid, B. Wang, X. Qiu, J. Java, S. Bandyopadhyay, H. Yang, J. Holden-Wiltse, H. A. Kessler, A. L. Gill, H. Huyck, A. R. Falsey, D. J. Topham, K. M. Scheible, M. T. Caserta, G. S. Pryhuber, and S. R. Gill. Neonatal gut and respiratory microbiota: coordinated development through time and space. *Microbiome*, 6(1):193, 2018. doi:10.1186/s40168-018-0566-5.

F. Guarner and J. R. Malagelada. Gut flora in health and disease. *Lancet*, 361(9356):512–9, 2003. doi:10.1016/S0140-6736(03)12489-0.

X. Guo, C. Sunil, O. Adeyanju, A. Parker, S. Huang, M. Ikebe, T. A. Tucker, S. Idell, and G. Qian. Pd-l1 mediates lung fibroblast to myofibroblast transition through smad3 and beta-catenin signaling pathways. *Sci Rep*, 12(1):3053, 2022. doi:10.1038/s41598-022-07044-3.

A. C. Habermann, A. J. Gutierrez, L. T. Bui, S. L. Yahn, N. I. Winters, C. L. Calvi, L. Peter, M. I. Chung, C. J. Taylor, C. Jetter, L. Raju, J. Roberson, G. Ding, L. Wood, J. M. S. Sucre, B. W. Richmond, A. P. Serezani, W. J. McDonnell, S. B. Mallal, M. J. Bacchetta, J. E. Loyd, C. M. Shaver, L. B. Ware, R. Bremner, R. Walia, T. S. Blackwell, N. E. Banovich, and J. A. Kropski. Single-cell rna sequencing reveals profibrotic roles of distinct epithelial and mesenchymal lineages in pulmonary fibrosis. *Sci Adv*, 6(28):eaba1972, 2020. doi:10.1126/sciadv.aba1972.

H. Hagiya, K. Kimura, I. Nishi, N. Yamamoto, H. Yoshida, Y. Akeda, and K. Tomono. Desulfovibrio desulfuricans bacteremia: A case report and literature review. *Anaerobe*, 49: 112–115, 2018. doi:10.1016/j.anaerobe.2017.12.013.

M. K. Han, Y. Zhou, S. Murray, N. Tayob, I. Noth, V. N. Lama, B. B. Moore, E. S. White, K. R. Flaherty, G. B. Huffnagle, F. J. Martinez, and Comet Investigators. Lung microbiome and disease progression in idiopathic pulmonary fibrosis: an analysis of the comet study. *Lancet Respir Med*, 2(7):548–56, 2014. doi:10.1016/S2213-2600(14)70069-4.

S. Hayashi, J. Yatsunami, Y. Fukuno, M. Kawashima, and E. J. Miller. Antileukinate, a hexapeptide inhibitor of cxc-chemokine receptor, suppresses bleomycin-induced acute lung injury in mice. *Lung*, 180(6):339–48, 2002. doi:10.1007/s00408-002-0106-7.

M. T. Henry, K. McMahon, A. J. Mackarel, K. Prikk, T. Sorsa, P. Maisi, R. Sepper, M. X. Fitzgerald, and C. M. O'Connor. Matrix metalloproteinases and tissue inhibitor of metalloproteinase-1 in sarcoidosis and ipf. *Eur Respir J*, 20(5):1220–7, 2002. doi:10.1183/09031936.02.00022302.

J. D. Herazo-Maya, I. Noth, S. R. Duncan, S. Kim, S. F. Ma, G. C. Tseng, E. Feingold, B. M. Juan-Guardela, T. J. Richards, Y. Lussier, Y. Huang, R. Vij, K. O. Lindell, J. Xue, K. F. Gibson, S. D. Shapiro, J. G. Garcia, and N. Kaminski. Peripheral blood mononuclear cell gene expression profiles predict poor outcome in idiopathic pulmonary fibrosis. *Sci Transl Med*, 5(205):205ra136, 2013. doi:10.1126/scitranslmed.3005964.

M. S. Herridge, M. Moss, C. L. Hough, R. O. Hopkins, T. W. Rice, O. J. Bienvenu, and E. Azoulay. Recovery and outcomes after the acute respiratory distress syndrome (ards) in patients and their family caregivers. *Intensive Care Med*, 42(5):725–738, 2016. doi:10.1007/s00134-016-4321-8.

P. Heukels, J. A. C. van Hulst, M. van Nimwegen, C. E. Boorsma, B. N. Melgert, J. H. von der Thusen, B. van den Blink, R. A. S. Hoek, J. R. Miedema, S. F. H. Neys, O. B. J. Corneth, R. W. Hendriks, M. S. Wijsenbeek, and M. Kool. Enhanced bruton's tyrosine kinase in b-cells and autoreactive iga in patients with idiopathic pulmonary fibrosis. *Respir Res*, 20(1):232, 2019. doi:10.1186/s12931-019-1195-7.

R. J. Hogan, E. J. Usherwood, W. Zhong, A. A. Roberts, R. W. Dutton, A. G. Harmsen, and D. L. Woodland. Activated antigen-specific cd8+ t cells persist in the lungs following recovery from respiratory virus infections. *J Immunol*, 166(3):1813–22, 2001. doi:10.4049/jimmunol.166.3.1813.

J. A. Hollenbach and J. R. Oksenberg. The immunogenetics of multiple sclerosis: A comprehensive review. *J Autoimmun*, 64:13–25, 2015. doi:10.1016/j.jaut.2015.06.010.

Z. Hou, Q. Ye, M. Qiu, Y. Hao, J. Han, and H. Zeng. Increased activated regulatory t cells proportion correlate with the severity of idiopathic pulmonary fibrosis. *Respir Res*, 18(1): 170, 2017. doi:10.1186/s12931-017-0653-3.

C. L. Hrusch, S. T. Manns, D. Bryazka, J. Casaos, C. A. Bonham, M. R. Jaffery, K. M. Blaine, K. A. M. Mills, P. A. Verhoef, A. O. Adegunsoye, J. W. Williams, M. Y. Tjota, T. V. Moore, M. E. Strek, I. Noth, and A. I. Sperling. Icos protects against mortality from acute lung injury through activation of il-5(+) ilc2s. *Mucosal Immunol*, 11(1):61–70, 2018. doi:10.1038/mi.2017.42.

G. B. Huffnagle. The microbiota and allergies/asthma. *PLoS Pathog*, 6(5):e1000549, 2010. doi:10.1371/journal.ppat.1000549.

T. Hussell, A. Pennycook, and P. J. Openshaw. Inhibition of tumor necrosis factor reduces the severity of virus-specific lung immunopathology. *Eur J Immunol*, 31(9):2566–73, 2001. doi:10.1002/1521-4141(200109)31:9<2566::aid-immu2566>3.0.co;2-l.

Network Idiopathic Pulmonary Fibrosis Clinical Research, G. Raghu, K. J. Anstrom, Jr. King, T. E., J. A. Lasky, and F. J. Martinez. Prednisone, azathioprine, and n-acetylcysteine for pulmonary fibrosis. *N Engl J Med*, 366(21):1968–77, 2012. doi:10.1056/NEJMoa1113354.

W. Ise, K. Fujii, K. Shiroguchi, A. Ito, K. Kometani, K. Takeda, E. Kawakami, K. Yamashita, K. Suzuki, T. Okada, and T. Kurosaki. T follicular helper cell-germinal center b cell interaction strength regulates entry into plasma cell or recycling germinal center cell fate. *Immunity*, 48(4):702–715 e4, 2018. doi:10.1016/j.immuni.2018.03.027.

II Ivanov, L. Frutos Rde, N. Manel, K. Yoshinaga, D. B. Rifkin, R. B. Sartor, B. B. Finlay, and D. R. Littman. Specific microbiota direct the differentiation of il-17-producing t-helper cells in the mucosa of the small intestine. *Cell Host Microbe*, 4(4):337–49, 2008. doi:10.1016/j.chom.2008.09.009.

II Ivanov, K. Atarashi, N. Manel, E. L. Brodie, T. Shima, U. Karaoz, D. Wei, K. C. Goldfarb, C. A. Santee, S. V. Lynch, T. Tanoue, A. Imaoka, K. Itoh, K. Takeda, Y. Umesaki, K. Honda, and D. R. Littman. Induction of intestinal th17 cells by segmented filamentous bacteria. *Cell*, 139(3):485–98, 2009. doi:10.1016/j.cell.2009.09.033.

J. T. Jacobsen, W. Hu, R. Castro TB, S. Solem, A. Galante, Z. Lin, S. J. Allon, L. Mesin, A. M. Bilate, A. Schiepers, A. K. Shalek, A. Y. Rudensky, and G. D. Victora. Expression of foxp3 by t follicular helper cells in end-stage germinal centers. *Science*, 373(6552), 2021. doi:10.1126/science.abe5146.

B. Jaeger, J. C. Schupp, L. Plappert, O. Terwolbeck, N. Artysh, G. Kayser, P. Engelhard, T. S. Adams, R. Zweigerdt, H. Kempf, S. Lienenklaus, W. Garrels, I. Nazarenko, D. Jonigk, M. Wygrecka, D. Klatt, A. Schambach, N. Kaminski, and A. Prasse. Airway basal cells show a dedifferentiated krt17(high)phenotype and promote fibrosis in idiopathic pulmonary fibrosis. *Nat Commun*, 13(1):5637, 2022. doi:10.1038/s41467-022-33193-0.

E. R. Johnson and M. A. Matthay. Acute lung injury: epidemiology, pathogenesis, and treatment. *J Aerosol Med Pulm Drug Deliv*, 23(4):243–52, 2010. doi:10.1089/jamp.2009.0775.

A. Jozwik, M. S. Habibi, A. Paras, J. Zhu, A. Guvenel, J. Dhariwal, M. Almond, E. H. C. Wong, A. Sykes, M. Maybeno, J. Del Rosario, M. B. Trujillo-Torralbo, P. Mallia, J. Sidney, B. Peters, O. M. Kon, A. Sette, S. L. Johnston, P. J. Openshaw, and C. Chiu. Rsv-specific airway resident memory cd8+ t cells and differential disease severity after experimental human infection. *Nat Commun*, 6:10224, 2015. doi:10.1038/ncomms10224.

S. Kadura and G. Raghu. Rheumatoid arthritis-interstitial lung disease: manifestations and current concepts in pathogenesis and management. *Eur Respir Rev*, 30(160), 2021. doi:10.1183/16000617.0011-2021.

R. A. Kahloon, J. Xue, A. Bhargava, E. Csizmadia, L. Otterbein, D. J. Kass, J. Bon, M. Soejima, M. C. Levesque, K. O. Lindell, K. F. Gibson, N. Kaminski, G. Banga, C. V. Oddis, J. M. Pilewski, F. C. Sciurba, M. Donahoe, Y. Zhang, and S. R. Duncan. Patients with idiopathic pulmonary fibrosis with antibodies to heat shock protein 70 have poor prognoses. *Am J Respir Crit Care Med*, 187(7):768–75, 2013. doi:10.1164/rccm.201203-0506OC.

O. Kalchiem-Dekel, J. R. Galvin, A. P. Burke, S. P. Atamas, and N. W. Todd. Interstitial lung disease and pulmonary fibrosis: A practical approach for general medicine physicians with focus on the medical history. *J Clin Med*, 7(12), 2018. doi:10.3390/jcm7120476.

L. A. Kalekar, J. N. Cohen, N. Prevel, P. M. Sandoval, A. N. Mathur, J. M. Moreau, M. M. Lowe, A. Nosbaum, P. J. Wolters, A. Haemel, F. Boin, and M. D. Rosenblum. Regulatory t cells in skin are uniquely poised to suppress profibrotic immune responses. *Sci Immunol*, 4(39), 2019. doi:10.1126/sciimmunol.aaw2910.

P. Kanellakis, T. N. Dinh, A. Agrotis, and A. Bobik. Cd4(+)cd25(+)foxp3(+) regulatory t cells suppress cardiac fibrosis in the hypertensive heart. *J Hypertens*, 29(9):1820–8, 2011. doi:10.1097/HJH.0b013e328349c62d.

M. Kaviratne, M. Hesse, M. Leusink, A. W. Cheever, S. J. Davies, J. H. McKerrow, L. M. Wakefield, J. J. Letterio, and T. A. Wynn. Il-13 activates a mechanism of tissue fibrosis that is completely tgf-beta independent. *J Immunol*, 173(6):4020–9, 2004. doi:10.4049/jimmunol.173.6.4020.

M. Kellner, S. Noonepalle, Q. Lu, A. Srivastava, E. Zemskov, and S. M. Black. Ros signaling in the pathogenesis of acute lung injury (ali) and acute respiratory distress syndrome (ards). *Adv Exp Med Biol*, 967:105–137, 2017. doi:10.1007/978-3-319-63245-2_8.

D. E. Kennedy, M. K. Okoreeh, M. Maienschein-Cline, J. Ai, M. Veselits, K. C. McLean, Y. Dhungana, H. Wang, J. Peng, H. Chi, M. Mandal, and M. R. Clark. Novel specialized cell state and spatial compartments within the germinal center. *Nat Immunol*, 21(6): 660–670, 2020. doi:10.1038/s41590-020-0660-2.

R. M. Kern, J. P. Singer, L. Koth, J. Mooney, J. Golden, S. Hays, J. Greenland, P. Wolters, E. Ghio, K. D. Jones, L. Leard, J. Kukreja, and P. D. Blanc. Lung transplantation for hypersensitivity pneumonitis. *Chest*, 147(6):1558–1565, 2015. doi:10.1378/chest.14-1543.

P. Kirgou, S. I. Sinis, I. E. Dimeas, I. C. Papanikolaou, K. Tatsis, A. Gogali, K. I. Gourgoulianis, D. P. Bogdanos, and Z. Daniil. Clinical relevance of circulating autoantibodies in idiopathic pulmonary fibrosis; a nat hard to break. *Front Med (Lausanne)*, 9:964722, 2022. doi:10.3389/fmed.2022.964722.

M. Kmieciak, M. Gowda, L. Graham, K. Godder, H. D. Bear, F. M. Marincola, and M. H. Manjili. Human t cells express cd25 and foxp3 upon activation and exhibit effector/memory phenotypes without any regulatory/suppressor function. *J Transl Med*, 7:89, 2009. doi:10.1186/1479-5876-7-89.

M. A. Koch, G. Tucker-Heard, N. R. Perdue, J. R. Killebrew, K. B. Urdahl, and D. J. Campbell. The transcription factor t-bet controls regulatory t cell homeostasis and function during type 1 inflammation. *Nat Immunol*, 10(6):595–602, 2009. doi:10.1038/ni.1731.

K. Kokubo, A. Onodera, M. Kiuchi, K. Tsuji, K. Hirahara, and T. Nakayama. Conventional and pathogenic th2 cells in inflammation, tissue repair, and fibrosis. *Front Immunol*, 13: 945063, 2022. doi:10.3389/fimmu.2022.945063.

I. Kotsianidis, E. Nakou, I. Bouchliou, A. Tzouvelekis, E. Spanoudakis, P. Steiropoulos, I. Sotiriou, V. Aidinis, D. Margaritis, C. Tsatalas, and D. Bouros. Global impairment of cd4+cd25+foxp3+ regulatory t cells in idiopathic pulmonary fibrosis. *Am J Respir Crit Care Med*, 179(12):1121–30, 2009. doi:10.1164/rccm.200812-1936OC.

M. C. Kullberg, J. M. Ward, P. L. Gorelick, P. Caspar, S. Hieny, A. Cheever, D. Jankovic, and A. Sher. Helicobacter hepaticus triggers colitis in specific-pathogen-free interleukin-10 (il-10)-deficient mice through an il-12- and gamma interferon-dependent mechanism. *Infect Immun*, 66(11):5157–66, 1998. doi:10.1128/IAI.66.11.5157-5166.1998.

M. C. Kullberg, A. G. Rothfuchs, D. Jankovic, P. Caspar, T. A. Wynn, P. L. Gorelick, A. W. Cheever, and A. Sher. Helicobacter hepaticus-induced colitis in interleukin-10-deficient mice: cytokine requirements for the induction and maintenance of intestinal inflammation. *Infect Immun*, 69(7):4232–41, 2001. doi:10.1128/IAI.69.7.4232-4241.2001.

R. Lamichhane, S. Patial, and Y. Saini. Higher susceptibility of males to bleomycin-induced pulmonary inflammation is associated with sex-specific transcriptomic differences in myeloid cells. *Toxicol Appl Pharmacol*, 454:116228, 2022. doi:10.1016/j.taap.2022.116228.

H. B. Larman, Z. Zhao, U. Laserson, M. Z. Li, A. Ciccia, M. A. Gakidis, G. M. Church, S. Kesari, E. M. Leproust, N. L. Solimini, and S. J. Elledge. Autoantigen discovery with a synthetic human peptidome. *Nat Biotechnol*, 29(6):535–41, 2011a. doi:10.1038/nbt.1856.

H. B. Larman, Z. Zhao, U. Laserson, M. Z. Li, A. Ciccia, M. A. M. Gakidis, G. M Church, S. Kesari, E. M. LeProust, N. L. Solimini, et al. Autoantigen discovery with a synthetic human peptidome. *Nature biotechnology*, 29(6):535–541, 2011b. doi:10.1038/nbt.1856.

C. G. Lee, R. J. Homer, Z. Zhu, S. Lanone, X. Wang, V. Koteliansky, J. M. Shipley, P. Gotwals, P. Noble, Q. Chen, et al. Interleukin-13 induces tissue fibrosis by selectively stimulating and activating transforming growth factor β1. *The Journal of experimental medicine*, 194(6):809–822, 2001. doi:10.1084/jem.194.6.809.

C. T. Lee, A. Adegunsoye, J. H. Chung, I. B. Ventura, R. Jablonski, S. Montner, R. Vij, S. E. Hines, and M. E. Strek. Characteristics and prevalence of domestic and occupational inhalational exposures across interstitial lung diseases. *Chest*, 160(1):209–218, 2021a. doi:10.1016/j.chest.2021.02.026.

C. T. Lee, M. E. Strek, A. Adegunsoye, A. W. Wong, D. Assayag, G. Cox, C. D. Fell, J. H. Fisher, A. S. Gershon, A. J. Halayko, N. Hambly, N. Khalil, M. Kolb, S. D. Lok, H. Manganas, V. Marcoux, J. Morisset, M. Sadatsafavi, S. Shapera, T. To, P. Wilcox, C. J. Ryerson, and K. A. Johannson. Inhalational exposures in patients with fibrotic interstitial lung disease: Presentation, pulmonary function and survival in the canadian registry for pulmonary fibrosis. *Respirology*, 27(8):635–644, 2022. doi:10.1111/resp.14267.

W. Lee, B. Kingstad-Bakke, R. M. Kedl, Y. Kawaoka, and M. Suresh. Ccr2 regulates vaccine-induced mucosal t-cell memory to influenza a virus. *J Virol*, 95(15):e0053021, 2021b. doi:10.1128/JVI.00530-21.

E. Lefrancais, B. Mallavia, H. Zhuo, C. S. Calfee, and M. R. Looney. Maladaptive role of neutrophil extracellular traps in pathogen-induced lung injury. *JCI Insight*, 3(3), 2018. doi:10.1172/jci.insight.98178.

F. J. Li, R. Surolia, H. Li, Z. Wang, T. Kulkarni, G. Liu, J. A. de Andrade, D. J. Kass, V. J. Thannickal, S. R. Duncan, and V. B. Antony. Autoimmunity to vimentin is associated with outcomes of patients with idiopathic pulmonary fibrosis. *J Immunol*, 199(5):1596–1605, 2017. doi:10.4049/jimmunol.1700473.

F. J. Li, R. Surolia, H. Li, Z. Wang, G. Liu, T. Kulkarni, A. V. F. Massicano, J. A. Mobley, S. Mondal, J. A. de Andrade, S. A. Coonrod, P. R. Thompson, K. Wille, S. E. Lapi, M. Athar, V. J. Thannickal, A. B. Carter, and V. B. Antony. Citrullinated vimentin mediates development and progression of lung fibrosis. *Sci Transl Med*, 13(585), 2021. doi:10.1126/scitranslmed.aba2927.

J. L. Linehan, T. Dileepan, S. W. Kashem, D. H. Kaplan, P. Cleary, and M. K. Jenkins. Generation of th17 cells in response to intranasal infection requires tgf-beta1 from dendritic cells and il-6 from cd301b+ dendritic cells. *Proc Natl Acad Sci U S A*, 112(41):12782–7, 2015. doi:10.1073/pnas.1513532112.

M. A. Linterman, W. Pierson, S. K. Lee, A. Kallies, S. Kawamoto, T. F. Rayner, M. Srivastava, D. P. Divekar, L. Beaton, J. J. Hogan, S. Fagarasan, A. Liston, K. G. Smith, and C. G. Vinuesa. Foxp3+ follicular regulatory t cells control the germinal center response. *Nat Med*, 17(8):975–82, 2011. doi:10.1038/nm.2425.

D. Liu, H. Xu, C. Shih, Z. Wan, X. Ma, W. Ma, D. Luo, and H. Qi. T-b-cell entanglement and icosl-driven feed-forward regulation of germinal centre reaction. *Nature*, 517(7533): 214–8, 2015. doi:10.1038/nature13803.

Q. Liu, G. K. Dwyer, Y. Zhao, H. Li, L. R. Mathews, A. B. Chakka, U. R. Chandran, J. A. Demetris, J. F. Alcorn, K. M. Robinson, L. A. Ortiz, B. R. Pitt, A. W. Thomson, M. H. Fan, T. R. Billiar, and H. R. Turnquist. Il-33-mediated il-13 secretion by st2+ tregs controls inflammation after lung injury. *JCI Insight*, 4(6), 2019. doi:10.1172/jci.insight.123919.

S. Lo Re, M. Lecocq, F. Uwambayinema, Y. Yakoub, M. Delos, J. B. Demoulin, S. Lucas, T. Sparwasser, J. C. Renauld, D. Lison, and F. Huaux. Platelet-derived growth factor-producing cd4+ foxp3+ regulatory t lymphocytes promote lung fibrosis. *Am J Respir Crit Care Med*, 184(11):1270–81, 2011. doi:10.1164/rccm.201103-0516OC.

C. Lozupone and R. Knight. Unifrac: a new phylogenetic method for comparing microbial communities. *Appl Environ Microbiol*, 71(12):8228–35, 2005. doi:10.1128/AEM.71.12.8228-8235.2005.

C. Lu, X. Huang, H. F. Ma, J. J. Gooley, J. Aparacio, D. J. Roof, C. Chen, D. F. Chen, and T. Li. Normal retinal development and retinofugal projections in mice lacking the

retina-specific variant of actin-binding lim domain protein. *Neuroscience*, 120(1):121–31, 2003. doi:10.1016/s0306-4522(03)00263-x.

Y. Lu and J. Craft. T follicular regulatory cells: Choreographers of productive germinal center responses. *Front Immunol*, 12:679909, 2021. doi:10.3389/fimmu.2021.679909.

A. R. Maceiras, S. C. P. Almeida, E. Mariotti-Ferrandiz, W. Chaara, F. Jebbawi, A. Six, S. Hori, D. Klatzmann, J. Faro, and L. Graca. T follicular helper and t follicular regulatory cells have different tcr specificity. *Nat Commun*, 8:15067, 2017. doi:10.1038/ncomms15067.

J. A. Mackintosh, A. U. Wells, V. Cottin, A. G. Nicholson, and E. A. Renzoni. Interstitial pneumonia with autoimmune features: challenges and controversies. *Eur Respir Rev*, 30 (162), 2021. doi:10.1183/16000617.0177-2021.

J. C. Madan, D. C. Koestler, B. A. Stanton, L. Davidson, L. A. Moulton, M. L. Housman, J. H. Moore, M. F. Guill, H. G. Morrison, M. L. Sogin, T. H. Hampton, M. R. Karagas, P. E. Palumbo, J. A. Foster, P. L. Hibberd, and G. A. O'Toole. Serial analysis of the gut and respiratory microbiome in cystic fibrosis in infancy: interaction between intestinal and respiratory tracts and impact of nutritional exposures. *mBio*, 3(4), 2012. doi:10.1128/mBio.00251-12.

T. M. Maher, T. J. Corte, A. Fischer, M. Kreuter, D. J. Lederer, M. Molina-Molina, J. Axmann, K. U. Kirchgaessler, K. Samara, F. Gilberg, and V. Cottin. Pirfenidone in patients with unclassifiable progressive fibrosing interstitial lung disease: a double-blind, randomised, placebo-controlled, phase 2 trial. *Lancet Respir Med*, 8(2):147–157, 2020. doi:10.1016/S2213-2600(19)30341-8.

L. Majlessi, F. Sayes, J. F. Bureau, A. Pawlik, V. Michel, G. Jouvion, M. Huerre, M. Severgnini, C. Consolandi, C. Peano, R. Brosch, E. Touati, and C. Leclerc. Colonization with helicobacter is concomitant with modified gut microbiota and drastic failure of the immune control of mycobacterium tuberculosis. *Mucosal Immunol*, 10(5):1178–1189, 2017. doi:10.1038/mi.2016.140.

D. Makrygiannakis, M. Hermansson, A. K. Ulfgren, A. P. Nicholas, A. J. Zendman, A. Eklund, J. Grunewald, C. M. Skold, L. Klareskog, and A. I. Catrina. Smoking increases peptidylarginine deiminase 2 enzyme expression in human lungs and increases citrullination in bal cells. *Ann Rheum Dis*, 67(10):1488–92, 2008. doi:10.1136/ard.2007.075192.

A. Mantovani, M. A. Cassatella, C. Costantini, and S. Jaillon. Neutrophils in the activation and regulation of innate and adaptive immunity. *Nat Rev Immunol*, 11(8):519–31, 2011. doi:10.1038/nri3024.

J. Marchal-Somme, Y. Uzunhan, S. Marchand-Adam, D. Valeyre, V. Soumelis, B. Crestani, and P. Soler. Cutting edge: nonproliferating mature immune cells form a novel type of organized lymphoid structure in idiopathic pulmonary fibrosis. *J Immunol*, 176(10): 5735–9, 2006. doi:10.4049/jimmunol.176.10.5735.

G. A. Margaritopoulos, E. Vasarmidi, J. Jacob, A. U. Wells, and K. M. Antoniou. Smoking and interstitial lung diseases. *Eur Respir Rev*, 24(137):428–35, 2015. doi:10.1183/16000617.0050-2015.

F. J. Martinez, E. Yow, K. R. Flaherty, L. D. Snyder, M. T. Durheim, S. R. Wisniewski, F. C. Sciurba, G. Raghu, M. M. Brooks, D. Kim, et al. Effect of antimicrobial therapy on respiratory hospitalization or death in adults with idiopathic pulmonary fibrosis: the cleanup-ipf randomized clinical trial. *Jama*, 325(18):1841–1851, 2021. doi:10.1001/jama.2021.4956.

F. Matesanz, A. Caro-Maldonado, M. Fedetz, O. Fernandez, R. L. Milne, M. Guerrero, C. Delgado, and A. Alcina. Il2ra/cd25 polymorphisms contribute to multiple sclerosis susceptibility. *J Neurol*, 254(5):682–4, 2007. doi:10.1007/s00415-006-0416-4.

E. Mathieu, U. Escribano-Vazquez, D. Descamps, C. Cherbuy, P. Langella, S. Riffault, A. Remot, and M. Thomas. Paradigms of lung microbiota functions in health and disease, particularly, in asthma. *Front Physiol*, 9:1168, 2018. doi:10.3389/fphys.2018.01168.

M. A. Matthay, R. L. Zemans, G. A. Zimmerman, Y. M. Arabi, J. R. Beitler, A. Mercat, M. Herridge, A. G. Randolph, and C. S. Calfee. Acute respiratory distress syndrome. *Nat Rev Dis Primers*, 5(1):18, 2019. doi:10.1038/s41572-019-0069-0.

G. Matute-Bello, C. W. Frevert, and T. R. Martin. Animal models of acute lung injury. *Am J Physiol Lung Cell Mol Physiol*, 295(3):L379–99, 2008. doi:10.1152/ajplung.00010.2008.

C. N. McBrien and A. Menzies-Gow. The biology of eosinophils and their role in asthma. *Front Med (Lausanne)*, 4:93, 2017. doi:10.3389/fmed.2017.00093.

L. M. McLane, M. S. Abdel-Hakeem, and E. J. Wherry. Cd8 t cell exhaustion during chronic viral infection and cancer. *Annu Rev Immunol*, 37:457–495, 2019. doi:10.1146/annurev-immunol-041015-055318.

P. J. McMurdie and S. Holmes. phyloseq: an r package for reproducible interactive analysis and graphics of microbiome census data. *PLoS One*, 8(4):e61217, 2013. doi:10.1371/journal.pone.0061217.

F. R. Millar, C. Summers, M. J. Griffiths, M. R. Toshner, and A. G. Proudfoot. The pulmonary endothelium in acute respiratory distress syndrome: insights and therapeutic opportunities. *Thorax*, 71(5):462–73, 2016. doi:10.1136/thoraxjnl-2015-207461.

H. Miyadera and K. Tokunaga. Associations of human leukocyte antigens with autoimmune diseases: challenges in identifying the mechanism. *J Hum Genet*, 60(11):697–702, 2015. doi:10.1038/jhg.2015.100.

M. Miyamoto, O. Prause, M. Sjostrand, M. Laan, J. Lotvall, and A. Linden. Endogenous il-17 as a mediator of neutrophil recruitment caused by endotoxin exposure in mouse airways. *J Immunol*, 170(9):4665–72, 2003. doi:10.4049/jimmunol.170.9.4665.

A. H. Moeller, T. A. Suzuki, M. Phifer-Rixey, and M. W. Nachman. Transmission modes of the mammalian gut microbiota. *Science*, 362(6413):453–457, 2018. doi:10.1126/science.aat7164.

T. Mogues, M. E. Goodrich, L. Ryan, R. LaCourse, and R. J. North. The relative importance of t cell subsets in immunity and immunopathology of airborne mycobacterium tuberculosis infection in mice. *J Exp Med*, 193(3):271–80, 2001. doi:10.1084/jem.193.3.271.

P. L. Molyneaux, M. J. Cox, S. A. Willis-Owen, P. Mallia, K. E. Russell, A. M. Russell, E. Murphy, S. L. Johnston, D. A. Schwartz, A. U. Wells, W. O. Cookson, T. M. Maher, and M. F. Moffatt. The role of bacteria in the pathogenesis and progression of idiopathic pulmonary fibrosis. *Am J Respir Crit Care Med*, 190(8):906–13, 2014. doi:10.1164/rccm.201403-0541OC.

P. L. Molyneaux, M. J. Cox, A. U. Wells, H. C. Kim, W. Ji, W. O. Cookson, M. F. Moffatt, D. S. Kim, and T. M. Maher. Changes in the respiratory microbiome during acute exacerbations of idiopathic pulmonary fibrosis. *Respir Res*, 18(1):29, 2017. doi:10.1186/s12931-017-0511-3.

C. Moon, M. T. Baldridge, M. A. Wallace, C. A. D, Burnham, H. W. Virgin, and T. S. Stappenbeck. Vertically transmitted faecal iga levels determine extra-chromosomal phenotypic variation. *Nature*, 521(7550):90–93, 2015. doi:10.1038/nature14139.

C. Morse, T. Tabib, J. Sembrat, K. L. Buschur, H. T. Bittar, E. Valenzi, Y. Jiang, D. J. Kass, K. Gibson, W. Chen, A. Mora, P. V. Benos, M. Rojas, and R. Lafyatis. Proliferating spp1/mertk-expressing macrophages in idiopathic pulmonary fibrosis. *Eur Respir J*, 54 (2), 2019. doi:10.1183/13993003.02441-2018.

T. Moua, F. Maldonado, P. A. Decker, C. E. Daniels, and J. H. Ryu. Frequency and implication of autoimmune serologies in idiopathic pulmonary fibrosis. *Mayo Clin Proc*, 89(3):319–26, 2014. doi:10.1016/j.mayocp.2013.11.018.

H. Narahara, E. Sakai, Y. Yamaguchi, S. Narahara, M. Iwatake, K. Okamoto, N. Yoshida, and T. Tsukuba. Actin binding lim 1 (ablim1) negatively controls osteoclastogenesis by regulating cell migration and fusion. *J Cell Physiol*, 234(1):486–499, 2018. doi:10.1002/jcp.26605.

R. Nasreddine, M. A. Argudin, M. Herpol, V. Y. Miendje Deyi, and N. Dauby. First case of desulfovibrio desulfuricans bacteraemia successfully identified using maldi-tof ms. *New Microbes New Infect*, 32:100614, 2019. doi:10.1016/j.nmni.2019.100614.

N. Neumark, Jr. Cosme, C., K. A. Rose, and N. Kaminski. The idiopathic pulmonary fibrosis cell atlas. *Am J Physiol Lung Cell Mol Physiol*, 319(6):L887–L893, 2020. doi:10.1152/ajplung.00451.2020.

I. Noth, D. Adegunsoye, T. Kulkarni, E. Otoupalova, and D. Zhu. Progressive fibrosing interstitial lung disease primer, 2020. URL `https://www.thoracic.org/education-center/ild/pdf/2020_ats_pf-ild_v13_web.pdf`.

B. O'Donovan, C. Mandel-Brehm, S. E. Vazquez, J. Liu, A. V. Parent, M. S. Anderson, T. Kassimatis, A. Zekeridou, S. L. Hauser, S. J. Pittock, E. Chow, M. R. Wilson, and J. L. DeRisi. High-resolution epitope mapping of anti-hu and anti-yo autoimmunity by programmable phage display. *Brain Commun*, 2(2):fcaa059, 2020. doi:10.1093/braincomms/fcaa059.

D. N. O'Dwyer, S. L. Ashley, S. J. Gurczynski, M. Xia, C. Wilke, N. R. Falkowski, K. C. Norman, K. B. Arnold, G. B. Huffnagle, M. L. Salisbury, M. K. Han, K. R. Flaherty, E. S. White, F. J. Martinez, J. R. Erb-Downward, S. Murray, B. B. Moore, and R. P. Dickson. Lung microbiota contribute to pulmonary inflammation and disease progression in pulmonary fibrosis. *Am J Respir Crit Care Med*, 199(9):1127–1138, 2019. doi:10.1164/rccm.201809-1650OC.

N. Ohsawa, M. Koebis, H. Mitsuhashi, I. Nishino, and S. Ishiura. Ablim1 splicing is abnormal in skeletal muscle of patients with dm1 and regulated by mbnl, celf and ptbp1. *Genes Cells*, 20(2):121–34, 2015. doi:10.1111/gtc.12201.

T. Okamoto, S. K. Mathai, C. E. Hennessy, L. A. Hancock, A. D. Walts, A. L. Stefanski, K. K. Brown, D. A. Lynch, G. P. Cosgrove, S. D. Groshong, C. D. Cool, M. I. Schwarz, N. K. Banda, J. M. Thurman, I. V. Yang, V. M. Holers, and D. A. Schwartz. The relationship between complement c3 expression and the muc5b genotype in pulmonary fibrosis. *Am J Physiol Lung Cell Mol Physiol*, 315(1):L1–L10, 2018. doi:10.1152/ajplung.00395.2017.

J. M. Oldham, A. Adegunsoye, E. Valenzi, C. Lee, L. Witt, L. Chen, A. N. Husain, S. Montner, J. H. Chung, V. Cottin, A. Fischer, I. Noth, R. Vij, and M. E. Strek. Characterisation of patients with interstitial pneumonia with autoimmune features. *Eur Respir J*, 47(6):1767–75, 2016. doi:10.1183/13993003.01565-2015.

B. O'Donovan, C. Mandel-Brehm, S. E. Vazquez, J. Liu, A. V. Parent, M. S. Anderson, T. Kassimatis, A. Zekeridou, S. L. Hauser, S. J. Pittock, et al. High-resolution epitope mapping of anti-hu and anti-yo autoimmunity by programmable phage display. *Brain communications*, 2(2):fcaa059, 2020. doi:10.1093/braincomms/fcaa059.

A. R. Panzer, S. V. Lynch, C. Langelier, J. D. Christie, K. McCauley, M. Nelson, C. K. Cheung, N. L. Benowitz, M. J. Cohen, and C. S. Calfee. Lung microbiota is related to smoking status and to development of acute respiratory distress syndrome in critically ill trauma patients. *Am J Respir Crit Care Med*, 197(5):621–631, 2018. doi:10.1164/rccm.201702-0441OC.

D. H. Parks, G. W. Tyson, P. Hugenholtz, and R. G. Beiko. Stamp: statistical analysis of taxonomic and functional profiles. *Bioinformatics*, 30(21):3123–4, 2014. doi:10.1093/bioinformatics/btu494.

E. R. Parra, R. A. Kairalla, C. R. Ribeiro de Carvalho, E. Eher, and V. L. Capelozzi. Inflammatory cell phenotyping of the pulmonary interstitium in idiopathic interstitial pneumonia. *Respiration*, 74(2):159–69, 2007. doi:10.1159/000097133.

C. Pattaroni, M. L. Watzenboeck, S. Schneidegger, S. Kieser, N. C. Wong, E. Bernasconi, J. Pernot, L. Mercier, S. Knapp, L. P. Nicod, C. P. Marsland, M. Roth-Kleiner, and B. J. Marsland. Early-life formation of the microbial and immunological environment of the human airways. *Cell Host Microbe*, 24(6):857–865 e4, 2018. doi:10.1016/j.chom.2018.10.019.

Robert K. Peet. The measurement of species diversity. *Annual Review of Ecology and Systematics*, 5(1):285–307, 1974. doi:10.1146/annurev.es.05.110174.001441.

M. Pepper, J. L. Linehan, A. J. Pagan, T. Zell, T. Dileepan, P. P. Cleary, and M. K. Jenkins. Different routes of bacterial infection induce long-lived th1 memory cells and short-lived th17 cells. *Nat Immunol*, 11(1):83–9, 2010. doi:10.1038/ni.1826.

J. K. Polansky, K. Kretschmer, J. Freyer, S. Floess, A. Garbe, U. Baron, S. Olek, A. Hamann, H. von Boehmer, and J. Huehn. Dna methylation controls foxp3 gene expression. *Eur J Immunol*, 38(6):1654–63, 2008. doi:10.1002/eji.200838105.

Q. Qi, Y. Liu, Y. Cheng, J. Glanville, D. Zhang, J. Y. Lee, R. A. Olshen, C. M. Weyand, S. D. Boyd, and J. J. Goronzy. Diversity and clonal selection in the human t-cell repertoire. *Proc Natl Acad Sci U S A*, 111(36):13139–44, 2014. doi:10.1073/pnas.1409155111.

G. Raghu, K. K. Brown, U. Costabel, V. Cottin, R. M. du Bois, J. A. Lasky, M. Thomeer, J. P. Utz, R. K. Khandker, L. McDermott, and S. Fatenejad. Treatment of idiopathic pulmonary fibrosis with etanercept: an exploratory, placebo-controlled trial. *Am J Respir Crit Care Med*, 178(9):948–55, 2008. doi:10.1164/rccm.200709-1446OC.

G. Raghu, M. Remy-Jardin, J. L. Myers, L. Richeldi, C. J. Ryerson, D. J. Lederer, J. Behr, V. Cottin, S. K. Danoff, F. Morell, K. R. Flaherty, A. Wells, F. J. Martinez, A. Azuma, T. J. Bice, D. Bouros, K. K. Brown, H. R. Collard, A. Duggal, L. Galvin, Y. Inoue, R. G. Jenkins, T. Johkoh, E. A. Kazerooni, M. Kitaichi, S. L. Knight, G. Mansour, A. G. Nicholson, S. N. J. Pipavath, I. Buendia-Roldan, M. Selman, W. D. Travis, S. Walsh, K. C. Wilson, European Respiratory Society Japanese Respiratory Society American Thoracic Society, and Society Latin American Thoracic. Diagnosis of idiopathic pulmonary fibrosis. an official ats/ers/jrs/alat clinical practice guideline. *Am J Respir Crit Care Med*, 198(5):e44–e68, 2018. doi:10.1164/rccm.201807-1255ST.

G. Raghu, M. Remy-Jardin, C. J. Ryerson, J. L. Myers, M. Kreuter, M. Vasakova, E. Bargagli, J. H. Chung, B. F. Collins, E. Bendstrup, H. A. Chami, A. T. Chua, T. J. Corte, J. C. Dalphin, S. K. Danoff, J. Diaz-Mendoza, A. Duggal, R. Egashira, T. Ewing, M. Gulati, Y. Inoue, A. R. Jenkins, K. A. Johannson, T. Johkoh, M. Tamae-Kakazu, M. Kitaichi, S. L. Knight, D. Koschel, D. J. Lederer, Y. Mageto, L. A. Maier, C. Matiz, F. Morell, A. G. Nicholson, S. Patolia, C. A. Pereira, E. A. Renzoni, M. L. Salisbury, M. Selman, S. L. F. Walsh, W. A. Wuyts, and K. C. Wilson. Diagnosis of hypersensitivity pneumonitis in adults. an official ats/jrs/alat clinical practice guideline. *Am J Respir Crit Care Med*, 202(3):e36–e69, 2020. doi:10.1164/rccm.202005-2032ST.

G. Raghu, M. Remy-Jardin, L. Richeldi, C. C. Thomson, Y. Inoue, T. Johkoh, M. Kreuter, D. A. Lynch, T. M. Maher, F. J. Martinez, M. Molina-Molina, J. L. Myers, A. G. Nicholson, C. J. Ryerson, M. E. Strek, L. K. Troy, M. Wijsenbeek, M. J. Mammen, T. Hossain, B. D. Bissell, D. D. Herman, S. M. Hon, F. Kheir, Y. H. Khor, M. Macrea, K. M. Antoniou, D. Bouros, I. Buendia-Roldan, F. Caro, B. Crestani, L. Ho, J. Morisset, A. L. Olson, A. Podolanczuk, V. Poletti, M. Selman, T. Ewing, S. Jones, S. L. Knight, M. Ghazipura, and K. C. Wilson. Idiopathic pulmonary fibrosis (an update) and progressive pulmonary fibrosis in adults: An official ats/ers/jrs/alat clinical practice guideline. *Am J Respir Crit Care Med*, 205(9):e18–e47, 2022. doi:10.1164/rccm.202202-0399ST.

J. P. Ray, H. D. Marshall, B. J. Laidlaw, M. M. Staron, S. M. Kaech, and J. Craft. Transcription factor stat3 and type i interferons are corepressive insulators for differentiation of follicular helper and t helper 1 cells. *Immunity*, 40(3):367–77, 2014. doi:10.1016/j.immuni.2014.02.005.

E. F. Redente, K. M. Jacobsen, J. J. Solomon, A. R. Lara, S. Faubel, R. C. Keith, P. M. Henson, G. P. Downey, and D. W. Riches. Age and sex dimorphisms contribute to the severity of bleomycin-induced lung injury and fibrosis. *Am J Physiol Lung Cell Mol Physiol*, 301(4):L510–8, 2011. doi:10.1152/ajplung.00122.2011.

P. A. Reyfman, J. M. Walter, N. Joshi, K. R. Anekalla, A. C. McQuattie-Pimentel, S. Chiu, R. Fernandez, M. Akbarpour, C. I. Chen, Z. Ren, R. Verma, H. Abdala-Valencia, K. Nam, M. Chi, S. Han, F. J. Gonzalez-Gonzalez, S. Soberanes, S. Watanabe, K. J. N. Williams, A. S. Flozak, T. T. Nicholson, V. K. Morgan, D. R. Winter, M. Hinchcliff, C. L. Hrusch, R. D. Guzy, C. A. Bonham, A. I. Sperling, R. Bag, R. B. Hamanaka, G. M. Mutlu, A. V. Yeldandi, S. A. Marshall, A. Shilatifard, L. A. N. Amaral, H. Perlman, J. I. Sznajder, A. C. Argento, C. T. Gillespie, J. Dematte, M. Jain, B. D. Singer, K. M. Ridge, A. P. Lam, A. Bharat, S. M. Bhorade, C. J. Gottardi, G. R. S. Budinger, and A. V. Misharin. Single-cell transcriptomic analysis of human lung provides insights into the pathobiology of pulmonary fibrosis. *Am J Respir Crit Care Med*, 199(12):1517–1536, 2019. doi:10.1164/rccm.201712-2410OC.

D. J. Roof, A. Hayes, M. Adamian, A. H. Chishti, and T. Li. Molecular characterization of ablim, a novel actin-binding and double zinc finger protein. *J Cell Biol*, 138(3):575–88, 1997. doi:10.1083/jcb.138.3.575.

J. A. Rutigliano and B. S. Graham. Prolonged production of tnf-alpha exacerbates illness during respiratory syncytial virus infection. *J Immunol*, 173(5):3408–17, 2004. doi:10.4049/jimmunol.173.5.3408.

E. P. A. Rutten, K. Lenaerts, W. A. Buurman, and E. F. M. Wouters. Disturbed intestinal integrity in patients with copd: effects of activities of daily living. *Chest*, 145(2):245–252, 2014. doi:10.1378/chest.13-0584.

P. T. Sage, A. M. Paterson, S. B. Lovitch, and A. H. Sharpe. The coinhibitory receptor

ctla-4 controls b cell responses by modulating t follicular helper, t follicular regulatory, and t regulatory cells. *Immunity*, 41(6):1026–39, 2014. doi:10.1016/j.immuni.2014.12.005.

S. Sakaguchi, N. Mikami, J. B. Wing, A. Tanaka, K. Ichiyama, and N. Ohkura. Regulatory t cells and human disease. *Annu Rev Immunol*, 38:541–566, 2020. doi:10.1146/annurev-immunol-042718-041717.

J. Salonen, H. Vahanikkila, M. Purokivi, and R. Kaarteenaho. Causes of acute respiratory hospitalizations predict survival in fibrosing interstitial lung diseases. *PLoS One*, 15(11): e0242860, 2020. doi:10.1371/journal.pone.0242860.

K. D. Samara, A. Trachalaki, E. Tsitoura, A. V. Koutsopoulos, E. D. Lagoudaki, I. Lasithiotaki, G. Margaritopoulos, P. Pantelidis, E. Bibaki, N. M. Siafakas, N. Tzanakis, A. U. Wells, and K. M. Antoniou. Upregulation of citrullination pathway: From autoimmune to idiopathic lung fibrosis. *Respir Res*, 18(1):218, 2017. doi:10.1186/s12931-017-0692-9.

C. A. Schneider, W. S. Rasband, and K. W. Eliceiri. Nih image to imagej: 25 years of image analysis. *Nature methods*, 9(7):671–675, 2012. doi:10.1038/nmeth.2089.

P. Schwarzenberger, V. La Russa, A. Miller, P. Ye, W. Huang, A. Zieske, S. Nelson, G. J. Bagby, D. Stoltz, R. L. Mynatt, M. Spriggs, and J. K. Kolls. Il-17 stimulates granulopoiesis in mice: use of an alternate, novel gene therapy-derived method for in vivo evaluation of cytokines. *J Immunol*, 161(11):6383–9, 1998.

P. Schwarzenberger, W. Huang, P. Ye, P. Oliver, M. Manuel, Z. Zhang, G. Bagby, S. Nelson, and J. K. Kolls. Requirement of endogenous stem cell factor and granulocyte-colony-stimulating factor for il-17-mediated granulopoiesis. *J Immunol*, 164(9):4783–9, 2000. doi:10.4049/jimmunol.164.9.4783.

C. J. Scotton and R. C. Chambers. Bleomycin revisited: towards a more representative model of ipf? *Am J Physiol Lung Cell Mol Physiol*, 299(4):L439–41, 2010. doi:10.1152/ajplung.00258.2010.

M. Selman and A. Pardo. Idiopathic pulmonary fibrosis: an epithelial/fibroblastic cross-talk disorder. *Respir Res*, 3:3, 2002. doi:10.1186/rr175.

V. Sencio, M. G. Machado, and F. Trottein. The lung-gut axis during viral respiratory infections: the impact of gut dysbiosis on secondary disease outcomes. *Mucosal Immunol*, 14(2):296–304, 2021. doi:10.1038/s41385-020-00361-8.

G. Serena, S. Yan, S. Camhi, S. Patel, R. S. Lima, A. Sapone, M. M. Leonard, R. Mukherjee, B. J. Nath, K. M. Lammers, and A. Fasano. Proinflammatory cytokine interferon-gamma and microbiome-derived metabolites dictate epigenetic switch between forkhead box protein 3 isoforms in coeliac disease. *Clin Exp Immunol*, 187(3):490–506, 2017. doi:10.1111/cei.12911.

A. P. M. Serezani, B. D. Pascoalino, J. M. R. Bazzano, K. N. Vowell, H. Tanjore, C. J. Taylor, C. L. Calvi, A. S. McCall, M. D. Bacchetta, C. M. Shaver, L. B. Ware, M. L. Salisbury, N. E. Banovich, P. L. Kendall, J. A. Kropski, and T. S. Blackwell. Multiplatform single-cell analysis identifies immune cell types enhanced in pulmonary fibrosis. *Am J Respir Cell Mol Biol*, 67(1):50–60, 2022. doi:10.1165/rcmb.2021-0418OC.

A. V. Shinde, C. Humeres, and N. G. Frangogiannis. The role of alpha-smooth muscle actin in fibroblast-mediated matrix contraction and remodeling. *Biochim Biophys Acta Mol Basis Dis*, 1863(1):298–309, 2017. doi:10.1016/j.bbadis.2016.11.006.

A. K. Shum, M. Alimohammadi, C. L. Tan, M. H. Cheng, T. C. Metzger, C. S. Law, W. Lwin, J. Perheentupa, H. Bour-Jordan, J. C. Carel, E. S. Husebye, F. De Luca, C. Janson, R. Sargur, N. Dubois, M. Kajosaari, P. J. Wolters, H. A. Chapman, O. Kampe, and M. S. Anderson. Bpifb1 is a lung-specific autoantigen associated with interstitial lung disease. *Sci Transl Med*, 5(206):206ra139, 2013. doi:10.1126/scitranslmed.3006998.

Y. Si, Y. Wen, S. H. Kelly, A. S. Chong, and J. H. Collier. Intranasal delivery of adjuvant-free peptide nanofibers elicits resident cd8(+) t cell responses. *J Control Release*, 282: 120–130, 2018. doi:10.1016/j.jconrel.2018.04.031.

S. Sleijfer. Bleomycin-induced pneumonitis. *Chest*, 120(2):617–24, 2001. doi:10.1378/chest.120.2.617.

J. Solomon, F. Castelino, and A. Mathur. Connective tissue-related interstitial lung disease primer, 2020. URL `https://www.thoracic.org/education-center/ild/pdf/2020_ats_ctd-ild_v13_web.pdf`.

C. Soto, R. G. Bombardi, M. Kozhevnikov, R. S. Sinkovits, E. C. Chen, A. Branchizio, N. Kose, S. B. Day, M. Pilkinton, M. Gujral, S. Mallal, and Jr. Crowe, J. E. High frequency of shared clonotypes in human t cell receptor repertoires. *Cell Rep*, 32(2):107882, 2020. doi:10.1016/j.celrep.2020.107882.

M. Stebegg, S. D. Kumar, A. Silva-Cayetano, V. R. Fonseca, M. A. Linterman, and L. Graca. Regulation of the germinal center response. *Front Immunol*, 9:2469, 2018. doi:10.3389/fimmu.2018.02469.

J. D. Storey. A direct approach to false discovery rates. *Journal of the Royal Statistical Society Series B-Statistical Methodology*, 64:479–498, 2002. doi:Unsp 1369-7412/02/64479.

M. E. Strek, J. M. Oldham, A. Adegunsoye, and R. Vij. A call for uniformity in implementing the ipaf (interstitial pneumonia with autoimmune features) criteria. *Eur Respir J*, 48(6): 1813–1814, 2016. doi:10.1183/13993003.01841-2016.

T. Tada, S. Yamamura, Y. Kuwano, and T. Abo. Level of myelopoiesis in the bone marrow is influenced by intestinal flora. *Cell Immunol*, 173(1):155–61, 1996. doi:10.1006/cimm.1996.0261.

N. W. Todd, R. G. Scheraga, J. R. Galvin, A. T. Iacono, E. J. Britt, I. G. Luzina, A. P. Burke, and S. P. Atamas. Lymphocyte aggregates persist and accumulate in the lungs of patients with idiopathic pulmonary fibrosis. *J Inflamm Res*, 6:63–70, 2013. doi:10.2147/JIR.S40673.

J. Travers and M. E. Rothenberg. Eosinophils in mucosal immune responses. *Mucosal Immunol*, 8(3):464–75, 2015. doi:10.1038/mi.2015.2.

A. Trompette, E. S. Gollwitzer, K. Yadava, A. K. Sichelstiel, N. Sprenger, C. Ngom-Bru, C. Blanchard, T. Junt, L. P. Nicod, N. L. Harris, and B. J. Marsland. Gut microbiota metabolism of dietary fiber influences allergic airway disease and hematopoiesis. *Nat Med*, 20(2):159–66, 2014. doi:10.1038/nm.3444.

N. J. Tubo and M. K. Jenkins. Cd4+ t cells: guardians of the phagosome. *Clin Microbiol Rev*, 27(2):200–13, 2014. doi:10.1128/CMR.00097-13.

S. J. Tzotzos, B. Fischer, H. Fischer, and M. Zeitlinger. Incidence of ards and outcomes in hospitalized patients with covid-19: a global literature survey. *Crit Care*, 24(1):516, 2020. doi:10.1186/s13054-020-03240-7.

B. B. Ural, D. P. Caron, P. Dogra, S. B. Wells, P. A. Szabo, T. Granot, T. Senda, M. M. L. Poon, N. Lam, P. Thapa, Y. S. Lee, M. Kubota, R. Matsumoto, and D. L. Farber. Inhaled particulate accumulation with age impairs immune function and architecture in human lung lymph nodes. *Nat Med*, 28(12):2622–2632, 2022. doi:10.1038/s41591-022-02073-x.

M. Vasakova, F. Morell, S. Walsh, K. Leslie, and G. Raghu. Hypersensitivity pneumonitis: Perspectives in diagnosis and management. *Am J Respir Crit Care Med*, 196(6):680–689, 2017. doi:10.1164/rccm.201611-2201PP.

S. E. Vazquez, E. M. Ferre, D. W. Scheel, S. Sunshine, B. Miao, C. Mandel-Brehm, Z. Quandt, A. Y. Chan, M. Cheng, M. German, M. Lionakis, J. L. DeRisi, and M. S. Anderson. Identification of novel, clinically correlated autoantigens in the monogenic autoimmune syndrome aps1 by proteome-wide phip-seq. *Elife*, 9, 2020a. doi:10.7554/eLife.55053.

S. E. Vazquez, E. M. N. Ferré, D. W. Scheel, S. Sunshine, B. Miao, C. Mandel-Brehm, Z. Quandt, A. Y. Chan, M. Cheng, M. German, et al. Identification of novel, clinically correlated autoantigens in the monogenic autoimmune syndrome aps1 by proteome-wide phip-seq. *Elife*, 9:e55053, 2020b. doi:10.7554/eLife.55053.

R. Vij and M. E. Strek. Diagnosis and treatment of connective tissue disease-associated interstitial lung disease. *Chest*, 143(3):814–824, 2013. doi:10.1378/chest.12-0741.

J. W. Voltz, J. W. Card, M. A. Carey, L. M. Degraff, C. D. Ferguson, G. P. Flake, J. C. Bonner, K. S. Korach, and D. C. Zeldin. Male sex hormones exacerbate lung function impairment after bleomycin-induced pulmonary fibrosis. *Am J Respir Cell Mol Biol*, 39 (1):45–52, 2008. doi:10.1165/rcmb.2007-0340OC.

L. J. Vuga, J. R. Tedrow, K. V. Pandit, J. Tan, D. J. Kass, J. Xue, D. Chandra, J. K. Leader, K. F. Gibson, N. Kaminski, F. C. Sciurba, and S. R. Duncan. C-x-c motif chemokine 13 (cxcl13) is a prognostic biomarker of idiopathic pulmonary fibrosis. *Am J Respir Crit Care Med*, 189(8):966–74, 2014. doi:10.1164/rccm.201309-1592OC.

L. E. Wagar, A. Salahudeen, C. M. Constantz, B. S. Wendel, M. M. Lyons, V. Mallajosyula, L. P. Jatt, J. Z. Adamska, L. K. Blum, N. Gupta, K. J. L. Jackson, F. Yang, K. Roltgen, K. M. Roskin, K. M. Blaine, K. D. Meister, I. N. Ahmad, M. Cortese, E. G. Dora, S. N. Tucker, A. I. Sperling, A. Jain, D. H. Davies, P. L. Felgner, G. B. Hammer, P. S. Kim, W. H. Robinson, S. D. Boyd, C. J. Kuo, and M. M. Davis. Modeling human adaptive immune responses with tonsil organoids. *Nat Med*, 27(1):125–135, 2021. doi:10.1038/s41591-020-01145-0.

K. B. Walsh, J. R. Teijaro, L. G. Brock, D. M. Fremgen, P. L. Collins, H. Rosen, and M. B. Oldstone. Animal model of respiratory syncytial virus: Cd8+ t cells cause a cytokine storm that is chemically tractable by sphingosine-1-phosphate 1 receptor agonist therapy. *J Virol*, 88(11):6281–93, 2014. doi:10.1128/JVI.00464-14.

J. D. Watson, E. Leung, M. Eszes, G. S. Le Gros, R. L. Prestidge, R. J. Booth, R. A. Overell, and S. Gillis. Expression of functional human interleukin-2 receptors in murine interleukin-3-dependent cells. *Immunol Cell Biol*, 66 (Pt 4):319–30, 1988. doi:10.1038/icb.1988.42.

J. S. Weinstein, E. I. Herman, B. Lainez, P. Licona-Limon, E. Esplugues, R. Flavell, and J. Craft. Tfh cells progressively differentiate to regulate the germinal center response. *Nat Immunol*, 17(10):1197–1205, 2016. doi:10.1038/ni.3554.

M. T. Whary, N. S. Taylor, Y. Feng, Z. Ge, S. Muthupalani, J. Versalovic, and J. G. Fox. Lactobacillus reuteri promotes helicobacter hepaticus-associated typhlocolitis in gnotobiotic b6.129p2-il-10(tm1cgn) (il-10(-/-)) mice. *Immunology*, 133(2):165–78, 2011. doi:10.1111/j.1365-2567.2011.03423.x.

M. Wijsenbeek and V. Cottin. Spectrum of fibrotic lung diseases. *N Engl J Med*, 383(10): 958–968, 2020. doi:10.1056/NEJMra2005230.

D. M. Willerford, J. Chen, J. A. Ferry, L. Davidson, A. Ma, and F. W. Alt. Interleukin-2 receptor alpha chain regulates the size and content of the peripheral lymphoid compartment. *Immunity*, 3(4):521–30, 1995. doi:10.1016/1074-7613(95)90180-9.

E. A. Wohlfert, J. R. Grainger, N. Bouladoux, J. E. Konkel, G. Oldenhove, C. H. Ribeiro, J. A. Hall, R. Yagi, S. Naik, R. Bhairavabhotla, W. E. Paul, R. Bosselut, G. Wei, K. Zhao, M. Oukka, J. Zhu, and Y. Belkaid. Gata3 controls foxp3(+) regulatory t cell fate during inflammation in mice. *J Clin Invest*, 121(11):4503–15, 2011. doi:10.1172/JCI57456.

M. Wolfl, J. Kuball, W. Y. Ho, H. Nguyen, T. J. Manley, M. Bleakley, and P. D. Greenberg. Activation-induced expression of cd137 permits detection, isolation, and expansion of the full repertoire of cd8+ t cells responding to antigen without requiring knowledge of epitope specificities. *Blood*, 110(1):201–10, 2007. doi:10.1182/blood-2006-11-056168.

I. Wollenberg, A. Agua-Doce, A. Hernandez, C. Almeida, V. G. Oliveira, J. Faro, and L. Graca. Regulation of the germinal center reaction by foxp3+ follicular regulatory t cells. *J Immunol*, 187(9):4553–60, 2011. doi:10.4049/jimmunol.1101328.

P. J. Wolters, T. S. Blackwell, O. Eickelberg, J. E. Loyd, N. Kaminski, G. Jenkins, T. M. Maher, M. Molina-Molina, P. W. Noble, G. Raghu, L. Richeldi, M. I. Schwarz, M. Selman, W. A. Wuyts, and D. A. Schwartz. Time for a change: is idiopathic pulmonary fibrosis still idiopathic and only fibrotic? *Lancet Respir Med*, 6(2):154–160, 2018. doi:10.1016/S2213-2600(18)30007-9.

D. E. Wood and S. L. Salzberg. Kraken: ultrafast metagenomic sequence classification using exact alignments. *Genome Biol*, 15(3):R46, 2014. doi:10.1186/gb-2014-15-3-r46.

W. A. Wuyts, A. Cavazza, G. Rossi, F. Bonella, N. Sverzellati, and P. Spagnolo. Differential diagnosis of usual interstitial pneumonia: when is it truly idiopathic? *Eur Respir Rev*, 23 (133):308–19, 2014. doi:10.1183/09059180.00004914.

T. A. Wynn. Cellular and molecular mechanisms of fibrosis. *The Journal of Pathology: A Journal of the Pathological Society of Great Britain and Ireland*, 214(2):199–210, 2008. doi:10.1002/path.2277.

H. Xia, V. Bodempudi, A. Benyumov, P. Hergert, D. Tank, J. Herrera, J. Braziunas, O. Larsson, M. Parker, D. Rossi, K. Smith, M. Peterson, A. Limper, J. Jessurun, J. Connett, D. Ingbar, S. Phan, P. B. Bitterman, and C. A. Henke. Identification of a cell-of-origin for fibroblasts comprising the fibrotic reticulum in idiopathic pulmonary fibrosis. *Am J Pathol*, 184(5):1369–83, 2014. doi:10.1016/j.ajpath.2014.01.012.

S. Xie, S. Li, B. Chen, Q. Zhu, L. Xu, and F. Li. Serum anti-citrullinated protein antibodies and rheumatoid factor increase the risk of rheumatoid arthritis-related interstitial lung disease: a meta-analysis. *Clin Rheumatol*, 40(11):4533–4543, 2021. doi:10.1007/s10067-021-05808-2.

M. Xu, M. Pokrovskii, Y. Ding, R. Yi, C. Au, O. J. Harrison, C. Galan, Y. Belkaid, R. Bonneau, and D. R. Littman. c-maf-dependent regulatory t cells mediate immunological tolerance to a gut pathobiont. *Nature*, 554(7692):373–377, 2018. doi:10.1038/nature25500.

J. Xue, B. R. Gochuico, A. S. Alawad, C. A. Feghali-Bostwick, I. Noth, S. D. Nathan, G. D. Rosen, I. O. Rosas, S. Dacic, I. Ocak, C. R. Fuhrman, K. T. Cuenco, M. A. Smith, S. S. Jacobs, A. Zeevi, P. A. Morel, J. M. Pilewski, V. G. Valentine, K. F. Gibson, N. Kaminski, F. C. Sciurba, Y. Zhang, and S. R. Duncan. The hla class ii allele drb1*1501 is over-represented in patients with idiopathic pulmonary fibrosis. *PLoS One*, 6(2):e14715, 2011. doi:10.1371/journal.pone.0014715.

B. H. Yang, S. Hagemann, P. Mamareli, U. Lauer, U. Hoffmann, M. Beckstette, L. Fohse, I. Prinz, J. Pezoldt, S. Suerbaum, T. Sparwasser, A. Hamann, S. Floess, J. Huehn, and

M. Lochner. Foxp3(+) t cells expressing rorgammat represent a stable regulatory t-cell effector lineage with enhanced suppressive capacity during intestinal inflammation. *Mucosal Immunol*, 9(2):444–57, 2016. doi:10.1038/mi.2015.74.

D. Yang, X. Chen, J. Wang, Q. Lou, Y. Lou, L. Li, H. Wang, J. Chen, M. Wu, X. Song, and Y. Qian. Dysregulated lung commensal bacteria drive interleukin-17b production to promote pulmonary fibrosis through their outer membrane vesicles. *Immunity*, 50(3): 692–706 e7, 2019. doi:10.1016/j.immuni.2019.02.001.

I. Yang, D. Eibach, F. Kops, B. Brenneke, S. Woltemate, J. Schulze, A. Bleich, A. D. Gruber, S. Muthupalani, J. G. Fox, C. Josenhans, and S. Suerbaum. Intestinal microbiota composition of interleukin-10 deficient c57bl/6j mice and susceptibility to helicobacter hepaticus-induced colitis. *PLoS One*, 8(8):e70783, 2013. doi:10.1371/journal.pone.0070783.

Y. Yang, J. Fujita, S. Bandoh, Y. Ohtsuki, I. Yamadori, T. Yoshinouchi, and T. Ishida. Detection of antivimentin antibody in sera of patients with idiopathic pulmonary fibrosis and non-specific interstitial pneumonia. *Clinical & Experimental Immunology*, 128(1): 169–174, 2002. doi:doi: 10.1046/j.1365-2249.2002.01811.x.

A. Yazar, S. Atis, K. Konca, C. Pata, E. Akbay, M. Calikoglu, and A. Hafta. Respiratory symptoms and pulmonary functional changes in patients with irritable bowel syndrome. *Am J Gastroenterol*, 96(5):1511–6, 2001. doi:10.1111/j.1572-0241.2001.03748.x.

Z. X. Yunt and J. J. Solomon. Lung disease in rheumatoid arthritis. *Rheum Dis Clin North Am*, 41(2):225–36, 2015. doi:10.1016/j.rdc.2014.12.004.

R. D. Yusen, L. B. Edwards, A. Y. Kucheryavaya, C. Benden, A. I. Dipchand, F. Dobbels, S. B. Goldfarb, B. J. Levvey, L. H. Lund, B. Meiser, J. Stehlik, Heart International Society for, and Transplantation Lung. The registry of the international society for heart and lung transplantation: thirty-first adult lung and heart-lung transplant report–2014; focus theme: retransplantation. *J Heart Lung Transplant*, 33(10):1009–24, 2014. doi:10.1016/j.healun.2014.08.004.

B. Zhang, X. Zhang, F. L. Tang, L. P. Zhu, Y. Liu, and P. E. Lipsky. Clinical significance of increased cd4+cd25-foxp3+ t cells in patients with new-onset systemic lupus erythematosus. *Ann Rheum Dis*, 67(7):1037–40, 2008. doi:10.1136/ard.2007.083543.

M. Zurkova, E. Kriegova, V. Kolek, V. Lostakova, M. Sterclova, V. Bartos, M. Doubkova, I. Binkova, M. Svoboda, J. Strenkova, M. Janotova, M. Plackova, L. Lacina, V. Rihak, F. Petrik, P. Lisa, R. Bittenglova, R. Tyl, G. Ondrejka, H. Suldova, J. Lnenicka, J. Psikalova, T. Snizek, J. Homolka, R. Kralova, J. Kervitzer, M. Vasakova, I. L. D. section, and I. P. F. registry. Effect of pirfenidone on lung function decline and survival: 5-yr experience from a real-life ipf cohort from the czech empire registry. *Respir Res*, 20 (1):16, 2019. doi:10.1186/s12931-019-0977-2.